

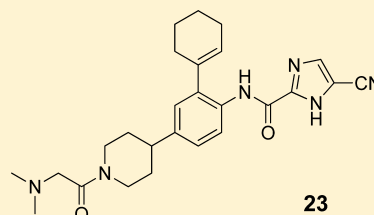
# Optimization of a Potent Class of Arylamide Colony-Stimulating Factor-1 Receptor Inhibitors Leading to Anti-inflammatory Clinical Candidate 4-Cyano-*N*-[2-(1-cyclohexen-1-yl)-4-[1-[(dimethylamino)-acetyl]-4-piperidiny]phenyl]-1*H*-imidazole-2-carboxamide (JNJ-28312141)

Carl R. Illig,\* Carl L. Manthey, Mark J. Wall, Sanath K. Meegalla, Jinsheng Chen, Kenneth J. Wilson, Shelley K. Ballentine, Renee L. DesJarlais, Carsten Schubert, Carl S. Crysler, Yanmin Chen, Christopher J. Molloy, Margery A. Chaikin, Robert R. Donatelli, Edward Yurkow, Zhao Zhou, Mark R. Player, and Bruce E. Tomczuk

Johnson & Johnson Pharmaceutical Research & Development, Welsh & McKean Roads, Spring House, Pennsylvania 19477, United States

## Supporting Information

**ABSTRACT:** A class of potent inhibitors of colony-stimulating factor-1 receptor (CSF-1R or FMS), as exemplified by **8** and **21**, was optimized to improve pharmacokinetic and pharmacodynamic properties and potential toxicological liabilities. Early stage absorption, distribution, metabolism, and excretion assays were employed to ensure the incorporation of druglike properties resulting in the selection of several compounds with good activity in a pharmacodynamic screening assay in mice. Further investigation, utilizing the type II collagen-induced arthritis model in mice, culminated in the selection of anti-inflammatory development candidate JNJ-28312141 (**23**, FMS  $IC_{50}$  = 0.69 nM, cell assay  $IC_{50}$  = 2.6 nM). Compound **23** also demonstrated efficacy in rat adjuvant and streptococcal cell wall-induced models of arthritis and has entered phase I clinical trials.



## ■ INTRODUCTION

Inflammation comprises a complex series of biochemical events that can be initiated by a number of stimuli including noxious chemical agents, pathogens, and autoimmune responses and, in pathological situations, may lead to the destruction of cells, tissues, and organs. Among autoimmune diseases, rheumatoid arthritis (RA) represents an area of significant unmet medical need and affects about 1% of the population. The annual economic burden caused by this disease in 2006 was estimated to be \$58 billion in Europe and \$54 billion in the United States,<sup>1</sup> while the global market for arthritis drugs was estimated to be as high as \$35 billion for 2008.<sup>2</sup>

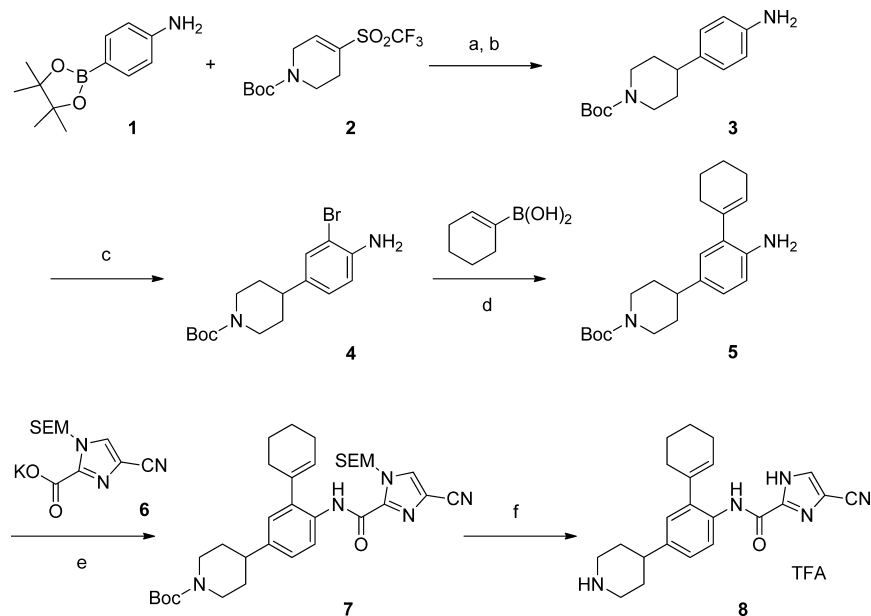
Low-dose methotrexate is the first-line therapy in RA. Although methotrexate has a very low associated cost, patients must be monitored several times a year for the development of hepatitis. Additional monitoring is also necessary to guard against the development of renal, pulmonary, or bone marrow disease. Many patients on this regimen experience side effects such as fatigue and nausea, and approximately half of all patients do not respond sufficiently to methotrexate monotherapy.<sup>3</sup> In these patients, methotrexate may then be combined with a biologic therapy, which includes anti-tumor necrosis factor (TNF) agents<sup>4</sup> such as infliximab or etanercept. Biologics, despite their effectiveness in reducing symptoms and structural damage, are of significantly higher cost and must be

given parenterally. Thus, there is a continuing need for an oral agent that effectively relieves the symptoms of RA, prevents structural damage, and is better tolerated than methotrexate.

Of the many cellular components of the inflammatory process, macrophages are known to play a critical role<sup>5</sup> where they contribute to antigen presentation and immunomodulation via the production of growth factors and activating cytokines such as TNF, IL-1, and IL-6. Of cell types present in rheumatoid synovium, macrophage numbers present in synovial biopsies provide the strongest correlation with clinical symptoms, including scores for knee pain.<sup>6</sup> The change in the number of these macrophages also correlates significantly with changes in the 28-joint count Disease Activity Score (DAS28) associated with disease therapy.<sup>7</sup> Synovial inflammation in RA is chronic and eventually organizes to form granulation tissue known as pannus, which is a highly invasive tissue that progressively erodes cartilage, bone, tendons, and ligaments and is associated with structural damage and irreversible loss of joint function. Moreover, pannus macrophages can differentiate to osteoclasts required for bone invasion. Therefore, the modulation of proliferation and activity of macrophages and osteoclasts is a potentially attractive approach for the treatment

**Received:** July 8, 2011

**Published:** October 31, 2011

Scheme 1<sup>a</sup>

<sup>a</sup>Reagents and conditions: (a)  $\text{Pd}(\text{PPh}_3)_4$ ,  $\text{LiCl}$ , 2 M  $\text{Na}_2\text{CO}_3$ , dioxane, 80 °C, 2 h. (b)  $\text{H}_2$ , 10%  $\text{Pd/C}$ , MeOH, 20 psi, 1 h. (c) NBS,  $\text{CH}_2\text{Cl}_2$ , room temperature, 10 h. (d)  $\text{Pd}(\text{PPh}_3)_4$ , 2 M  $\text{Na}_2\text{CO}_3$ , toluene, EtOH, 80 °C, 3 h. (e) EDCI, HOBt, DIEA,  $\text{CH}_2\text{Cl}_2$ , room temperature, 10 h. (f) TFA,  $\text{CH}_2\text{Cl}_2$ , room temperature, 1 h.

of RA, and as such, we became interested in one of the key signaling pathways for the macrophage lineage.

The colony-stimulating factor-1 receptor (CSF-1R) is alternatively known as FMS, that is, the product of the cellular proto-oncogene homologue of the feline McDonough sarcoma virus oncogene (v-fms). FMS is a member of the class III receptor tyrosine kinases that include FMS-like tyrosine kinase-3 (FLT-3), stem cell factor receptor (KIT), and platelet-derived growth factor receptors (PDGFR)  $\alpha$  and  $\beta$ . FMS is the exclusive cell-surface protein receptor for colony-stimulating factor-1 (CSF-1, or macrophage colony-stimulating factor, M-CSF),<sup>8</sup> which, upon binding to the extracellular domain of FMS, induces dimerization and trans-autophosphorylation of the intracellular FMS kinase domain on Tyr723 and other tyrosine residues. These phosphorylated sites subsequently act as binding sites for several cytoplasmic Src homology-2 (SH2) domain-containing signaling molecules, which promote de novo gene expression, proliferation, and differentiation. High expression of FMS is restricted to monocytes, tissue macrophages, oocytes, trophoblasts, and osteoclasts, and CSF-1 is the predominant growth factor for macrophages and macrophage-lineage cells including osteoclasts.

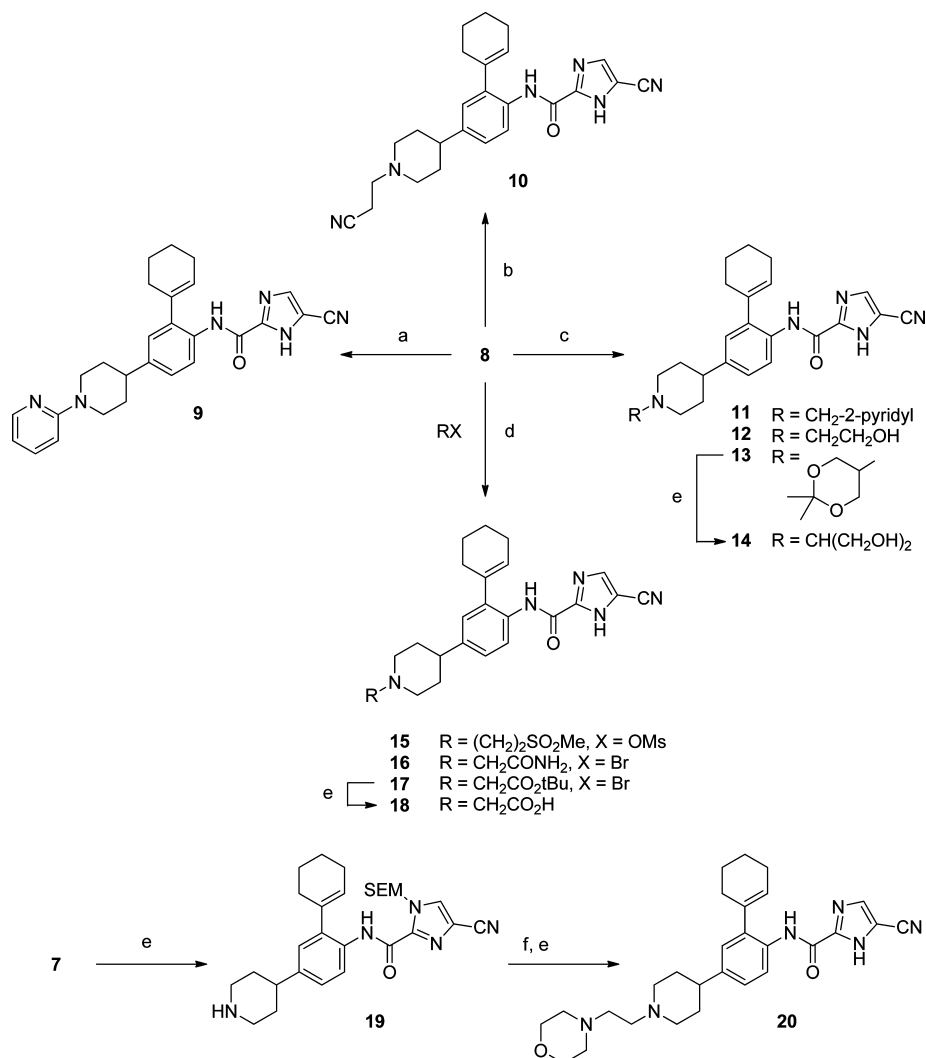
There is evidence that CSF-1 may drive the macrophage population in RA.<sup>9</sup> Although CSF-1 is expressed constitutively, expression is strongly induced in fibroblasts, endothelial cells, and chondrocytes by TNF and IL-1.<sup>10,11</sup> Endothelial cells from rheumatoid synovium express more CSF-1 than endothelial cells purified from other anatomical sites,<sup>12</sup> and CSF-1 levels are significantly elevated in rheumatoid plasma, synovium, and synovial fluid.<sup>13–15</sup> Furthermore, it has been shown that administered CSF-1 will exacerbate arthritis in rodents,<sup>16–18</sup> and CSF-1 deficient (op/op) mice were highly resistant to arthritis in a collagen-induced model.<sup>18</sup> Thus, it is expected that FMS inhibitors could intervene advantageously in diseases where osteoclasts and macrophages are pathogenic, particularly RA. In fact, in collagen-induced arthritis (CIA) models in

rodents, researchers have demonstrated decreases in overall progression of clinical scores, destruction of bone and cartilage, and macrophage numbers using specific oral FMS inhibitors,<sup>19–21</sup> as well as other nonspecific kinase inhibitors possessing known FMS inhibitory activity such as imatinib mesylate,<sup>22,23</sup> and also with CSF-1-specific antibodies.<sup>18</sup> FMS inhibitors may also find therapeutic applications for other immune-modulated inflammatory or remodeling diseases with high macrophage or osteoclast involvement, such as metastatic bone disease.<sup>24</sup>

## CHEMISTRY

The methodology for constructing the core structure of the compounds is outlined in Scheme 1. The synthesis commences with a Suzuki–Miyaura coupling<sup>25</sup> between the anilino boronic ester 1 and the enol triflate ester derivative of *N*-Boc-protected piperidinone 2.<sup>26</sup> After hydrogenation of the olefin, the resulting aniline 3 was brominated with *N*-bromosuccinimide (NBS) to give 4. This set up the next Suzuki–Miyaura coupling with 1-cyclohexeneboronic acid to afford the tricyclic aniline 5. The potassium salt of the trimethylsilylethoxymethyl (SEM)-protected imidazole-2-carboxylate 6 previously reported in these laboratories<sup>27</sup> is coupled to 5 using *N*-(3-dimethylaminopropyl)-*N'*-ethylcarbodiimide hydrochloride (EDCI), 1-hydroxybenzotriazole (HOBt), and *N,N*-diisopropylethylamine (DIEA) to provide amide 7. Simultaneous removal of both the Boc and the SEM groups with trifluoroacetic acid (TFA) afforded a common intermediate 8 that was widely employed for derivatizations of the piperidine ring.

Scheme 2 outlines the chemistry used to introduce the various *N*-alkyl and *N*-aryl substitutions on the piperidine nitrogen. Reaction of 8 with 2-fluoropyridine at 120 °C afforded the aminopyridine 9. Conjugate addition of 8 to acrylonitrile led to the cyanoethyl derivative 10. Reductive amination of the appropriate aldehyde or ketone with 8 in the presence of sodium triacetoxyborohydride was useful for the

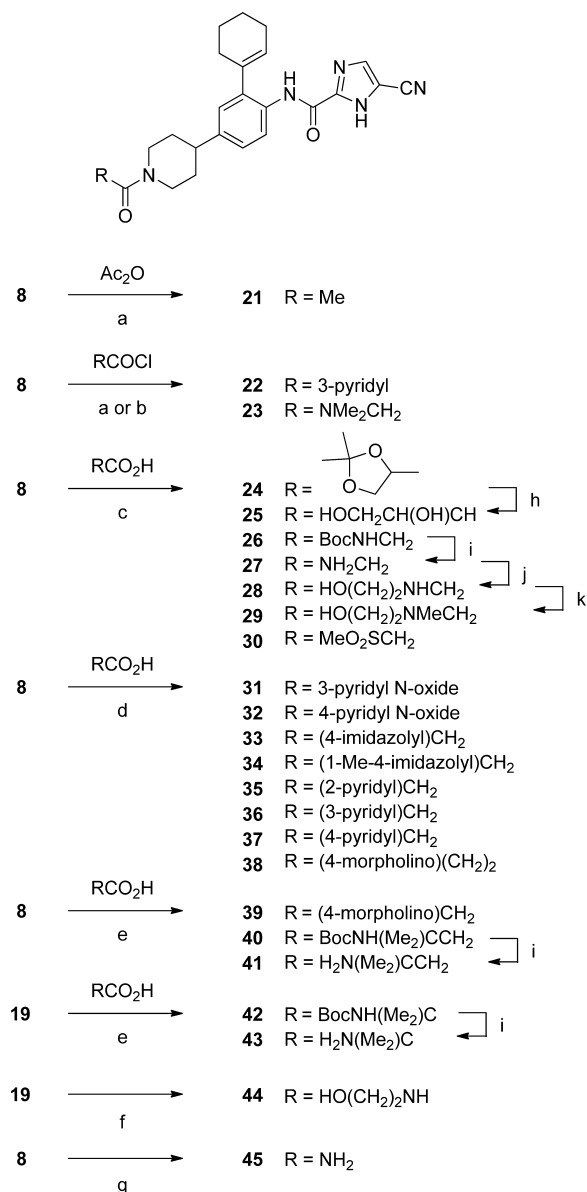
Scheme 2<sup>a</sup>

<sup>a</sup>Reagents and conditions: (a) 2-Fluoropyridine, DMA, 120 °C. (b) Acrylonitrile, Et<sub>3</sub>N, MeOH, DCE, 80 °C. (c) Aldehyde or ketone, NaBH(OAc)<sub>3</sub>, DIEA, 1,2-dichloroethane, room temperature. (d) DIEA, CH<sub>2</sub>Cl<sub>2</sub>, room temperature. (e) TFA, EtOH, CH<sub>2</sub>Cl<sub>2</sub>, 0 °C to room temperature. (f) 4-(2-Chloroethyl)morpholine HCl, NaI, DMA, 80 °C.

addition of a 2-pyridylmethyl group as on **11**, a hydroxyethyl group as on **12**, and, after deprotection of **13**, a 1,3-dihydroxy-2-propyl group as on **14**. Direct alkylation chemistry was also employed to produce a number of piperidines appended with a methylsulfonyl group as in **15**, a carbamylmethyl group as in **16**, and a carboxymethyl group, along with its corresponding *t*-butyl ester, as in compounds **18** and **17**, respectively. In some instances, protection of the imidazole was beneficial during reactions with the piperidine; thus, selective deprotection of the Boc group was effected by careful treatment of the doubly protected **7** with TFA in the presence of ethanol to afford **19**. Alkylation of **19** with 4-(2-chloroethyl)-morpholine in DMA at 80 °C followed by final acidic removal of the SEM group afforded the morpholinoethyl analogue **20**.

The numerous *N*-acyl analogues of the core structure were synthesized as shown in Scheme 3. Reaction of **8** with acetic anhydride afforded *N*-acetylpiperidine **21**. Acylation of **8** with the acid chlorides of nicotinic acid and *N,N*-dimethylglycine produced compounds **22** and **23**, respectively. The remainder of the analogues was synthesized by means of amide coupling chemistry with the corresponding carboxylic acids. Thus,

various derivatives, including *N*-acetyl derivatives substituted  $\alpha$  to the carbonyl with amino, methylsulfonyl, various pyridyl *N*-oxides, imidazoys, and pyridyls, were all made by reaction of the appropriate carboxylic acids and EDCI resulting in compounds **24**, **26**, and **30–38**. Hydrolysis of the ketal of **24** with aqueous HCl afforded 2,3-dihydroxypropionyl compound **25**. Deprotection of *N*-Boc-protected **28** with TFA followed by sodium triacetoxyborohydride and glyoxal gave *N*-hydroxyethylglycyl derivative **28**. Further treatment of **28** with sodium triacetoxyborohydride and formalin then gave the *N*-methyl analogue of **28**, compound **29**. Similarly, bromotripyrrolidino-phosphonium hexafluorophosphate (PyBrop) was used as the coupling agent in the production of the morpholinoacetyl analogue **39**, the *N*-Boc-protected amine **40**, as well as compound **42**, where SEM-protected compound **19** was the precursor. Removal of the Boc group in **40** and simultaneous removal of both the Boc and the SEM groups in **42** with TFA yielded the final compounds **41** and **43**, respectively. When intermediate **19** was treated with triphosgene followed by 2-aminoethanol and then deprotected as before, *N*-(2-hydroxyethyl)urea **44** was produced. Finally, the unsubstituted

Scheme 3<sup>a</sup>

<sup>a</sup>Reagents and conditions: (a) Et<sub>3</sub>N, CH<sub>2</sub>Cl<sub>2</sub>, room temperature. (b) DIEA, CH<sub>2</sub>Cl<sub>2</sub>, room temperature. (c) EDCl, HOBt, DIEA or Et<sub>3</sub>N, CH<sub>2</sub>Cl<sub>2</sub>, room temperature. (d) EDCl, HOBt, DIEA, DMF, room temperature. (e) PyBrop, DIEA, CH<sub>2</sub>Cl<sub>2</sub>, room temperature. (f) Triphosgene, DIEA, H<sub>2</sub>N(CH<sub>2</sub>)<sub>2</sub>OH, CH<sub>2</sub>Cl<sub>2</sub>, -78 °C, then TFA, EtOH, CH<sub>2</sub>Cl<sub>2</sub>, room temperature. (g) TMS-NCO, Et<sub>3</sub>N, CH<sub>2</sub>Cl<sub>2</sub>, room temperature. (h) 2 M HCl, MeOH–H<sub>2</sub>O, room temperature. (i) TFA, EtOH, CH<sub>2</sub>Cl<sub>2</sub>, room temperature. (j) Na(OAc)<sub>3</sub>BH, glyoxal, CH<sub>2</sub>Cl<sub>2</sub>, room temperature. (k) Na(OAc)<sub>3</sub>BH, CH<sub>2</sub>O, MeOH, room temperature.

urea **45** was derived by treatment of **8** with trimethylsilyliso-cyanate followed by hydrolysis during aqueous purification by reverse HPLC.

## RESULTS AND DISCUSSION

We embarked on this discovery program with a focused screening effort within our chemical library collection. This endeavor resulted in three promising chemical classes: a series of quinolones<sup>28</sup> and pyrimidinopyridones,<sup>20</sup> both of which have been reported previously, and, the subject of this article, a series

of arylamides as represented by **46** in Figure 1. It seemed evident from the initial collection of screening hits that an *ortho*-aminophenyl heteroarylcarboxamide comprised the basic pharmacophore of this series. Subsequent hit-to-lead efforts<sup>29</sup> resulted in significant improvements in binding affinity as in, for example, **47**, and eventually resulted in an initial lead compound **48**. This compound, in addition to improved druglike properties, also stabilized the crystal packing of an engineered chimeric form of the FMS kinase domain, thereby providing our first crystallographic information on the binding mode of this interesting new series<sup>30</sup> and supplying us with an avenue to rapid structure-based optimization.

Further optimization studies and investigation of the structure–activity relationship (SAR) produced proof-of-concept compounds, for example, furans and pyrroles **49–52**, of excellent potency (Figure 1),<sup>31</sup> which permitted confirmation of in vivo efficacy for this class of compounds. Compound **52**, for example, in addition to possessing subnanomolar potency, displayed a very favorable pharmacokinetic profile and demonstrated significant efficacy in a collagen-induced model of arthritis in mice at doses as low as 5 mg/kg po BID. Histological evaluation of the tissues was consistent with the reductions in arthritis clinical scores, revealing that this agent reduced pannus invasion as well as destruction of both bone and cartilage, competitive in degree to that seen with biological anti-TNF agents in similar models. Moreover, the significant reductions in the number of macrophages in the joints of **52**-treated mice were consistent with both the observed macroscopic results and the hypothesized mechanism of action for these agents, viz., FMS inhibition.

Despite these promising data, it was important to remain mindful of the latent liability of a 1,2,4-phenylenetriamine core structure, possessed by these proof-of-concept compounds, to undergo possible in vivo oxidation to form reactive quinonediimine metabolites. Such reactive species could potentially haptenize proteins as well as deplete glutathione concentrations, culminating in tissue damage via an idiosyncratic drug reaction (IDR).<sup>32</sup> In this respect, in vitro glutathione conjugation assays<sup>33</sup> partly corroborated this prospective risk.

Hoping to circumvent this anticipated liability and armed with the knowledge of the binding mode of this class from X-ray studies, a focused structure-based design effort was initiated to replace two of the three nitrogen substituents on the benzene core to derive the 2- and 4-substituted carbon-based analogues.<sup>34</sup> Although the challenge of instituting such major structural changes was recognized with regard to maintaining potency and good pharmacological properties, it was deemed necessary to ensure the long-term safety characteristics for a drug candidate.

The SAR at the 4-position proved tolerant to replacement of the piperazine with a range of lipophilic rings and substituents (data not shown) where the direct replacement of a piperazine with a 4-piperidine resulted in derivatives, such as **53**, with no loss in potency. This was consistent with structural evidence indicating that substituents at the 4-position have close contact with a lipophilic region of the protein proximal to the attachment point at the benzene ring. The region more distal to the attachment point is largely directed out into solvent and is therefore open for more variation.

Unlike the 4-position, the SAR surrounding the 2-position revealed that a piperidine group was very specific in its steric and conformational requirements. Hence, the best carbocyclic analogue that could be obtained for the piperidine, a

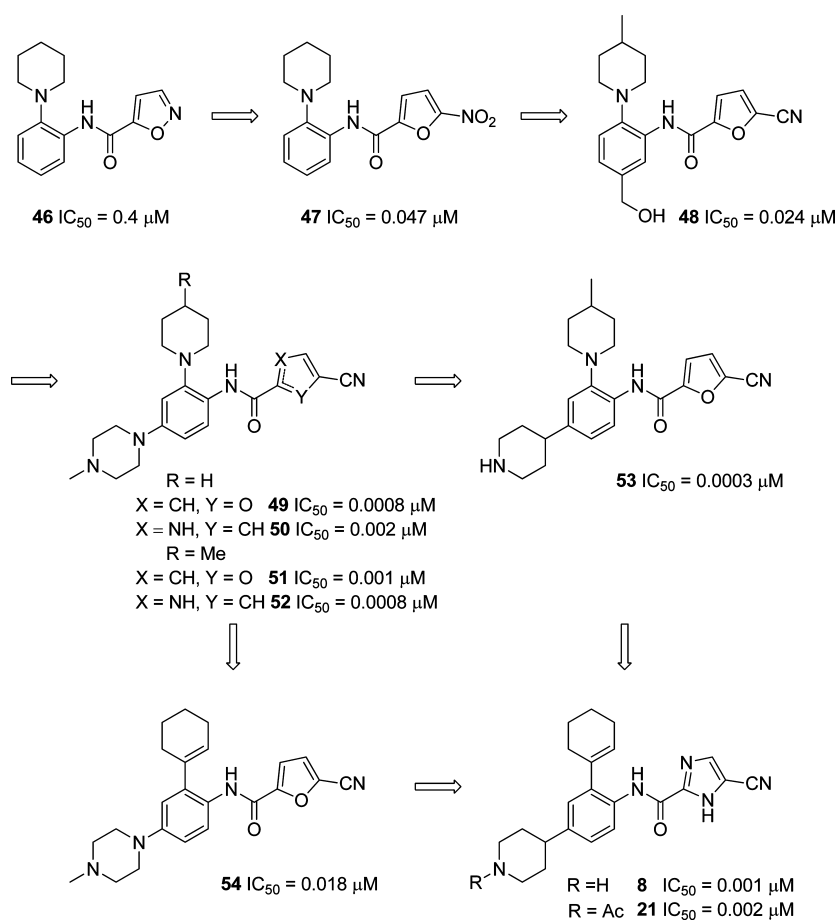


Figure 1.

1-cyclohexenyl group, resulted in an unavoidable 20–30-fold erosion of the potency as illustrated by **54**. Ultimately, this significant loss of potency was mitigated by further optimization of the terminal acyl heterocycle.

It was hypothesized through modeling that the equipotent nature of cyanofurans and cyanopyrroles in this acyl heterocyclic location was a result of two different hydrogen-bonding scenarios. An intramolecular hydrogen bond was thought to form between the amide NH and the furan oxygen, which assisted in holding the inhibitor in the conformation required for binding. This hydrogen bond was confirmed in the now-available X-ray cocrystal structure (PDB ID: 3KRL) of **49**<sup>35</sup> in FMS as shown in Figure 2A. In the contrasting case of the pyrrole **50**<sup>35</sup> modeled into FMS (Figure 2B), the internal hydrogen bond cannot form. However, the anticipated reduction in binding affinity from the loss of this interaction was not observed. This appears to have been the result of an alternate intermolecular hydrogen bond that can form between the pyrrole NH and the carbonyl of Glu664, which, from modeling, would exist where the dashed line in Figure 2B is placed. Using this information, it was possible to combine the individually advantageous hydrogen-bonding characteristics of the two heterocycles. The result was the corresponding class of cyanoimidazoles, for example, **8** and **21**, which show approximately 10-fold improvement in affinity over either the furan or the pyrrole analogues compensating for the loss induced by replacement of the piperidine in the 2-position with the suboptimally potent 1-cyclohexenyl group. A cocrystal structure of **8** in FMS (PDB ID: 3KRJ), also reported here for

the first time and shown in Figure 2C, confirmed the hypothesis for increased potency where the two complementary internal and external hydrogen bonds were unmistakably present.

As shown in Table 1, these molecules also demonstrated low nanomolar potency in a cellular assay that measured the ability of compounds to inhibit the proliferation of murine bone marrow-derived macrophages (BMDM).<sup>20</sup> More importantly, these compounds did not show the potential for reactive metabolite formation as gauged by the glutathione conjugation assay previously described.<sup>33</sup>

Secure in the knowledge that these were potent inhibitors, which were less likely to present an IDR liability, we investigated the pharmacokinetic (PK) and pharmacodynamic (PD) properties of **8** and **21**. A PD assay in mice<sup>20,24</sup> was developed based on the ability of CSF-1 to induce the expression of *c-fos* mRNA in macrophages.<sup>39</sup> Tail-vein injection of CSF-1 caused an increase in *c-fos* mRNA concentrations of more than 10-fold in the spleen within 15 min but returned toward baseline by 30 min. The CSF-1-induced expression of *c-fos* was dose-dependent and specific as it was blocked completely in mice predosed with a neutralizing antibody to CSF-1.<sup>24</sup> Table 2 shows the PD effect of compounds **8**, **21**, and the earlier proof-of-concept compound **51**, at a time of 8 h following an oral dose of 50 mg/kg. This PD assay was used routinely throughout the program. With initial assessment at relatively high doses, compounds were often triaged on the basis of the presence or absence of robust (80–100%) inhibition of *c-fos* induction. Thus, the 70% inhibition of



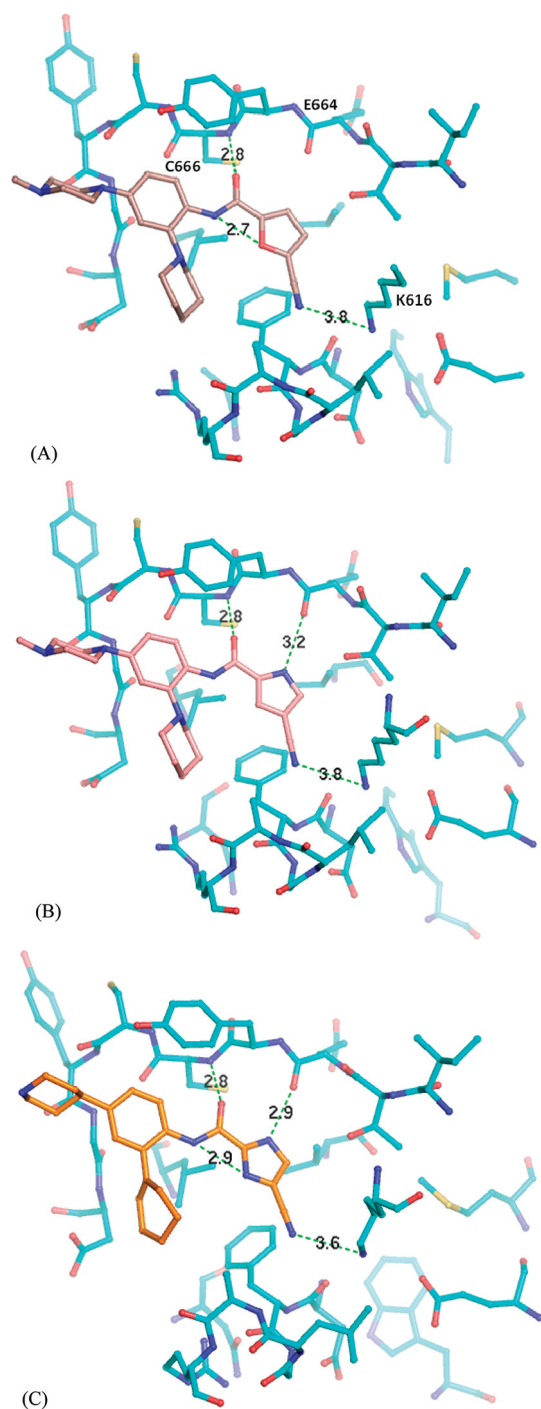


**Figure 2.** (A) Crystal structure of FMS, cyan carbons, with furan-containing compound **49**, brown carbons (PDB ID: 3KRL).<sup>36</sup> (B) Model of FMS, cyan carbons, with pyrrole-containing compound **50**, salmon carbons. (C) Crystal structure of FMS, cyan carbons, with imidazole-containing compound **8**, orange carbons (PDB ID: 3KRJ).<sup>37</sup> Hydrogen bonds between the inhibitor and FMS and the inhibitor intramolecular hydrogen bonds are shown as green dashed lines. The figures were prepared with PyMol.<sup>38</sup>

compound **8** and the 24% inhibition of compound **21** fell short of this criterion, while compound **51**, by comparison, which had excellent oral efficacy in a mouse CIA model,<sup>31</sup> had strong inhibition (96%) even at a dose that is significantly lower (20 mg/kg) than for either of the two candidates **8** and **21**. Table 2 also presents some of the PK properties of **8** and **21**. In mice,

**Table 1.** FMS and Cell Potency and Potential for Reactive Metabolite Formation of Early Leads **8** and **21**

compd	R	mean IC <sub>50</sub> (nM)		
		FMS	BMDM assay	glutathione conjugation <sup>a</sup>
<b>8</b>	H	1.1 ( <i>n</i> = 31)	7.2 ( <i>n</i> = 5)	no
<b>21</b>	Ac	2.4 ( <i>n</i> = 2)	5.6 ( <i>n</i> = 2)	no

<sup>a</sup>The test compound at 20 or 40  $\mu$ M was incubated with NADPH (1 mM), GSH (5 mM) in PBS (0.1 mM), and 1 mg/mL of mouse liver microsomes at 37 °C for 1 h. The products were then analyzed by LC/MS for the glutathione conjugate of the parent (P + GSH), the amide bond cleavage product (ACP + GSH), and their fragments.

the oral exposures of **51** at 4 and 8 h postdose were robust as compared to **8** and **21** and provided the apparent explanation of the superior PD activity. The superior exposures were largely a consequence of the good oral bioavailability of **51** vs the poor oral bioavailability of **8** and **21**. All three compounds exhibited moderate to high clearance relative to liver blood flow, together with moderate to high volumes of distribution. It seemed apparent from these results, in particular the failure of both **8** and **21** to attain adequate bioavailability, that the early evaluation of the in vivo properties of subsequent candidates would be essential for the rapid progression of this program.

To investigate the potential for side effects, **8** and **21** at 10  $\mu$ M were examined in a battery of 50 counterscreen assays<sup>40</sup> for activity against a wide variety of receptors, transporters, and ion channels. Compound **8** hit nine targets with greater than 50% inhibition of specific control ligand binding, whereas **21** gave greater than 50% inhibition at only three targets. It is not uncommon to see significant levels of off-target binding with relatively basic compounds such as piperidine **8** (calculated  $pK_a = 10.2 \pm 0.1$ ).<sup>41</sup> Many groups have investigated the target promiscuity of compounds as a function of their basicity and, in general, it seems clear that increased basicity as well as the potential for a positive charge at physiological pH are strong contributors to off-target activity.<sup>42</sup>

Of particular concern was that higher levels of binding at ion channels, in particular sodium<sup>43</sup> and calcium ion channels,<sup>44</sup> for basic compounds may lead to an increased risk of adverse cardiovascular effects. Indeed, it was demonstrated<sup>45</sup> that the highly basic compound **8** inhibited Ca<sup>2+</sup> channel, L, reference compound binding by 91% and Na<sup>+</sup> channel, site 2 reference compound binding by 96% at 10  $\mu$ M, and had somewhat greater undesirable effects in a guinea pig right atrium assay than the less basic amide derivative **21**, which inhibited Ca<sup>2+</sup> channel and Na<sup>+</sup> channel binding by 46 and 27%, respectively. The strategy of reducing the basicity of compounds to mitigate off-target ion channel effects has been used for calcium and sodium channels<sup>46</sup> and for potassium channels such as human ether-a-go-go-related gene potassium channel (hERG).<sup>47</sup> Thus, we hypothesized that moderating the basicity of future analogues would be beneficial and, so, the majority of analogues in this paper were selected with that concept in mind.

Leads also were optimized against a battery of in vitro tests for ADMET properties including the in vitro metabolic stability in human and rodent liver microsomes as a means to separate out compounds that may not withstand first-pass metabolism. A compound stability of at least 70% remaining after a 10 min exposure to the microsomal mixture was preferred. In addition, in vitro assays for inhibition of recombinant cytochrome P450 (CYP) enzymes provided a means to predict future problems with drug–drug interactions,<sup>48</sup> and we routinely monitored

Table 2. PK and PD Data for Compounds **8**, **21**, and **51**

compd	PD (po)	PK (iv) <sup>b</sup>			PK (po) <sup>c</sup>						
	c-fos assay (% inhib at 8 h <sup>a</sup> )	t <sub>1/2</sub> (h)	V <sub>z</sub> (L/kg)	Cl (mL/min/kg)	t <sub>1/2</sub> (h)	F (%)	T <sub>max</sub> (h)	C <sub>max</sub> (ng/mL)	AUC <sub>last</sub> (min ng/mL)	concn at 4 h (ng/mL)	concn at 8 h (ng/mL)
8	70 (50 mg/kg)	7.2	32	52	2.0	12	0.25	50	5715	7	BLQ <sup>d</sup>
21	24 (50 mg/kg)	1.2	2.8	27	1.9	15	0.5	209	27218	54	9
51 <sup>e</sup>	96 (20 mg/kg)	3.0	12.3	46	3.1	75	0.5–4.0	285	69711	183	64

<sup>a</sup>See the text for details of PD assay. <sup>b</sup>Compounds **8** and **51** administered in 20% HPβCD (pH 2 by HCl) at 0.5 mg/kg iv and 5 mg/kg po.

<sup>c</sup>Compound **21** administered in 20% DMSO/80% PEG400 at 0.5 mg/kg iv and in 1% Tween 80/0.5% hydroxypropylmethylcellulose at 5 mg/kg po.

<sup>d</sup>Below the limit of quantitation. <sup>e</sup>PK values for **51** are the mean of multiple studies (*n* = 4).

four of the CYP enzyme subtypes (CYP1A2, CYP2C9, CYP2C19, and CYP3A4) responsible for metabolism of a majority of drugs.<sup>49</sup> IC<sub>50</sub> values below 3 μM were considered suspect requiring follow-up in secondary assays, and values below 1 μM can often prove problematic.

As mentioned above, many of the derivatives for this optimization process were selected to modulate the basicity of the piperidine nitrogen. The predictable effects on basicity of various electron-withdrawing groups, electronegative heteroatoms, and heteroaryl rings placed two to three bonds away from an amine nitrogen are well-documented,<sup>50</sup> and selections based on these principles resulted in a group of *N*-alkyl and *N*-aryl piperidines (compounds **9**–**20**). The data for these analogues are displayed in Table 3 where the unsubstituted piperidine lead **8** is included as a reference.

As a first screening criterion, we sought compounds with an IC<sub>50</sub> potency better than 15 nM in the cellular BMDM proliferation assay based on experience that compounds with higher values often did not exhibit PD activity at reasonable (<50 mg/kg) doses. In general, the data in the tables are formatted in bold when they met the criteria as discussed above for a particular assay. Thus, bolded values for all assay results within a given row indicate compounds of greater interest for secondary studies.

It is immediately apparent that this entire group of compounds displayed good in vitro stability in the presence of both human and mouse liver microsomal preparations. It is possible that the additional functionality present on the various *N*-alkyl groups prevents metabolism commonly observed with simpler *N*-alkyl groups. In vitro potency in the FMS enzyme assay was also excellent with the only exception being the 2-pyridylpiperidine **9** (IC<sub>50</sub> = 22 nM), which was further compromised by significant inhibition of CYP3A4 (IC<sub>50</sub> = 1.7 μM). Of the remaining candidates, the highest IC<sub>50</sub> values in the group did not exceed 2.4 nM.

In the cellular BMDM assay, only two compounds (**14** and **18**) failed to give IC<sub>50</sub> values below 15 nM. In the case of the carboxymethyl derivative **18**, the low p*K*<sub>a</sub> expected for an amino acid of this type likely resulted in insufficient concentration of the free acid at physiological pH to provide adequate cell membrane penetration.

The values for inhibition of the four cytochrome P450 enzymes assayed also did not strongly rule out any additional compounds. A number of the compounds were also tested for inhibition of [<sup>3</sup>H]-astemizole binding at the hERG potassium channel as a predictor for compounds that may prolong cardiac action potential duration, potentially resulting in long QT

syndrome.<sup>51</sup> None of the compounds tested gave results that merited concern. Thus, the six compounds from the *N*-alkylpiperidine analogues with the greatest cell potency (**10**–**12**, **15**, **16**, and **20**) were selected for further evaluation.

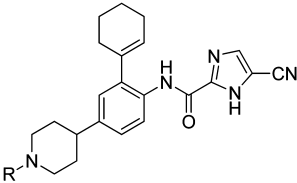
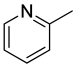
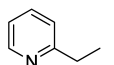
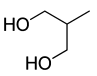
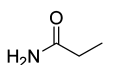
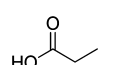
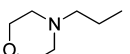
Data for the corresponding collection of *N*-acylpiperidine derivatives (compounds **22**–**45**) are displayed in Table 4. Because acylation of the piperidine to give nonbasic amides could potentially impact the solubility, some acyl groups were selected that still contained amines to retain a solubilizing feature. As discussed above, however, the proximity of the added amine to the acyl carbonyl or other heteroatoms was maintained to modulate the p*K*<sub>a</sub> and limit ion-channel and other off-target activity. As before, one of the early leads, *N*-acetyl piperidine **21**, is included as an *N*-acyl reference for this group.

All compounds in this series also exhibited excellent in vitro potency in the FMS enzyme assay with no IC<sub>50</sub> values exceeding 3.8 nM. Five compounds were discarded based on relatively modest cellular potency, viz., the isonicotinic amide *N*-oxide **32**, the 4-imidazolyl amides **33** and **34**, the aminoalkylamide **41**, and the primary urea **45**. Additionally, the 4-imidazolyl amides, **33** and **34**, showed greater CYP inhibition with **33** being a particularly potent inhibitor of CYP2C9 and CYP2C19. With regard to the relatively weak cellular potency of **41**, one may postulate that the more strongly basic nature of the α-branched amine results in a more charged species at physiological pH that does not pass easily through cell membranes, whereas, by comparison, the closer proximity of the amino group to the carbonyl in **43** attenuates the p*K*<sub>a</sub> such that **43** does not suffer the same fate and retains good cellular activity.

When the remaining 14 candidates were subsequently incubated in the presence of liver microsomes, a significant number demonstrated less-than-desirable stability. All of the pyridylmethyl amides, **35**–**37**, were very unstable in both species. In addition, nicotinic amide **22**, the two hydroxyethylaminomethyl amides **28** and **29**, both morpholinoalkyl amides **38** and **39**, as well as the hydroxyethylurea **44** all suffered varying degrees of reduced stability in the presence of one or both species of microsomes, which did meet our threshold for desired stability. Nicotinic amide **22** also displayed submicromolar inhibition of CYP2C9.

Finally, of the remaining five most potent and stable derivatives within this group, nicotinic amide *N*-oxide **31** and aminoalkylamide **43** showed low micromolar CYP inhibition. More importantly, the *N*-oxide **31**, despite its apparent in vitro microsomal stability, also carried the liability that any in vivo

Table 3. FMS and Cell Potency and Early ADMET Properties of *N*-Alkyl/*N*-Aryl Piperidines<sup>a</sup>

										
Cmpd	R	FMS IC <sub>50</sub> (nM)	BMDM Assay IC <sub>50</sub> (nM)	Liver Micros Stability (% remaining at 10 min)		CYP450 IC <sub>50</sub> (μM)				hERG IC <sub>50</sub> (μM)
				Human	Mouse	1A2	2C9	2C19	3A4	
8	H	<b>1.1</b>	<b>7.2</b>	<b>100</b>	<b>96</b>	<b>&gt;10</b>	<b>4.1</b>	<b>&gt;10</b>	<b>&gt;10</b>	<b>&gt;10</b>
9		22	na <sup>b</sup>	77	77	na	<b>&gt;10</b>	3.7	1.7	na
10	NC-CH <sub>2</sub> -CH <sub>2</sub> -CH <sub>3</sub>	<b>1.8</b>	<b>11</b>	<b>100</b>	<b>93</b>	na	<b>&gt;10</b>	<b>&gt;10</b>	na	na
11		<b>2.4</b>	<b>4.9</b>	<b>75</b>	<b>79</b>	<b>&gt;10</b>	<b>&gt;10</b>	<b>&gt;10</b>	<b>5.6</b>	<b>7.7</b>
12	HO-CH <sub>2</sub> -CH <sub>2</sub> -CH <sub>3</sub>	<b>1.1</b>	<b>4.7</b>	<b>100</b>	<b>89</b>	na	<b>&gt;10</b>	<b>&gt;10</b>	<b>&gt;10</b>	<b>&gt;10</b>
14		<b>1.6</b>	21	<b>100</b>	<b>94</b>	na	na	na	na	na
15	MeO <sub>2</sub> S-CH <sub>2</sub> -CH <sub>2</sub> -CH <sub>3</sub>	<b>1.5</b>	<b>3.1</b>	<b>94</b>	<b>98</b>	<b>&gt;10</b>	<b>&gt;10</b>	<b>&gt;10</b>	<b>&gt;10</b>	<b>&gt;10</b>
16		<b>1.4</b>	<b>11</b>	<b>81</b>	<b>79</b>	<b>&gt;10</b>	<b>&gt;10</b>	<b>&gt;10</b>	<b>&gt;10</b>	na
18		<b>1.3</b>	>500	<b>98</b>	<b>70</b>	na	na	na	na	na
20		<b>1.1</b>	<b>3.2</b>	<b>77</b>	<b>96</b>	<b>&gt;10</b>	<b>&gt;10</b>	<b>&gt;10</b>	<b>3.8</b>	<b>&gt;10</b>

<sup>a</sup>For comparative purposes, data in the table are formatted in bold when they met desired subjective criteria (FMS IC<sub>50</sub> < 10 nM (bolded but not used as a selection criterion), BMDM IC<sub>50</sub> < 15 nM, liver microsomal stability 70–100%, CYP450 IC<sub>50</sub> > 3 μM, and hERG IC<sub>50</sub> > 3.2 μM). <sup>b</sup>na, not assayed.

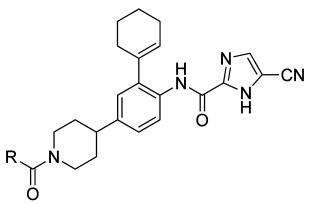
metabolic loss of the *N*-oxide would result in the formation of the potent CYP2C9 inhibitor **22**, a concern that also removed it from further consideration. Again, of the compounds tested for inhibition of binding of astemizole to hERG, none appeared to have a hERG liability. The remaining compounds appeared quite promising in their profile. Unfortunately, the attrition of compounds from this group of *N*-acyl derivatives shown in Table 4 was significantly greater than from the *N*-alkyl and *N*-aryl compounds shown in Table 3, resulting in only three analogues (**23**, **25**, and **30**) for advancement to further studies.

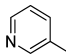
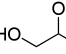
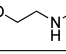
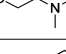
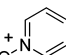
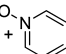
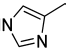
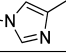
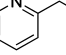
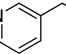
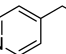
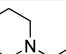
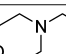
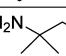
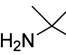
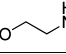
At this stage, there remained a collection of nine promising candidates from Tables 3 and 4, and it was clear from the shortcomings of **8** and **21** that an early assessment of in vivo efficacy would be useful for the most efficient selection of improved candidates. Because the activity in the PD model was presumably an integrated function of potency and tissue

exposure, the performance in the PD model was deemed the most efficient way to prioritize compounds for further advancement. However, the resource-intensive nature of this assay at multiple doses and time points required an abbreviated approach be used to screen this collection. Therefore, the top candidates were investigated in this model initially at a single dose of 50 mg/kg and at a time of 8 h after oral administration.

The results of these PD screening studies are presented in Table 5. Of the nine compounds, two (**11** and **25**) were not tested. After Cerep counterscreening for other activities, compound **11** demonstrated greater than 50% inhibition against 12 targets at 10 μM, and compound **25**, as a chiral compound, was also excluded. Lead compounds **8** and **21** are included again in this table for reference. To ensure that the in vitro screens based on cellular activity and microsomal stability were not excluding potentially useful compounds, a selection of



Table 4. FMS and Cell Potency and Early ADMET Properties of *N*-Acyl Piperidines<sup>a</sup>


Cmpd	R	FMS IC <sub>50</sub> (nM)	BMDM Assay IC <sub>50</sub> (nM)	Liver Micros Stability (% remaining at 10 min)		CYP450 IC <sub>50</sub> (μM)				hERG IC <sub>50</sub> (μM) <sup>d</sup>
				Human	Mouse	1A2	2C9	2C19	3A4	
21	Me	<b>2.4</b>	<b>5.6</b>	<b>95</b>	<b>86</b>	<b>&gt;10</b>	<b>&gt;10</b>	<b>9.2</b>	<b>&gt;10</b>	<b>&gt;3.2</b>
22		2.7	<b>4.4</b>	56	<b>66</b>	na <sup>b</sup>	0.54	<b>5.5</b>	<b>6.1</b>	<b>&gt;10</b>
23	Me <sub>2</sub> N	<b>0.69</b>	<b>2.6</b>	<b>87</b>	<b>81</b>	<b>&gt;10</b>	<b>&gt;10</b>	<b>&gt;10</b>	<b>4.8</b>	<b>&gt;10</b>
25		1.2	<b>2.3</b>	<b>89</b>	<b>100</b>	<b>&gt;10</b>	<b>&gt;10</b>	<b>9.8</b>	<b>8.2</b>	na
28		<b>0.83</b>	<b>4.4</b>	67	<b>79</b>	<b>&gt;10</b>	na	7.7	<b>5.1</b>	na
29		1.0	<b>0.64</b>	69	60	<b>&gt;10</b>	na	<b>&gt;10</b>	<b>6.7</b>	<b>&gt;10</b>
30	MeO <sub>2</sub> S	<b>2.6</b>	<b>6.8</b>	<b>100</b>	<b>86</b>	na <sup>c</sup>	na <sup>c</sup>	na <sup>c</sup>	na <sup>c</sup>	<b>&gt;10</b>
31		<b>1.4</b>	<b>9.5</b>	<b>100</b>	<b>89</b>	<b>&gt;10</b>	na	na	1.9	na
32		<b>1.3</b>	18	<b>100</b>	<b>92</b>	na	<b>&gt;10</b>	na	<b>&gt;10</b>	na
33		<b>1.1</b>	49	<b>89</b>	<b>100</b>	na	0.33	0.81	na	na
34		<b>1.6</b>	23	<b>82</b>	<b>90</b>	<b>&gt;10</b>	na	na	2.3	<b>&gt;10</b>
35		<b>2.5</b>	<b>13</b>	34	37	<b>&gt;10</b>	na	na	1.5	na
36		<b>1.7</b>	<b>3.1</b>	<b>28</b>	<b>21</b>	na	na	na	na	<b>&gt;10</b>
37		<b>1.3</b>	<b>4.7</b>	11	24	<b>&gt;10</b>	<b>&gt;10</b>	2.9	1.0	<b>&gt;3.2</b>
38		<b>1.7</b>	<b>3.2</b>	57	23	na	<b>&gt;10</b>	<b>9.1</b>	na	na
39		<b>3.8</b>	<b>6.4</b>	66	23	<b>&gt;10</b>	<b>&gt;10</b>	<b>4.3</b>	1.8	<b>&gt;10</b>
41		<b>0.62</b>	22	na	na	na	na	na	na	na
43		<b>1.3</b>	<b>4.0</b>	<b>94</b>	<b>93</b>	<b>&gt;10</b>	<b>&gt;10</b>	2.2	<b>&gt;10</b>	<b>&gt;10</b>
44		<b>0.70</b>	<b>13</b>	<b>80</b>	61	<b>&gt;10</b>	<b>&gt;10</b>	<b>&gt;10</b>	<b>6.4</b>	<b>&gt;10</b>
45	NH <sub>2</sub>	<b>3.3</b>	25	<b>78</b>	<b>70</b>	na	na	na	na	na

<sup>a</sup>For comparative purposes, data in the table are formatted in bold when they met desired subjective criteria (FMS IC<sub>50</sub> < 10 nM (bolded but not used as a selection criterion), BMDM IC<sub>50</sub> < 15 nM, liver microsomal stability 70–100%, CYP450 IC<sub>50</sub> > 3 μM, and hERG IC<sub>50</sub> > 3.2 μM). <sup>b</sup>na, not assayed. <sup>c</sup>Insufficient solubility in PBS to determine. <sup>d</sup>On different occasions, hERG assays were run with a maximum concentration that limited the determination of IC<sub>50</sub> values to either 3.2 or 10 μM.

compounds that did not meet the cutoff criteria were also added as controls. These included **35–37** and **44**, which had excellent cellular potency for inhibition of BMDM proliferation but which had marginal to poor stability in mouse liver microsomes. Also added as a control was **34**, which, by contrast,

had good mouse microsomal stability but poor cellular BMDM activity.

The negative control compounds **34–37** and **44** gave little or no PD response, as expected. Also, the seven top primary screen candidates did not all perform equally well in this screen.

Table 5. PD, PK, and Solubility Properties of Selected Compounds

compd	PD assay % inhibition at 8 h <sup>a</sup> (50 mpk po)	PK parameters <sup>b,d</sup>							solubility in PBS (μM)
		iv			po				
		<i>t</i> <sub>1/2</sub> (h)	Vz (L/kg)	Cl (mL/min/kg)	<i>t</i> <sub>1/2</sub> (h)	C <sub>max</sub> (ng/mL)	AUC <sub>last</sub> (min ng/mL)	% F	
8	70	7.16	32	51.7	2.00	50	5715	12	38.8
21	24	1.21 <sup>c</sup>	2.84 <sup>c</sup>	27.0 <sup>c</sup>	1.88 <sup>c</sup>	209 <sup>c</sup>	27218	15 <sup>c</sup>	26.1
10	28	na	na	na	na	na	na	na	11.8
12	76	na	na	na	na	na	na	na	>40
15	88–93	1.44	3.84	30.7	1.55	866	127845	88	4.2
16	<51	1.39	6.43	53.3	0.88	55	8445	9.8	28.6
20	86	0.23	8.99	46.6	2.37	461	93173	101	25.9
23	88–100	1.36	7.11	60.6	2.33	296	61365	83	37.3
30	33	1.20 <sup>c</sup>	1.58 <sup>c</sup>	23.9 <sup>c</sup>	1.55 <sup>c</sup>	24 <sup>c</sup>	7500	2.3 <sup>c</sup>	0.91
34	13	0.54	3.85	81.8	0.40	81	6075	13	36.7
35	36	na	na	na	na	na	na	na	1.6
36	0	na	na	na	na	na	na	na	10.4
37	0	0.41	7.27	205	0.23	118	4080	18	0.39
44	23	2.41	10.3	49.2	1.63	24	7740	9.3	8.2

<sup>a</sup>PD model in B6C3F1 mice with all compounds administered po in 20% HP $\beta$ CD (see the details in the Experimental Section). <sup>b</sup>PK studies in 30–40 g male CD-1 mice. All compounds administered in 20% HP $\beta$ CD (pH 2 by HCl) at 0.5 mg/kg iv and 5 mg/kg po except where indicated otherwise. <sup>c</sup>Compounds administered in 20% DMSO/80% PEG400 at 0.5 mg/kg iv and in 1% Tween 80/0.5% hydroxypropyl- methylcellulose at 5 mg/kg po. <sup>d</sup>na, not assayed.

Table 6. Kinase Inhibition by 23

kinases inhibited more than 50% by 0.1 $\mu$ M 23	kinases not inhibited 50% by 0.1 $\mu$ M 23 but more than 50% by 1 $\mu$ M 23	kinases not inhibited 50% by 1 $\mu$ M 23
FMS, FLT3, KIT, AXL, TRKA, and LCK	ALK, BLK, BMX, FES, FGR, FYN, PDGFRA, PDGFRB, TRKB, and YES	Abl1, Akt1, Akt2, Akt3, Arg, Brk, BTKC, aMKII- $\alpha$ , CHK1, CHK2, CK2- $\alpha$ 1, MET, Csk, EGFR, EphA3, EphB4, ERK1, ERK2, FGFR1, FGFR2, FGFR3, FGFR4, GSK3- $\beta$ , Hck, Hyl, IGF1R, IRAK4, Lyn A, Lyn B, MAPKAP-K2, MAPKAP-K3, MAPKAP-K5, NEK2, PHKG2, PKA, PKC ( $\alpha$ , $\beta$ I, $\beta$ II, $\delta$ , $\epsilon$ , $\eta$ , $\gamma$ , $\iota$ , $\theta$ , $\zeta$ ), RSK2, Src, AMPK, Aurora-A, CaMKIV, CDK/cyclinB, CDK2/cyclinA, CDK2/cyclinE, CDK3/cyclinE, CDK5/p35, CDK6/cyclinD3, CDK7/cyclinH, CK1, CK1d, c-RAF, CSK, EphB2, IKK $\alpha$ , IKK $\beta$ , IR, JNK1 $\alpha$ 1, JNK $\alpha$ 2, JNK3, MAPK1, MAPK2, MEK1, MKK4, MKK6, MKK7b, MSK1, MST2, NEK2, p70S6K, PAK2, PAR-1Ba, PDK1, PKB $\alpha$ , PKB $\beta$ , PKBy, PRAK, PRK2, ROCK-II, Ros, Rsk1, Rsk3, SAPK2a, SAPK2b, SAPK3, SAPK4, SGK, Syk, Tie, and ZAP-70

Ultimately, three candidates, **15**, **20**, and **23**, gave good to excellent results.

In an effort to understand some of the factors that contributed to the ineffectiveness of some compounds in this assay, PK parameters and solubility values in PBS are included in this table for selected compounds. In general, it seems clear that nearly all of the compounds within this series suffer from moderate to high clearance rates, ranging from values of 24 up to as high as 82 mL/min/kg. Nevertheless, in some cases, correspondingly high volumes of distribution result in compounds that still retain iv half-lives of reasonable length. Control compound **44**, which was below the desired threshold for stability in the mouse microsomal assay, had low bioavailability and low C<sub>max</sub> values in plasma, consistent with the poor PD activity seen, and although poor microsomal stability may often be a predictor of high clearance, compounds with good microsomal stability may still suffer from high clearance for other reasons (such as phase II metabolism), as shown by control compound **34**, which possessed one of the highest clearance values of those tested. Among the remaining compounds, the poor C<sub>max</sub> and bioavailability of compounds **16** and **30** appear to explain the low PD inhibition effects observed. The three compounds that demonstrated the most promising PD activities, **15**, **20**, and **23**, all possessed good PK. Moderate to high clearance values of each compound were compensated for by excellent bioavailabilities (all greater than

80%) and by high volumes of distribution resulting in good oral half-lives (1.6–2.4 h).

Solubility may play a role in the PK behavior observed. It can be seen that the solubility in phosphate buffered saline (PBS) of the control compounds **35–37** and **44** and for test compounds **10** and **30** was lower than for the reference compounds **8** and **21** and may have been an additional contributing factor in the poor PK observed for compounds **30** and **44**. However, good solubility is only one helpful characteristic and, clearly, somewhat lower solubility did not impact the good PK seen for test compound **15**.

To assess kinase selectivity, compounds **15**, **20**, and **23** were screened against a large number of tyrosine, serine-threonine, or mixed kinases. Differences in the profiles of the three compounds were not pronounced (data not shown). For example, as shown in Table 6, compound **23** was assessed at 1  $\mu$ M for activity vs 39 tyrosine kinases and 79 serine-threonine or mixed kinases. Seventy-eight of the serine-threonine or mixed kinases were inhibited less than 50%; one serine-threonine kinase, ALK, was inhibited by 51%. Sixteen of the 39 tyrosine kinases were inhibited by more than 50% by 1  $\mu$ M **23**. Of these, six were inhibited by more than 50% at 0.1  $\mu$ M, and the IC<sub>50</sub> values of **23** vs these six kinases were determined and are reported in Table 7. IC<sub>50</sub> values are also reported in Table 7 for **15** and **20**. All three compounds were found to be relatively potent inhibitors of FLT3, AXL, KIT, and TRKA with modest

Table 7. Kinase Selectivities of 15, 20 and 23

kinase	IC <sub>50</sub> (nM)		
	15	20	23
FMS	1.5	1.1	0.69
KIT	12	23	5.0
AXL	16	6.0	12
TRKA	30	19	15
FLT3	58	23	30
LCK	860	200	88

selectivities for FMS ranging from 7- to 43-fold. The inhibition of FLT3 and KIT can suppress functions in dendritic cells and mast cells, suggesting that the presence of these activities may have beneficial effects toward inflammation. However, there is also evidence that potent inhibition of KIT can produce myelosuppression and anemia.<sup>52</sup> We also tested these compounds in cell-based assays designed to exhibit dependence on these kinases (Table 8). While the selectivity for FMS vs FLT3 and KIT was modest for compound 23 and the selectivity for FMS vs FLT3 was minimal for compound 20, compound 15 exhibited the highest selectivity for FMS among the three compounds with FMS selectivity in cells ranging from ca. 32- to 161-fold. Although compound 23 was a potent inhibitor of AXL and LCK enzyme assays, only high (>2  $\mu$ M) concentrations inhibited these targets in cellular assays.

Compounds 15, 20, and 23 had properties from the abbreviated in vivo screening studies that more than qualified each to advance to more extensive efficacy studies. Therefore, to better characterize and compare them, a more detailed dose–response PD study was performed. Each compound was dosed at high and medium doses of 50 and 20 mg/kg, respectively, and at a lower dose of either 10 mg/kg for compounds 20 and 23 or at 8 mg/kg for compound 15 (Table 9).

Differences in the in vivo activity of the three compounds became apparent in the dose–response comparison. By the mid-dose of 20 mg/kg, the performance of 15 had fallen off sharply, while the responses of 20 and 23 remained robust (77–79% inhibition). At the lowest dose, 20 and 23 still showed substantial responses with 20 (51% inhibition) appearing somewhat superior to 23 (32% inhibition).

The three candidates, compounds 15, 20, and 23, were subsequently evaluated in a type II CIA model in mice.<sup>53,54</sup> This model has been particularly useful in evaluating the beneficial effects of soluble TNF receptors and other cytokine inhibitors.<sup>55</sup> Although 15 had demonstrated a reduced response relative to the other two candidates in the previous PD assay, it was still included in the CIA study at a high dose.

Male B10RII mice were administered Freund's complete adjuvant containing bovine type II collagen and supplemental *Mycobacterium tuberculosis* H37 RA at the base of the tail on day 0 and again on day 15. Groups of 15 mice received twice daily oral administration of either the vehicle (20% HP $\beta$ CD) in a disease control group or the test compound on days 12–26. Compounds 20 and 23 were tested at doses of 60 and 20 mg/kg po BID and 15 at a single dose of 60 mg/kg po BID. One untreated naive group was used as a normal (nondisease) control. Efficacy was based on four individual histopathological parameters, that is, inflammation, pannus formation, cartilage damage, and bone erosion. Histopathology scores were recorded for each category in a range of 0 (normal) to 5 (severe), and the mean value was calculated for the four paws. Statistical significance ( $p < 0.05$ , Student's  $t$  test) was based, in

each group, relative to the vehicle-treated disease control group and, when achieved, is indicated in the charts with an asterisk. A separate, overall, four-paw, animal score based on the sum of the four histological scores was also calculated to provide a more generalized indication of efficacy.

The vehicle-treated disease control animals developed arthritis symptoms with histological changes in most paws with scores ranging from minimal (1) to severe (5). As shown in Figure 3, the vehicle-treated disease control group displayed a greatly elevated four-paw summary score (mean = 5.45) relative to the disease-free naive group. Compound 15 at 60 mg/kg produced a significant 61% reduction in the four-paw score relative to the vehicle-treated disease control. This was the result of significant inhibition, ranging from 57 to 63%, in all four of the measured individual histological parameters as shown in Figure 4. Compound 20 proved the most efficacious of the three candidates in this model. However, the 60 mg/kg dose of 20 caused acute weight loss in a subset of mice and resulted in the deaths of two animals by day 17. As a result of this toxicity and the subsequent deaths, the dose of compound 20 was reduced to 40 mg/kg beginning day 18 and maintained at the lower dose through day 26. Even so, compound 20 produced a significant overall reduction of 82% in the summary score. This is a result of marked reductions in inflammation, pannus, cartilage damage, and bone damage, all in the range of 77–88%. When the dose of 20 was reduced to 20 mg/kg, the toxicity seen at the higher dose was not seen, but the overall efficacy was still impressive with a summary score of 74% inhibition. The inhibition of the individual histological parameters for 20 at this lower dose displayed a range of 69–77% reduction relative to the disease controls. Compound 23 at 60 mg/kg produced a significant 73% reduction of the four-paw score (Figure 3). The inhibition of individual histological parameters ranged from 65 to 79% (Figure 4) with the reductions in the scores for both pannus formation (79%) and bone erosion (79%) of particular note. When administered at the lower dose of 20 mg/kg, compound 23 was less effective overall, providing a nonsignificant 20% reduction in the summary score. This reflected nonsignificant reductions in inflammation and cartilage damage of 16 and 18%, respectively, and significant 25% reductions in pannus formation and bone erosions (Figure 4). With the exception of the 60 mg/kg dose of 20, the candidates had no deleterious effects on body weight or any clinical signs of toxicity.

Although compound 20 showed a clear advantage in terms of efficacy over 15 and 23, the toxicity observed at the high dose was worrisome. In further studies, 20 and 23 were examined in a battery of 50 counterscreen assays<sup>40</sup> for activity against a wide variety of receptors, transporters, and ion channels. While 23 hit four targets with greater than 50% inhibition of specific control ligand binding, 20 gave greater than 50% inhibition at seven targets. The apparent increased off-target activity of 20 was also reflected in unambiguous conductance effects in guinea pig acute cardiovascular (CV) safety<sup>56</sup> and guinea pig right atrium studies.<sup>57</sup> Consequently, despite the lack of overt toxicity at the lower dose of 20 mg/kg in the arthritis study, the potential for safety issues was of significant concern, and the decision was made to eliminate 20 as a candidate. Thus, compound 23, which was superior to 15 at a comparable dose for every histological parameter and in its summary score, was chosen as the best candidate in the group for further evaluation. To better characterize the potential of compound 23 as a

Table 8. Cell-Based Kinase Selectivities of 15, 20, and 23<sup>a</sup>

target	cells/cell line	stimulus	end point	IC <sub>50</sub> (nM) <sup>a</sup>		
				15	20	23
FMS	BMDM <sup>b</sup>	CSF-1	proliferation	3.1	3.2	2.6
ITD-FLT 3	MV-4–11 <sup>c</sup>	none	proliferation	98	8.0	21
KIT	Mo7e <sup>c</sup>	SCF	proliferation	210	na <sup>f</sup>	41
TRKA	TF-1 <sup>c</sup>	NGF	proliferation	500	na	150
LCK	Jurkat <sup>d</sup>	anti-CD3, PMA	IL-2	na	na	3900
AXL	AXL/HEK <sup>e</sup>	GAS6	phospho-AXL	na	na	2600

<sup>a</sup>Assays were performed as described in the Experimental Section or as described previously.<sup>24</sup> <sup>b</sup>Mouse BMDMs. <sup>c</sup>Leukemia cell lines. <sup>d</sup>T-cell lymphoma cell line. <sup>e</sup>HEK cells were transfected to overexpress AXL. <sup>f</sup>na, not assayed.

Table 9. PD Dose–Response Studies of 15, 20, and 23

compd	PD assay			
	% inhibition at 8 h (po) <sup>a</sup>			
	mg/kg			
	50	20	10	8
15	93	5	na <sup>b</sup>	0
20	86	77	51	na
23	88–100	79	32	na

<sup>a</sup>PD model in B6C3F1 mice with all compounds administered in 20% HP/CD (see the details in the Experimental Section). <sup>b</sup>na, not assayed.

potential treatment for RA, it was subsequently characterized in additional models of this disease.

Rat adjuvant arthritis is an experimental model of polyarthritis that has been widely employed for preclinical testing of antiarthritic agents.<sup>58–61</sup> Two characteristics of this model are the reliable onset and progression of robust, easily measurable, periarticular inflammation, and marked bone resorption. Cartilage destruction also occurs but is disproportionately mild in comparison to the inflammation and bone destruction that takes place. This is a fairly aggressive model especially when used, as in this case, in a therapeutic mode for evaluation of compounds administered after the symptoms of the disease have emerged.

Arthritis was induced in male Lewis rats by injection of Freund's complete adjuvant containing lipoidal amine [*N,N*-dioctyldecyl-*N,N*-bis(2-hydroxyethyl)propanediamine] at the base of the tail on day 0. Clinical signs of disease began to emerge on day 8 postinjection. Beginning on day 8, randomized groups of rats received twice daily oral administration of either the vehicle (0.5% hydroxypropylmethylcellulose/0.5% Tween 80) or compound 23 at 5, 20, and 60 mg/kg. All adjuvant-injected control rats developed clinical signs of arthritis as evidenced by increased ankle joint diameter. Mean body weights were similar in all groups at the start of the study, and none of the treatment groups with established arthritis had significant mean body weight changes as compared to the established arthritis vehicle controls (data not shown).

After euthanization on day 14, the hind paws were removed, weighed, processed, and scored for histopathology assessment. Paw weights were increased nearly 2-fold in rats with adjuvant arthritis (Figure 5A). The increase in paw weights was reduced by 23 in a dose-dependent fashion with 60 mg/kg reducing the gain in paw weight by 49%. Suppression of paw weight increase by 23 correlated with suppression in the histological scores of inflammation (Figure 5B). The abundance of periarticular macrophages was assessed in sections following immunohis-

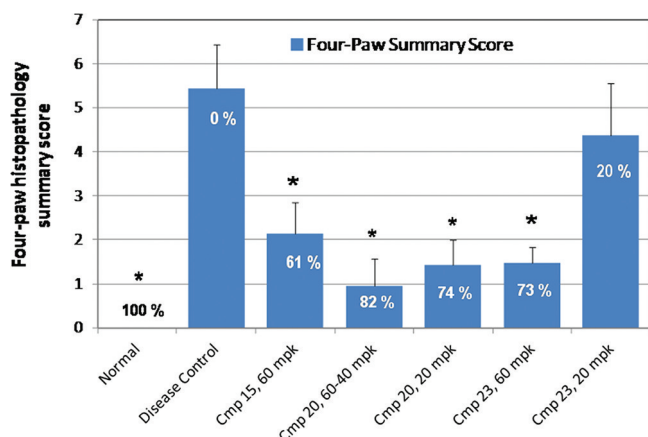


Figure 3. Compounds 15, 20, and 23 reduced four-paw histopathology summary scores in mouse CIA. CIA was induced in mice as described in the Experimental Section. Group mean values (SEM) are plotted, and percent inhibition values relative to the vehicle-treated disease control are indicated in text within the bars (mpk = mg/kg); \**p* < 0.01 vs disease control (vehicle).

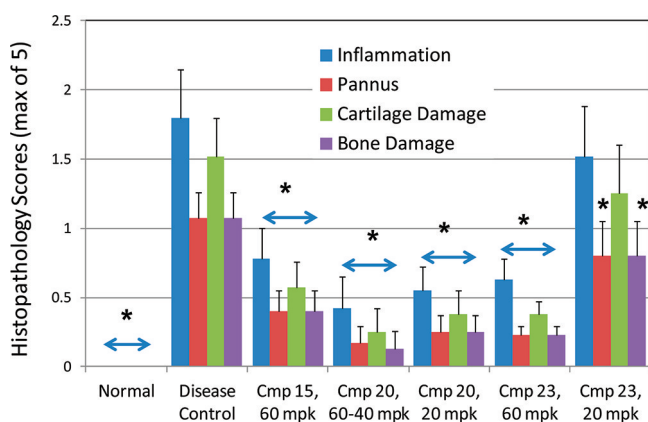


Figure 4. Compounds 15, 20, and 23 reduced the histopathology evidence of inflammation, pannus, cartilage, and bone damage. CIA was induced in mice, and scores for each histopathology parameters were determined as described in the Experimental Section. Group mean values (SEM) are plotted. \**p* < 0.01 vs disease control (vehicle).

tochemical detection of ED-1 antigen (CD68), a marker of macrophage lineage cells. ED-1<sup>+</sup> macrophages were reduced by 23 in a dose-dependent fashion with significant reductions at all doses (Figure 5C). Splenomegaly, an additional manifestation of the immune inflammatory response to adjuvant, was reduced by 23 in a similar dose-dependent fashion (Figure 5D).



Paws were examined further for histopathological evidence of bone erosion (Figure 5E). By day 14, all 16 evaluated tibio-tarsal joints of the vehicle-treated group exhibited signs of bone erosion ranging from minimal to severe. Loss of medullary trabecular bone was readily observed at low power in most paws from vehicle-treated diseased rats. Osteoclast numbers per 400 $\times$  field were averaged from examining the five fields of greatest bone resorption. In vehicle-treated rats, areas of bone erosion were characterized by numerous osteoclasts (average of 12.6 osteoclasts per 400 $\times$  field). The occurrence of erosions and erosion-associated osteoclasts was completely prevented in rats dosed with 60 or 20 mg/kg **23**. Even in rats receiving 5 mg/kg **23**, 11 of 16 evaluated joints were characterized by an absence of bone erosion, and the remaining five joints had mild erosions. At all three doses of **23**, osteoclast numbers were similar to disease-free joints. Adjuvant arthritis was additionally associated with periosteal new bone formation. The formation of new bone was proportional to inflammation scores and was reduced 67% by a dose of 60 mg/kg **23** but was not reduced by lower doses.

In a third model, polyarthritis was induced in female Lewis rats following intraperitoneal (ip) administration of streptococcal cell wall (SCW) proteoglycan-polysaccharides (PG-PS). This model has an acute nonerosive phase (days 3–7) that is complement- and neutrophil-dependent and that resolves. A chronic erosive phase then begins at about day 10 and is dependent on macrophages and on the development of specific T-cell immunity to SCW.<sup>62,63</sup> In an initial study, dosing of **23** was commenced on day 8 when the acute phase was resolving and transitioning to the chronic phase. Rats treated with vehicle progressively developed a severe arthritis until study termination (day 19). Administration of **23** at 20 mg/kg (po, BID) blocked the emergence of the chronic arthritic phase with a significant effects on ankle thickness (Figure 6A) and clinical scores (Figure 6B) observed as early as day 12, 4 days after dose initiation. Histological assessment of the ankles of vehicle-treated rats revealed recruitment of numerous ED-1 positive macrophages into the periarticular tissues together with fibroplasia (Figure 6C). Also notable were the greatly increased numbers osteoclasts (also ED-1 positive) eroding many large areas of trabecular bone in all vehicle-treated rats (Figure 6C). Compound **23** reduced the recruitment of macrophages into the periarticular tissues (Figure 6D). Furthermore, osteoclast counts and distribution were normal, and the large areas of trabecular bone loss observed in all vehicle-treated rats were not observed in rats treated with **23**. The bone protective effects of **23** were corroborated when imaged by micro-radiography (Figure 7). When compared to disease-free controls (Figure 7A), the ankle bones of vehicle-treated rats appeared pitted and deformed (Figure 7B). Consistent with the observed histological effects, joints of rats dosed from day 8 to day 19 with 20 mg/kg **23** appeared normal (Figure 7C) with the exception of one rat that exhibited minimal signs of pitting. On the basis of a four-point severity scale, the mean (SD) bone deformation score in vehicle-treated rats was  $2.83 \pm 0.41$  vs  $0.17 \pm 0.41$  for rats dosed with **23**.

In a second study, dosing was commenced on day 18 when chronic arthritis was well-established (Figure 8). Treatment with **23** induced a dose-dependent decrease in arthritis scores with significant effects observed by day 21 for the 6 and 20 mg/kg dose groups and for all dose groups by day 26. Both ankle swelling and arthritic scores continued to decrease in the 6 and 20 mg/kg dose groups 1 day prior to study termination (day

39). On day 39, the ankle thickness measurements for the SCW vehicle group rats were  $13.78 \pm 0.57$  mm, and the ankle thickness measurements of 2 mg/kg **23** group rats were  $11.56 \pm 1.54$ ; the ankle thickness measurements of 6 mg/kg **23** group rats were  $9.91 \pm 0.41$  mm; the ankle thickness measurements of 20 mg/kg **23** group rats were  $9.30 \pm 0.39$  and  $7.58 \pm 0.03$  mm for naïve disease-free rats.

Collectively, **23** was shown to prevent osteoclastogenesis and to reduce synovial and periarticular macrophages in three models of RA together with reductions in histopathology scores or joint swelling and erosion. These data suggest the potential for substantial disease modification with **23** in RA as a single agent. Furthermore, because the antirheumatic effects of low-dose methotrexate (MTX) are currently ascribed to the capacity of the drug to suppress the development of a fully activated T-cell phenotype, **23** and MTX might be expected to have complementary effects in suppressing autoimmune disease, macrophage-derived inflammation, and bone erosion. Because of the overall promising preclinical profile of **23** and the potential to provide benefit to RA patients, **23** was selected as a candidate for clinical studies in humans pending the results of safety testing.

## CONCLUSION

Two previous lead FMS inhibitors, **8** and **21**, which possessed excellent in vitro potency against FMS and cells, were found to have poor PK characteristics resulting in less than ideal in vivo PD activity. A sequence of analogues of the piperidine group was prepared to optimize both the ADME and the PK/PD properties of this series, resulting in three potent and efficacious compounds, **15**, **20**, and **23**, with relatively good selectivity against a number of kinases. In vivo PD dose–response behavior, CIA efficacy, and toxicity observations were used to ultimately select **23** as the most promising clinical candidate. Compound **23** was shown to effectively reduce inflammation and bone erosion in mouse CIA as well as in rat adjuvant and SCW models of arthritis, indicating that this agent may be beneficial in the treatment of RA.

## EXPERIMENTAL SECTION

**Chemistry.** Reagents and solvents were obtained from commercial suppliers and used without further purification. <sup>1</sup>H NMR spectra were measured in the indicated solvent with tetramethylsilane (TMS) or the residual solvent peak as the internal standard on a Bruker B-ACS-120 (400 MHz) spectrophotometer at room temperature. Chemical shifts are given in ppm ( $\delta$ ) relative to the internal standard, and coupling constants (*J*) are in Hertz (Hz). Abbreviations for the multiplicities of the signals are as follows: s (singlet), d (doublet), t (triplet), q (quartet), quin (quintet), sep (septet), m (multiplet), br s (broad singlet), and combinations thereof. All reactions were monitored by thin-layer chromatography (TLC) carried out on EMD silica gel plates (2.5 cm  $\times$  7.5 cm, 250  $\mu$ m thick, 60 F<sub>254</sub>), visualized by using UV (254 nm) or stains such as KMnO<sub>4</sub>, *p*-anisaldehyde, and ceric ammonium molybdate (CAM). All organic solutions were dried over anhydrous MgSO<sub>4</sub> or Na<sub>2</sub>SO<sub>4</sub> and concentrated on a rotary evaporator. Hydrogenation was performed at atmospheric pressures under a balloon of hydrogen and at higher pressures on a shaker type hydrogenation apparatus (Parr Instrument Co.). Flash chromatography was performed using Fisher Chemical Silica Gel Sorbent (230–400 mesh, grade 60) or on prepacked silica solid-phase extraction (SPE) columns (Biotage IST Isolute or Waters Sep-Pak columns). Preparative TLC was performed on Analtech Silica Gel GF plates (1000 or 2000  $\mu$ m, 20 cm  $\times$  20 cm). Preparative high-performance liquid chromatography (HPLC) was carried out on a Varian Prep Star system equipped with a Varian model 325 UV detector (monitoring

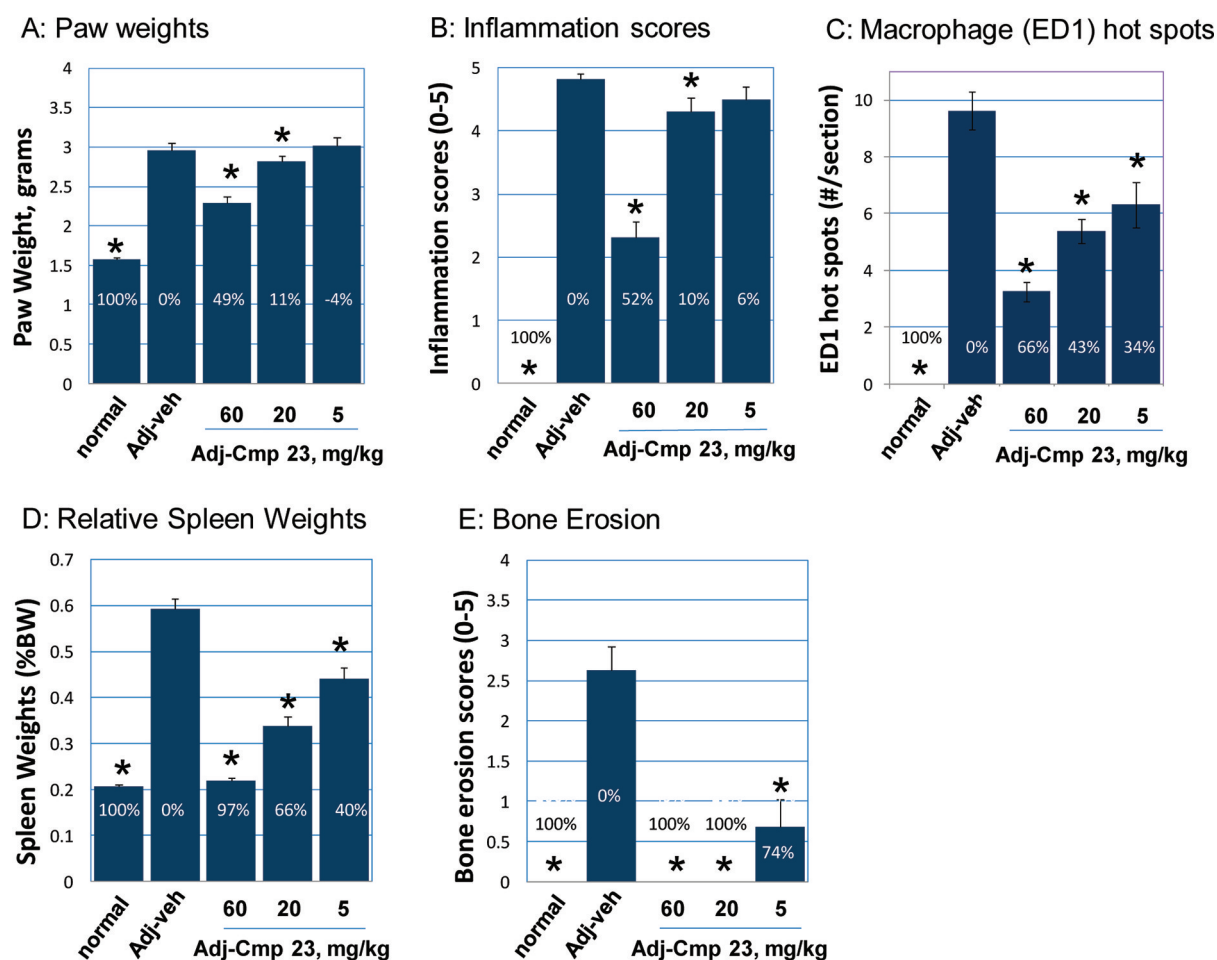


**Figure 5.** Compound 23 reduced disease activity in rats with adjuvant arthritis. Adjuvant arthritis was induced in rats as described in the Experimental Section. Commencing on day 8, adjuvant-induced rats (Adj) received twice daily oral doses of vehicle (veh) or 5, 20, or 60 mg/kg of 23 until study termination on day 14. An additional group of rats was not adjuvant induced and served as the disease-free (normal) control. All end points were determined as described in the Experimental Section. (A) Hind paws were severed at the level of the medial and lateral malleolus and weighed. (B) H&E-stained sections of formalin-fixed hind paws were scored for inflammation by histopathology assessment using a five-point scale. (C) Soft tissue regions of sections stained for ED-1 antigen (CD68) positive macrophages were assessed for the number of areas (hot spots) with marked numbers of positive cells. (D) Spleens were weighed at necropsy. (E) H&E-stained sections of formalin-fixed hind paws were scored for bone erosions using a five-point scale. All values represent group means ( $n = 16$  hind limbs or 8 spleens). Error bars represent standard errors of the means. Percent inhibition values relative to adjuvant-induced, vehicle-treated rats were provided as white text within bars.  $*p < 0.05$ .

at 254 nm) and a Varian Pro Star fraction collector and using a ThermoElectron Betasil C<sub>18</sub> (150 mm × 21.2 mm, 10 μm particle size) reverse phase column. The solvents, both acetonitrile (MeCN) and water, contained 0.05% of trifluoroacetic acid (TFA, v/v). LC-MS was performed on a system consisting of an electrospray ionization (ESI) source on a Finnigan LCQ Classics ion trap mass spectrometer, an Agilent 1100 DAD UV detector (214 nm wavelength), an Agilent 1100-LC binary gradient pumping system, a Gilson 215 configured as an autosampler, and a PrincetonSPHER HTS 60A (Princeton Chromatography Inc.) C<sub>12</sub> HPLC column (5 μm, 50 mm × 3.0 mm). The purities of the key target compounds were determined on the Finnigan LCQ instrument, which gave both the MS and LC trace of the compound in a 5 min run. The HPLC method used was as follows: column, PrincetonSPHER HTS 60A C<sub>12</sub> HPLC column (5 μm, 50 mm × 3.0 mm); column temperature, ambient; flow rate, 1.5 mL/min; and gradient, 10% acetonitrile in water to 100% acetonitrile in water in 5 min, both MeCN and water contained 0.05% of TFA, v/v. All compounds used for biological assays were at least of 95% purity based on HPLC analytical results, unless otherwise noted.

**4-Cyano-1H-imidazole-2-carboxylic Acid (2-Cyclohex-1-enyl-4-piperidin-4-yl-phenyl)-amide Trifluoroacetic Acid Salt (8).** a. 4-(4-Amino-phenyl)-3,6-dihydro-2H-pyridine-1-carboxylic Acid *tert*-Butyl Ester. A solution of 4-(4,4,5,5-tetramethyl-1,3,2-

dioxaborolan-2-yl)-phenylamine **1** (4.0 g, 18 mmol), 4-trifluoromethanesulfonyloxy-3,6-dihydro-2H-pyridine-1-carboxylic acid *tert*-butyl ester<sup>64</sup> **2** (7.4 g, 22 mmol), and 2 M aqueous Na<sub>2</sub>CO<sub>3</sub> (80 mL) in toluene (160 mL) and EtOH (80 mL) was placed under Ar and heated to 80 °C for 3 h. The mixture was washed with 1 M aqueous NaOH, and the organic layer was removed, dried (Na<sub>2</sub>SO<sub>4</sub>), and concentrated in vacuo. The residue was purified by silica gel chromatography, eluting with 20% EtOAc/hexanes to afford 3.2 g (63%) of the title compound as a yellow foam. <sup>1</sup>H NMR (CDCl<sub>3</sub>, 400 MHz): δ 7.18–7.23 (m, 2H, *J* = 8.4 Hz), 6.64–6.69 (m, 2H, *J* = 8.6 Hz), 5.90 (br s, 1H), 4.02–4.08 (m, 2H), 3.68 (s, 2H), 3.62 (t, 2H, *J* = 5.6 Hz), 2.48 (br s, 2H), 1.49 (s, 9H). Mass spectrum (ESI, *m/z*): calcd for C<sub>16</sub>H<sub>22</sub>N<sub>2</sub>O<sub>2</sub>, 275.2 (*M* + *H*); found, 275.1.

b. 4-(4-Amino-phenyl)-piperidine-1-carboxylic Acid *tert*-Butyl Ester (**3**). A solution of 4-(4-amino-phenyl)-3,6-dihydro-2H-pyridine-1-carboxylic acid *tert*-butyl ester (0.350 g, 1.28 mmol) (as prepared in the previous step) in methanol was hydrogenated over 10% Pd/C at 20 psi for 1 h. The solution was filtered through diatomaceous earth, and the filtrate was concentrated to give 0.35 g (100%) of the title compound **3** as a yellow solid. <sup>1</sup>H NMR (CDCl<sub>3</sub>, 400 MHz): δ 6.96–7.01 (d, 2H, *J* = 8.4 Hz), 6.62–6.67 (d, 2H, *J* = 8.4 Hz), 4.21 (br s, 2H), 3.58 (br s, 2H), 2.77 (t, 2H, *J* = 12.6 Hz), 2.53 (tt, 1H, *J* = 12.1, 3.5 Hz), 1.77 (d, 2H, *J* = 12.3 Hz), 1.52–1.59

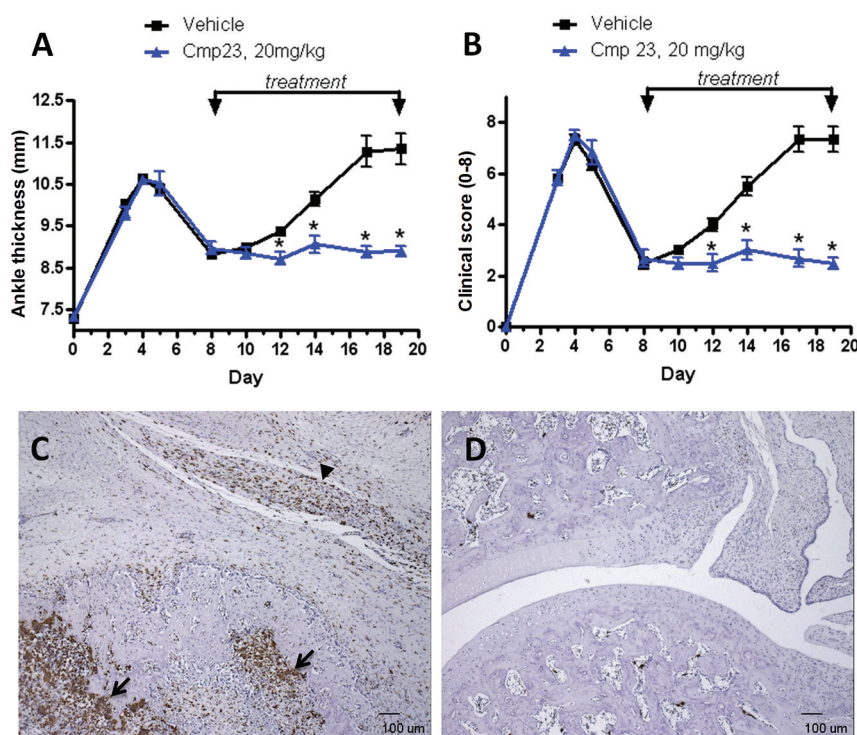


**Figure 6.** Compound 23 prevented the chronic phase of SCW arthritis and the recruitment of macrophages and osteoclasts and bone erosion. Arthritis was induced in rats following a single ip injection of SCW as described in the Experimental Section. Following partial resolution of the acute phase, twice daily oral dosing was commenced on day 8 with vehicle or with 20 mg/kg compound 23. Ankle thickness was determined using calipers (A), and clinical scores were assigned as described in the Experiment Section (B). Immunohistochemistry was used to assess formalin-fixed sections of hind-limb ankles for ED-1 antigen positive cells. Representative low power (20X) fields of rats treated with vehicle (C) or with 20 mg/kg compound 23 (D) are provided. The arrow head indicates periarticular tissue with intense infiltration of macrophages. Arrows indicated erosions in trabecular bone associated with large numbers of osteoclasts. All values represent group means ( $n = 6$ ). Error bars represent standard errors of the means. \* $p < 0.05$ .

(m, 2H), 1.48 (s, 9H). Mass spectrum (ESI,  $m/z$ ): calcd for  $C_{16}H_{24}N_2O_2$ , 277.2 (M + H); found, 277.1.

**c. 4-(4-Amino-3-bromo-phenyl)-piperidine-1-carboxylic Acid tert-Butyl Ester (4).** To a solution of 4-(4-amino-phenyl)-piperidine-1-carboxylic acid tert-butyl ester (0.20 g, 0.71 mmol) (as prepared in the previous step) in  $CH_2Cl_2$  (3 mL) was added *N*-bromosuccinimide (NBS) (0.13 g, 0.71 mmol), and the reaction was stirred at room temperature for 10 h. The reaction was diluted with EtOAc (10 mL) and washed with saturated aqueous  $NaHCO_3$  ( $2 \times 10$  mL) and brine (10 mL). Concentration of the organic layer gave 0.26 g (100%) of the title compound 4 as a yellow foam.  $^1H$  NMR ( $CDCl_3$ , 400 MHz):  $\delta$  7.27 (d, 1H,  $J = 2.1$  Hz), 6.96 (dd, 1H,  $J = 8.1, 1.9$  Hz), 6.73 (d, 1H,  $J = 8.1$  Hz), 4.24 (br s, 2H), 4.01 (br s, 2H), 2.78 (t, 2H,  $J = 12.2$  Hz), 2.53 (tt, 1H,  $J = 12.2, 3.3$  Hz), 1.79 (d, 2H,  $J = 12.6$  Hz), 1.52–1.59 (m, 2H), 1.50 (s, 9H). Mass spectrum (ESI,  $m/z$ ): calcd for  $C_{16}H_{23}BrN_2O_2$ , 355.1 (M + H); found, 355.1.

**d. 4-(4-Amino-3-cyclohex-1-enyl-phenyl)-piperidine-1-carboxylic Acid tert-Butyl Ester (5).** 4-(4-Amino-3-bromo-phenyl)-piperidine-1-carboxylic acid tert-butyl ester (0.13 g, 0.36 mmol) (as prepared in the previous step), cyclohex-1-enyl boronic acid 4 (0.060 g, 0.48 mmol),  $Pd(PPh_3)_4$  (0.04 g, 10 mol %), aqueous 2 M  $Na_2CO_3$  (1.5 mL), ethanol (1.5 mL), and toluene (3 mL) were heated at 80 °C for 3 h. The reaction was diluted with EtOAc (10 mL) and washed with saturated aqueous  $NaHCO_3$  ( $2 \times 10$  mL) and brine (10 mL), and the organic layer was dried over  $Na_2SO_4$  and then concentrated. The residue was purified on a 20 g SPE cartridge (silica) with 30% EtOAc/hexane to give 0.10 g (85%) of the title compound 5 as a yellow oil.  $^1H$  NMR ( $CDCl_3$ , 400 MHz):  $\delta$  6.90 (dd, 1H,  $J = 8.1, 2.1$  Hz), 6.85 (d, 1H,  $J = 1.9$  Hz), 6.67 (d, 1H,  $J = 8.1$  Hz), 5.76 (dq, 1H,  $J = 3.5, 1.8$  Hz), 4.23 (br s, 2H), 3.71 (s, 2H), 2.79 (t, 2H,  $J = 12.7$  Hz), 2.54 (tt, 1H,  $J = 12.3, 3.4$  Hz), 2.22–2.29 (m, 2H), 2.16–2.22 (m, 2H), 1.62–

1.85 (m, 8H), 1.50 (s, 9H). Mass spectrum (ESI,  $m/z$ ): calcd for  $C_{22}H_{32}N_2O_2$ , 357.2 (M + H); found, 357.1.

**e. (4-[[4-Cyano-1-(2-trimethylsilylanyl-ethoxymethyl)-1H-imidazole-2-carbo-nyl]-amino]-3-cyclohex-1-enyl-phenyl)-piperidine-1-carboxylic Acid tert-Butyl Ester (7).** To a solution of 4-cyano-1-(2-trimethylsilylanyl-ethoxymethyl)-1H-imidazole-2-carboxylate potassium salt<sup>27</sup> 6 (3.34 g, 10.9 mmol) in 20 mL of  $CH_2Cl_2$  were added DIEA (3.80 mL, 21.8 mmol) and PyBroP (5.59 g, 12.0 mmol), and the reaction was stirred at 25 °C for 15 min. A solution of 4-(4-amino-3-cyclohex-1-enyl-phenyl)-piperidine-1-carboxylic acid tert-butyl ester (3.92 g, 11.0 mmol) (as prepared in the previous step) in 10 mL of  $CH_2Cl_2$  was added, and the reaction was stirred for 8 h at 25 °C. The reaction was diluted with EtOAc (60 mL) and washed with saturated aqueous  $NaHCO_3$  ( $2 \times 60$  mL) and brine (100 mL), and the organic layer was dried over  $Na_2SO_4$  and then concentrated. The residue was purified by flash chromatography (silica gel, 2% EtOAc/ $CH_2Cl_2$ ) to give 5.5 g (85%) of the title compound 7 as a yellow oil.  $^1H$  NMR ( $CDCl_3$ , 400 MHz):  $\delta$  9.68 (s, 1H), 8.25 (d, 1H,  $J = 8.4$  Hz), 7.78 (s, 1H), 7.12 (dd, 1H,  $J = 8.6, 2.1$  Hz), 7.02 (d, 1H,  $J = 2.1$  Hz), 5.96 (s, 2H), 5.83 (dt, 1H,  $J = 3.6, 1.9$  Hz), 4.25 (br s, 2H), 3.63–3.69 (m, 2H), 2.80 (t, 2H,  $J = 11.7$  Hz), 2.63 (tt, 1H,  $J = 12.2, 3.5$  Hz), 2.27–2.33 (m, 2H), 2.20–2.27 (m, 2H), 1.77–1.87 (m, 6H), 1.56–1.68 (m, 2H), 1.49 (s, 9H), 0.95–1.00 (m, 2H), 0.01 (s, 9H). Mass spectrum (ESI,  $m/z$ ): calcd for  $C_{33}H_{47}N_5O_4Si$ , 606.2 (M + H); found, 606.2.

**f. 4-Cyano-1H-imidazole-2-carboxylic Acid (2-Cyclohex-1-enyl-4-piperidin-4-yl-phenyl)-amide Trifluoroacetic Acid Salt (8).** To a solution of 4-[[4-cyano-1-(2-trimethylsilylanyl-ethoxymethyl)-1H-imidazole-2-carboxyl]-amino]-3-cyclohex-1-enyl-phenyl)-piperidine-1-carboxylic acid tert-butyl ester 7 (1.50 g, 2.48 mmol) (as prepared in the previous step) in 10 mL of  $CH_2Cl_2$  and 0.3 mL of EtOH was added 3 mL of TFA, and the solution was stirred for 3 h at 25 °C. The reaction was diluted with 5 mL of EtOH and then concentrated.



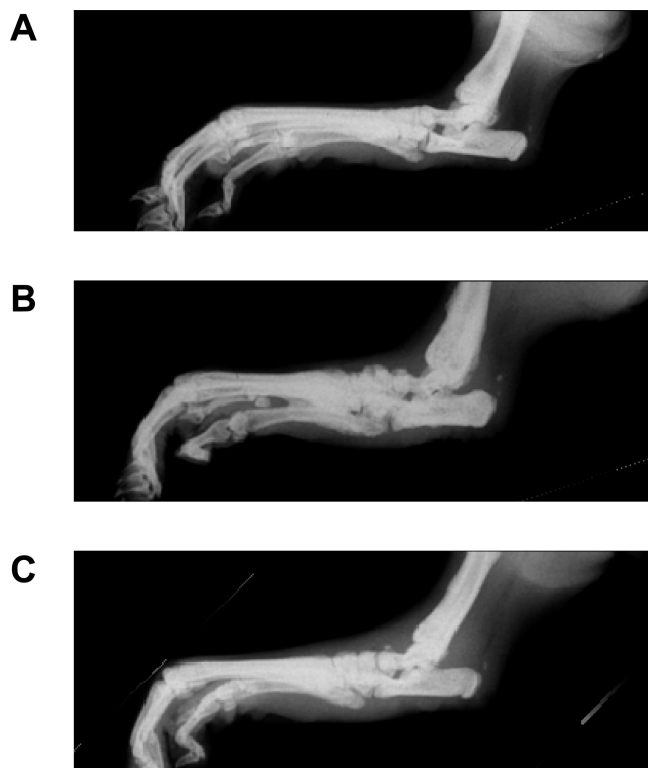
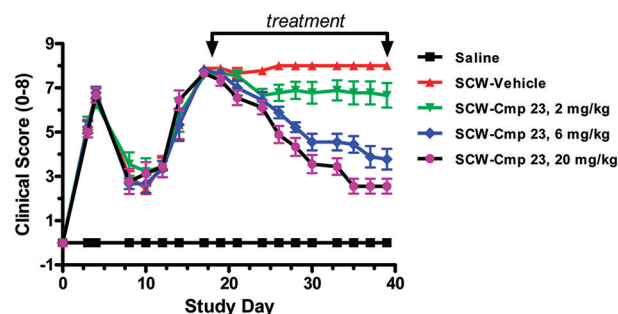


**Figure 7.** Compound 23 prevented the development of bone deformation. Following necropsy on day 19, microradiographic images were prepared of tibial tarsal joints. Representative images are shown obtained from a disease-free rat (A), a rat with adjuvant arthritis treated with vehicle (B), and a rat with adjuvant arthritis treated with 20 mg/kg 23 (C). Bones in vehicle-treated rats with adjuvant arthritis appeared pitted and lacked fine definition, while bones from rats treated with 23 appeared normal.



**p value vs. SCW-Vehicle**

	Day 21	Day 24	Day 26	Day 28	Day 30	Day 33	Day 35	Day 37	Day 39
SCW-Vehicle									
SCW-Cmp 23, 2mg/kg			P < 0.05	P < 0.05					
SCW-Cmp 23, 6mg/kg	P < 0.05	P < 0.05	P < 0.01	P < 0.01	P < 0.01	P < 0.01	P < 0.01	P < 0.01	P < 0.01
SCW-Cmp 23, 20mg/kg	P < 0.05	P < 0.05	P < 0.01	P < 0.01	P < 0.01	P < 0.01	P < 0.01	P < 0.01	P < 0.01

**Figure 8.** SCW model of arthritis. Dosing commenced after the establishment of chronic arthritis.

The residue was crystallized from methanol and ethyl ether to give 0.85 g (70%) of the title compound as a white solid.  $^1\text{H}$  NMR ( $\text{CD}_3\text{OD}$ , 400 MHz):  $\delta$  8.18 (d, 1H,  $J$  = 8.4 Hz), 8.04 (s, 1H), 7.22 (dd, 1H,  $J$  = 8.6, 2.1 Hz), 7.12 (d, 1H,  $J$  = 2.3 Hz), 5.76 (m, 1H), 3.54 (m, 2H), 3.16 (m, 2H), 2.92 (m, 1H), 2.30 (m, 4H), 2.10 (m, 2H), 1.87 (m, 6H). Mass spectrum (ESI,  $m/z$ ): calcd for  $\text{C}_{22}\text{H}_{25}\text{N}_5\text{O}$ , 376.2 ( $M + \text{H}$ ); found, 376.2.

**4-Cyano-1H-imidazole-2-carboxylic Acid [2-Cyclohex-1-enyl-4-[3,4,5,6-tetrahydro-2H-[1,2']bipyridinyl-4-yl]-phenyl]-amide Trifluoroacetic Acid Salt (9).** 4-Cyano-1H-imidazole-2-

carboxylic acid (2-cyclohex-1-enyl-4-piperidin-4-yl-phenyl)-amide TFA salt **8** (75.0 mg, 0.153 mmol),  $\text{K}_2\text{CO}_3$  (84.7 mg, 0.613 mmol), 2-fluoropyridine (26.4  $\mu\text{L}$ , 0.306 mmol), and 0.3 mL of *N,N*-dimethylacetamide were stirred for 8 h at 120  $^\circ\text{C}$ . The reaction was diluted with 3 mL of  $\text{H}_2\text{O}$ , and the residue was purified by RP-HPLC ( $\text{C}_{18}$ ), eluting with 30–50%  $\text{CH}_3\text{CN}$  in 0.1% TFA/ $\text{H}_2\text{O}$  over 9 min to give 50 mg (75%) of the title compound as a white solid.  $^1\text{H}$  NMR ( $\text{CD}_3\text{OD}$ , 400 MHz):  $\delta$  8.18 (d, 1H,  $J$  = 8.4 Hz), 8.06 (m, 1H), 8.02 (s, 1H), 7.94 (dd, 1H,  $J$  = 6.3, 1.6 Hz), 7.48 (d, 1H, 9.5 Hz), 7.22 (dd, 1H,  $J$  = 8.5, 2.2 Hz), 7.12 (d, 1H,  $J$  = 2.1 Hz), 6.98 (t, 1H,  $J$  = 7.1 Hz), 5.82 (m, 1H), 4.32 (m, 2H), 3.46 (m, 2H), 3.00 (m, 1H), 2.30 (m, 4H), 2.18 (m, 2H), 1.96–1.74 (m, 6H). Mass spectrum (ESI,  $m/z$ ): calcd for  $\text{C}_{27}\text{H}_{28}\text{N}_6\text{O}$ , 453.2 ( $M + \text{H}$ ); found, 453.2.

**4-Cyano-1H-imidazole-2-carboxylic Acid [4-[1-(2-Cyano-ethyl)-piperidin-4-yl]-2-cyclohex-1-enyl-phenyl]-amide Trifluoroacetic Acid Salt (10).** 4-Cyano-1H-imidazole-2-carboxylic acid (2-cyclohex-1-enyl-4-piperidin-4-yl-phenyl)-amide TFA salt **8** (77.0 mg, 0.157 mmol),  $\text{Et}_3\text{N}$  (21.9  $\mu\text{L}$ , 0.157 mmol), acrylonitrile (12.4  $\mu\text{L}$ , 0.188 mmol), 0.1 mL of MeOH, and 1.0 mL of 1,2-dichloroethane were stirred for 1 h at 80  $^\circ\text{C}$ . The reaction was concentrated, and the residue was purified by RP-HPLC ( $\text{C}_{18}$ ), eluting with 30–50%  $\text{CH}_3\text{CN}$  in 0.1% TFA/ $\text{H}_2\text{O}$  over 12 min to give 83 mg (95%) of the title compound as a white solid.  $^1\text{H}$  NMR ( $\text{CD}_3\text{OD}$ , 400 MHz):  $\delta$  8.18 (d, 1H,  $J$  = 8.6 Hz), 8.06 (m, 1H), 7.22 (dd, 1H,  $J$  = 8.4, 1.9 Hz), 7.12 (d, 1H,  $J$  = 1.9 Hz), 5.82 (m, 1H), 3.76 (m, 2H), 3.60 (m, 2H), 3.28 (t, 2H,  $J$  = 12.6 Hz), 3.12 (t, 2H,  $J$  = 7.2), 2.92 (m, 1H), 2.30 (m, 4H), 2.18–1.98 (m, 4H), 1.92–1.74 (m, 4H). Mass spectrum (ESI,  $m/z$ ): calcd for  $\text{C}_{25}\text{H}_{28}\text{N}_6\text{O}$ , 429.2 ( $M + \text{H}$ ); found, 429.2.

**4-Cyano-1H-imidazole-2-carboxylic Acid [2-Cyclohex-1-enyl-4-[1-(pyridin-2-ylmethyl)-piperidin-4-yl]-phenyl]-amide Trifluoroacetic Acid Salt (11).** 4-Cyano-1H-imidazole-2-carboxylic acid (2-cyclohex-1-enyl-4-piperidin-4-yl-phenyl)-amide TFA salt **8** (88.0 mg, 0.180 mmol), pyridine-2-carbaldehyde (20.5  $\mu\text{L}$ , 0.216 mmol),  $\text{Et}_3\text{N}$  (30.1  $\mu\text{L}$ , 0.216 mmol), sodium triacetoxymethylborohydride (53.4 mg, 0.252 mmol), and 0.8 mL of 1,2-dichloroethane were stirred for 10 h at 25  $^\circ\text{C}$ . The solvent was evaporated, and the residue was purified by RP-HPLC ( $\text{C}_{18}$ ), eluting with 30–50%  $\text{CH}_3\text{CN}$  in 0.1% TFA/ $\text{H}_2\text{O}$  over 20 min to give 81 mg (78%) of the title compound as a white solid.  $^1\text{H}$  NMR ( $\text{CDCl}_3$ , 400 MHz):  $\delta$  9.62 (s, 1H), 8.62 (ddd, 1H,  $J$  = 4.9, 1.7, 0.8 Hz), 8.25 (d, 1H,  $J$  = 8.4 Hz), 7.72–7.77 (m, 2H), 7.57 (d, 1H,  $J$  = 7.7 Hz), 7.26–7.31 (m, 1H), 7.17 (dd, 1H,  $J$  = 8.5, 2.0 Hz), 7.05 (d, 1H,  $J$  = 1.9 Hz), 5.84 (dt, 1H,  $J$  = 3.5, 1.8 Hz), 3.99 (s, 2H), 3.51 (s, 1H), 3.28 (d, 2H,  $J$  = 11.6 Hz), 2.59 (tt, 1H,  $J$  = 11.8, 4.0 Hz), 2.44–2.54 (m, 2H), 2.27–2.34 (m, 2H), 2.21–2.27 (m, 2H), 1.75–2.05 (m, 8H). Mass spectrum (ESI,  $m/z$ ): calcd for  $\text{C}_{28}\text{H}_{30}\text{N}_6\text{O}$ , 467.2 ( $M + \text{H}$ ); found, 467.2.

**4-Cyano-1H-imidazole-2-carboxylic Acid [2-Cyclohex-1-enyl-4-[1-(2-hydroxy-ethyl)-piperidin-4-yl]-phenyl]-amide Trifluoroacetic Acid Salt (12).** The title compound was prepared in 85% yield from 4-cyano-1H-imidazole-2-carboxylic acid (2-cyclohex-1-enyl-4-piperidin-4-yl-phenyl)-amide TFA salt **8** and hydroxyacetaldehyde according to the procedure in the preparation of **11**.  $^1\text{H}$  NMR ( $\text{CD}_3\text{OD}$ , 400 MHz):  $\delta$  8.18 (d, 1H,  $J$  = 8.6 Hz), 8.02 (s, 1H), 7.22 (dd, 1H,  $J$  = 8.4, 2.1 Hz), 7.14 (d, 2H,  $J$  = 2.1 Hz), 5.82 (m, 1H), 3.94 (m, 2H), 3.74 (m, 2H), 3.30 (m, 2H), 3.18 (t, 2H), 2.92 (m, 1H), 2.30 (m, 4H), 2.20–1.98 (m, 4H), 1.96–1.74 (m, 4H). Mass spectrum (ESI,  $m/z$ ): calcd for  $\text{C}_{24}\text{H}_{29}\text{N}_5\text{O}_2$ , 420.2 ( $M + \text{H}$ ); found, 420.2.

**4-Cyano-1H-imidazole-2-carboxylic Acid [2-Cyclohex-1-enyl-4-[1-(2-hydroxy-1-hydroxymethyl-ethyl)-piperidin-4-yl]-phenyl]-amide Trifluoroacetic Acid Salt (14).** To a slurry of 4-cyano-1H-imidazole-2-carboxylic acid (2-cyclohex-1-enyl-4-piperidin-4-yl-phenyl)-amide trifluoroacetic acid salt **8** (81 mg, 0.16 mmol) in  $\text{CH}_2\text{Cl}_2$  (3 mL) was added  $\text{Et}_3\text{N}$  (33  $\mu\text{L}$ , 0.24 mmol). The solution was then treated with 2,2-dimethyl-[1,3]dioxan-5-one (31 mg, 0.24 mmol), and the reaction was allowed to stir for 3 h. At this time,  $\text{NaBH}(\text{OAc})_3$  (51 mg, 0.24 mmol) was added in one portion, and the reaction was allowed to stir for an additional 4 h. The reaction was diluted with  $\text{H}_2\text{O}$  (10 mL) and extracted with  $\text{EtOAc}$  (2  $\times$  25 mL). The organic extracts were dried ( $\text{Na}_2\text{SO}_4$ ) and concentrated in vacuo. Purification by silica gel preparative TLC (10% MeOH– $\text{CHCl}_3$ ) afforded 22 mg (28%) of 4-cyano-1H-imidazole-2-carboxylic acid



{2-cyclohex-1-enyl-4-[1-(2,2-dimethyl-[1,3]dioxan-5-yl)-piperidin-4-yl]-phenyl}-amide (13) as an off-white semisolid. Mass spectrum (ESI,  $m/z$ ): calcd for  $C_{28}H_{35}N_5O_3$ , 490.2 ( $M + H$ ); found, 490.6.

To a solution of 4-cyano-1*H*-imidazole-2-carboxylic acid {2-cyclohex-1-enyl-4-[1-(2,2-dimethyl-[1,3]dioxan-5-yl)-piperidin-4-yl]-phenyl}-amide 13 (22 mg, 0.045 mmol, as prepared above) in THF–H<sub>2</sub>O (1 mL, 4:1 v/v) was added TFA (0.4 mL), and the reaction was allowed to stir for 1 h. Removal of the solvent under vacuum afforded 14 mg (60%) of the title compound as an amber foam. <sup>1</sup>H NMR (CD<sub>3</sub>OD, 400 MHz):  $\delta$  8.17 (d, 1H,  $J = 8.4$  Hz), 8.03 (s, 1H), 7.22 (dd, 1H,  $J = 8.4, 2.0$  Hz), 7.13 (d, 1H,  $J = 2.0$  Hz), 5.83 (s, 1H), 3.98 (d, 4H,  $J = 4.9$  Hz), 3.74–3.78 (m, 2H), 3.46–3.53 (m, 2H), 3.37–3.40 (m, 1H), 2.88–2.96 (m, 1H), 2.29 (br s, 4H), 2.03–2.16 (m, 4H), 1.78–1.90 (m, 4H). Mass spectrum (ESI,  $m/z$ ): calcd for  $C_{25}H_{31}N_5O_3$ , 450.2 ( $M + H$ ); found, 450.2.

**4-Cyano-1*H*-imidazole-2-carboxylic Acid {2-Cyclohex-1-enyl-4-[1-(2-methanesulfonyl-ethyl)-piperidin-4-yl]-phenyl}-amide (15).** *a. Methanesulfonic Acid 2-Methanesulfonyl-ethyl Ester.* To a solution of methanesulfonyl chloride (484 mg, 4.23 mmol) in 15 mL of CH<sub>2</sub>Cl<sub>2</sub> at 0 °C was added 2-methanesulfonyl-ethanol (500 mg, 4.03 mmol) in 10 mL of CH<sub>2</sub>Cl<sub>2</sub> followed by DIEA (1.05 mL, 6.05 mmol) under Ar. The mixture was warmed to room temperature and stirred for 20 h under Ar. The mixture was treated with 100 mL of EtOAc and washed with H<sub>2</sub>O (3  $\times$  20 mL) and brine (20 mL) and was dried (Na<sub>2</sub>SO<sub>4</sub>). Removal of the solvent in vacuo gave 534 mg (66%) of the title compound as a brown oil, which was used directly in the following step without purification. <sup>1</sup>H NMR (CDCl<sub>3</sub>, 400 MHz):  $\delta$  4.67 (d, 2H,  $J = 5.5$  Hz), 3.46 (d, 2H,  $J = 5.5$  Hz), 3.11 (s, 3H), 3.04 (s, 3H).

*b. 4-Cyano-1*H*-imidazole-2-carboxylic Acid {2-Cyclohex-1-enyl-4-[1-(2-methanesulfonyl-ethyl)-piperidin-4-yl]-phenyl}-amide (15).* To a solution of 4-cyano-1*H*-imidazole-2-carboxylic acid (2-cyclohex-1-enyl-4-piperidin-4-yl-phenyl)-amide trifluoroacetic acid salt 8 (85 mg, 0.17 mmol) and DIEA (91  $\mu$ L, 0.52 mmol) in 3 mL of CH<sub>2</sub>Cl<sub>2</sub> at room temperature was added 2-methanesulfonic acid 2-methanesulfonyl-ethyl ester (as prepared in the previous step, 42 mg, 0.21 mmol). The resulting mixture was stirred at room temperature for 3 h. Treated with 50 mL of EtOAc, the mixture was washed with H<sub>2</sub>O (2  $\times$  20 mL) and brine (10 mL) and was dried (Na<sub>2</sub>SO<sub>4</sub>). Removal of the solvent in vacuo followed by flash chromatography of the residue on silica gel (1–3% MeOH/CH<sub>2</sub>Cl<sub>2</sub>) gave 54 mg (65%) of the title compound as a white solid. <sup>1</sup>H NMR (CDCl<sub>3</sub>, 400 MHz):  $\delta$  9.54 (s, 1H), 8.25 (d, 1H,  $J = 8.4$  Hz), 7.72 (s, 1H), 7.15 (dd, 1H,  $J = 8.4, 2.0$  Hz), 7.04 (d, 1H,  $J = 2.0$  Hz), 5.85 (m, 1H), 3.21 (t, 2H,  $J = 6.5$  Hz), 3.09 (s, 3H), 3.02–3.11 (m, 2H), 2.92 (t, 2H,  $J = 6.5$  Hz), 2.52 (dddd, 1H,  $J = 12.1, 12.1, 3.3, 3.3$  Hz), 2.18–2.34 (m, 4H), 2.18 (t, 2H,  $J = 10.8$  Hz), 1.64–1.94 (m, 9H). Mass spectrum (ESI,  $m/z$ ): calcd for  $C_{23}H_{31}N_5O_3S$ , 482.2 ( $M + H$ ); found, 482.2.

**4-Cyano-1*H*-imidazole-2-carboxylic Acid [4-(1-Carbamoylmethyl-piperidin-4-yl)-2-cyclohex-1-enyl-phenyl]-amide Trifluoroacetic Acid Salt (16).** 4-Cyano-1*H*-imidazole-2-carboxylic acid (2-cyclohex-1-enyl-4-piperidin-4-yl-phenyl)-amide TFA salt 8 (50.0 mg, 0.102 mmol), Et<sub>3</sub>N (32.7  $\mu$ L, 0.235 mmol), 2-bromoacetamide (16.9 mg, 0.123 mmol), and 0.5 mL of CH<sub>2</sub>Cl<sub>2</sub> were stirred for 4 h at 25 °C. The reaction was concentrated, and the residue was purified by RP-HPLC (C<sub>18</sub>), eluting with 30–50% CH<sub>3</sub>CN in 0.1% TFA/H<sub>2</sub>O over 12 min to give 42 mg (75%) of the title compound as a white solid. <sup>1</sup>H NMR (CD<sub>3</sub>OD, 400 MHz):  $\delta$  8.14 (d, 1H,  $J = 8.6$  Hz), 8.00 (s, 1H), 7.19 (d, 1H,  $J = 8.4$  Hz), 7.11 (s, 1H), 5.75–5.83 (m, 1H), 3.99 (s, 2H), 3.73 (d, 2H,  $J = 11.4$  Hz), 3.14–3.29 (m, 2H), 2.78–2.97 (m, 1H), 2.19–2.32 (m, 4H), 2.01–2.16 (m, 4H), 1.71–1.90 (m, 4H). Mass spectrum (ESI,  $m/z$ ): calcd for  $C_{24}H_{28}N_6O_2$ , 433.2 ( $M + H$ ); found, 433.2.

**[4-{4-[(4-Cyano-1*H*-imidazole-2-carbonyl)-amino]-3-cyclohex-1-enyl-phenyl}-piperidin-1-yl]-acetic Acid Trifluoroacetic Acid Salt (18).** 4-Cyano-1*H*-imidazole-2-carboxylic acid (2-cyclohex-1-enyl-4-piperidin-4-yl-phenyl)-amide TFA salt 8 (33 mg, 0.067 mmol), *t*-butyl bromoacetate (9.90  $\mu$ L, 0.0675 mmol), Et<sub>3</sub>N (18.8  $\mu$ L, 0.135 mmol), and 0.25 mL of CH<sub>2</sub>Cl<sub>2</sub> were stirred for 10 h at 25 °C. The reaction mixture was loaded on a 5 g SPE cartridge (silica), and 23 mg (70%) of 4-{4-[(4-cyano-1*H*-imidazole-2-carbonyl)-

amino]-3-cyclohex-1-enyl-phenyl}-piperidin-1-yl]-acetic acid *tert*-butyl ester 17 was eluted with 25% EtOAc/CH<sub>2</sub>Cl<sub>2</sub>. This compound was dissolved in 1 mL of CH<sub>2</sub>Cl<sub>2</sub>, 20  $\mu$ L of EtOH and 1 mL of TFA were added, and the reaction was stirred for 3 h at 25 °C. The residue was purified by RP-HPLC (C<sub>18</sub>), eluting with 30–50% CH<sub>3</sub>CN in 0.1% TFA/H<sub>2</sub>O over 12 min to give 10 mg (40%) of the title compound as a white solid. <sup>1</sup>H NMR (CD<sub>3</sub>OD, 400 MHz):  $\delta$  8.16 (d, 1H,  $J = 8.4$  Hz), 8.02 (s, 1H), 7.22 (dd, 1H,  $J = 8.5, 2.0$  Hz), 7.10 (d, 1H,  $J = 1.9$  Hz), 5.72 (m, 1H), 4.04 (s, 2H), 3.76 (m, 2H), 3.22 (m, 2H), 2.90 (m, 1H), 2.29 (m, 4H), 2.10 (m, 4H), 1.82 (m, 4H). Mass spectrum (ESI,  $m/z$ ): calcd for  $C_{24}H_{27}N_5O_3$ , 434.2 ( $M + H$ ); found, 434.2.

**4-Cyano-1-(2-trimethylsilyl-ethoxymethyl)-1*H*-imidazole-2-carboxylic Acid {2-Cyclohex-1-enyl-4-piperidin-4-yl-phenyl}-amide Trifluoroacetic Acid Salt (19).** To a solution of 4-{4-[(4-cyano-1-(2-trimethylsilyl-ethoxymethyl)-1*H*-imidazole-2-carbonyl)-amino]-3-cyclohex-1-enyl-phenyl}-piperidine-1-carboxylic acid *tert*-butyl ester 7 (81 mg, 0.12 mmol) in 18 mL of CH<sub>2</sub>Cl<sub>2</sub> was added 1 mL of EtOH followed by 5 mL of TFA at 0 °C. The resulting solution was stirred at room temperature for only 0.5 h and treated with 20 mL of EtOH followed by 20 mL of *n*-PrOH and 5 mL of H<sub>2</sub>O. The mixture was then concentrated under reduced pressure to give a slightly yellow solid. Flash chromatography of the compound on silica gel (2–4% MeOH/CH<sub>2</sub>Cl<sub>2</sub>) gave 0.87 g (85%) of the title compound as a white solid. <sup>1</sup>H NMR (CDCl<sub>3</sub>, 400 MHz):  $\delta$  9.70 (s, 1H), 9.66 (br s, 1H), 9.15 (m, 1H), 8.29 (d, 1H,  $J = 8.3$  Hz), 7.78 (s, 1H), 7.13 (dd, 1H,  $J = 8.3, 2.2$  Hz), 7.03 (d, 1H,  $J = 2.2$  Hz), 5.95 (s, 2H), 5.83 (m, 1H), 3.66 (t, 2H,  $J = 8.4$  Hz), 3.55 (d, 2H,  $J = 12.3$  Hz), 2.95–3.11 (m, 2H), 2.76 (m, 1H), 2.18–2.33 (m, 4H), 1.99–2.15 (m, 4H), 1.82 (m, 4H), 0.97 (t, 2H,  $J = 8.3$  Hz), 0.00 (s, 9H). Mass spectrum (ESI,  $m/z$ ): calcd for  $C_{28}H_{39}N_5O_2Si$ , 506.3 ( $M + H$ ); found, 506.1.

**4-Cyano-1*H*-imidazole-2-carboxylic Acid {2-Cyclohex-1-enyl-4-[1-(2-morpholin-4-yl-ethyl)-piperidin-4-yl]-phenyl}-amide Bis-trifluoroacetic Acid Salt (20).** *a. 4-Cyano-1-(2-trimethylsilyl-ethoxymethyl)-1*H*-imidazole-2-carboxylic Acid {2-Cyclohex-1-enyl-4-[1-(2-morpholin-4-yl-ethyl)-piperidin-4-yl]-phenyl}-amide. 4-Cyano-1-(2-trimethylsilyl-ethoxymethyl)-1*H*-imidazole-2-carboxylic acid (2-cyclohex-1-enyl-4-piperidin-4-yl-phenyl)-amide TFA salt 19 (830 mg, 1.34 mmol), K<sub>2</sub>CO<sub>3</sub> (600 mg, 4.34 mmol), sodium iodide (40.2 mg, 0.268 mmol), 4-(2-chloroethyl)-morpholine hydrochloride (260 mg, 1.40 mmol), and 5.0 mL of *N,N*-dimethylacetamide were stirred for 8 h at 80 °C. The reaction was diluted with EtOAc (50 mL), washed with saturated aqueous NaHCO<sub>3</sub> (2  $\times$  50 mL) and brine (50 mL), and concentrated. The residue was purified by flash chromatography (silica gel, 5% MeOH/CH<sub>2</sub>Cl<sub>2</sub>) to give 650 mg (78%) of the title compound as a white solid. <sup>1</sup>H NMR (CDCl<sub>3</sub>, 400 MHz):  $\delta$  9.67 (s, 1H), 8.23 (d, 1H,  $J = 8.6$  Hz), 7.78 (s, 1H), 7.14 (dd, 1H,  $J = 8.5, 2.0$  Hz), 7.04 (d, 1H,  $J = 1.9$  Hz), 5.95 (s, 2H), 5.78–5.85 (m, 1H), 3.70–3.74 (m, 4H), 3.62–3.68 (m, 2H), 2.58–2.67 (m, 4H), 2.46–2.57 (m, 4H), 2.24–2.40 (m, 4H), 2.10–2.20 (m, 4H), 1.73–1.92 (m, 7H), 1.60–1.68 (m, 2H), 0.92–1.00 (m, 2H), 0.00 (s, 9H). Mass spectrum (ESI,  $m/z$ ): calcd for  $C_{34}H_{50}N_6O_3Si$ , 619.4 ( $M + H$ ); found, 619.3.*

*b. 4-Cyano-1*H*-imidazole-2-carboxylic Acid {2-Cyclohex-1-enyl-4-[1-(2-morpholin-4-yl-ethyl)-piperidin-4-yl]-phenyl}-amide Trifluoroacetic Acid Salt (20).* To a solution of 4-cyano-1-(2-trimethylsilyl-ethoxymethyl)-1*H*-imidazole-2-carboxylic acid {2-cyclohex-1-enyl-4-[1-(2-morpholin-4-yl-ethyl)-piperidin-4-yl]-phenyl}-amide 19 (650 mg, 1.05 mmol) (as prepared in the previous step) in 10 mL of CH<sub>2</sub>Cl<sub>2</sub> were added 0.3 mL of EtOH and 3.0 mL of TFA, and the reaction was allowed to proceed for 2 h at 25 °C. The reaction was diluted with 10 mL of EtOH and concentrated. The residue was purified by RP-HPLC (C<sub>18</sub>), eluting with 30–50% CH<sub>3</sub>CN in 0.1% TFA/H<sub>2</sub>O over 9 min to give 600 mg (80%) of the title compound as a white solid. <sup>1</sup>H NMR (CD<sub>3</sub>OD, 400 MHz):  $\delta$  8.18 (d, 1H,  $J = 8.4$  Hz), 8.04 (s, 1H), 7.24 (dd, 1H,  $J = 8.4, 2.1$  Hz), 7.14 (d, 1H,  $J = 2.1$  Hz), 5.84 (m, 1H), 3.84 (m, 4H), 3.76 (m, 2H), 3.50 (m, 2H), 3.30–3.10 (m, 4H), 2.92 (m, 5H), 2.30 (m, 4H), 2.20–2.00 (m, 4H), 1.90–1.74 (m, 4H). Mass spectrum (ESI,  $m/z$ ): calcd for  $C_{28}H_{36}N_6O_2$ , 489.2; found, 489.2.

**4-Cyano-1H-imidazole-2-carboxylic Acid [4-(1-Acetyl-piperidin-4-yl)-2-cyclohex-1-enyl-phenyl]-amide (21).** 4-Cyano-1H-imidazole-2-carboxylic acid (2-cyclohex-1-enyl-4-piperidin-4-yl-phenyl)-amide trifluoroacetic acid salt **8** (22.3 mg, 0.0456 mmol) in  $\text{CH}_2\text{Cl}_2$  (1 mL) was treated with  $\text{Et}_3\text{N}$  (22.2  $\mu\text{L}$ , 0.159 mmol) and acetic anhydride (6.03  $\mu\text{L}$ , 0.0638 mmol) at room temperature for 30 min using a procedure similar to that used in the preparation of **23**. Purification of the mixture on a 10 g silica gel SPE cartridge with 10%  $\text{MeOH}/\text{CH}_2\text{Cl}_2$  afforded the title compound (20 mg, 95%) as a white solid.  $^1\text{H}$  NMR ( $\text{CDCl}_3$ , 400 MHz):  $\delta$  13.12 (br s, 1H), 9.58 (s, 1H), 8.34 (d, 1H,  $J = 8.4$  Hz), 7.76 (s, 1H), 7.21 (dd, 1H,  $J = 8.6$ , 2.1 Hz), 7.05 (d, 1H,  $J = 2.1$  Hz), 5.86 (s, 1H), 4.84 (m, 1H), 4.00 (m, 1H), 3.22 (m, 1H), 2.72 (m, 2H), 2.30 (m, 4H), 2.21 (s, 3H), 1.80 (m, 8H). Mass spectrum (ESI,  $m/z$ ): calcd for  $\text{C}_{24}\text{H}_{27}\text{N}_5\text{O}_4$ , 418.2 (M + H); found, 418.1.

**4-Cyano-1H-imidazole-2-carboxylic Acid {2-Cyclohex-1-enyl-4-[1-(pyridine-3-carbonyl)-piperidin-4-yl]-phenyl}-amide (22).** A solution of 4-cyano-1H-imidazole-2-carboxylic acid (2-cyclohex-1-enyl-4-piperidin-4-yl-phenyl)-amide trifluoroacetic acid salt **8** (75.0 mg, 0.152 mmol) in  $\text{CH}_2\text{Cl}_2$  (10 mL) was treated with  $\text{Et}_3\text{N}$  (64.1  $\mu\text{L}$ , 0.460 mmol) and cooled to 0 °C. The mixture was treated with nicotinoyl chloride hydrochloride (30.0 mg, 0.169 mmol) and stirred at 0 °C for 15 min and then at room temperature for 17 h. The reaction mixture was adsorbed directly onto silica gel. Silica gel chromatography (10%  $\text{MeOH}$  in  $\text{EtOAc}$ ) afforded the title compound (61.0 mg, 83%) as a white solid.  $^1\text{H}$  NMR ( $\text{CDCl}_3$ , 400 MHz):  $\delta$  9.51 (br s, 1H), 8.77 (s, 1H), 8.70–8.66 (m, 1H), 8.32 (d, 1H,  $J = 8.4$  Hz), 7.86–7.81 (m, 1H), 7.70 (s, 1H), 7.42–7.37 (m, 1H), 7.17 (d, 1H,  $J = 8.4$  Hz), 7.06–7.04 (m, 1H), 5.87–5.82 (m, 1H), 4.98–4.87 (m, 1H), 3.94–3.84 (m, 1H), 3.29–3.18 (m, 1H), 2.98–2.86 (m, 1H), 2.86–2.76 (m, 1H), 2.34–2.20 (m, 4H), 1.94–1.72 (m, 9H). Mass spectrum (ESI,  $m/z$ ): calcd for  $\text{C}_{28}\text{H}_{28}\text{N}_6\text{O}_2$ , 481.2 (M + H); found, 481.3.

**4-Cyano-1H-imidazole-2-carboxylic Acid {2-Cyclohex-1-enyl-4-[1-(2-dimethylamino-acetyl)-piperidin-4-yl]-phenyl}-amide (23).** A suspension of 4-cyano-1H-imidazole-2-carboxylic acid (2-cyclohex-1-enyl-4-piperidin-4-yl-phenyl)-amide trifluoroacetic acid salt **8** (655 mg, 1.34 mmol) in  $\text{CH}_2\text{Cl}_2$  (15 mL) was cooled to 0 °C, and DIEA (0.932 mL, 5.35 mmol) was added. Dimethylaminoacetyl chloride hydrochloride (211 mg, 1.34 mmol) was then added portion wise over 10 min. The reaction mixture was stirred at 0 °C for 30 min and allowed to warm to room temperature and stir for 2 h. The solvent was removed in vacuo, and the resulting residue was partitioned between brine and  $\text{CH}_2\text{Cl}_2$ . The organic layer was separated, dried ( $\text{Na}_2\text{SO}_4$ ), and concentrated. The residue obtained was purified on silica (5%  $\text{MeOH}:\text{CH}_2\text{Cl}_2$ ) to obtain 432 mg (70%) of the title compound as a white solid.  $^1\text{H}$  NMR ( $\text{CDCl}_3$ , 400 MHz):  $\delta$  9.49 (s, 1H), 8.24 (d, 1H,  $J = 8.3$  Hz), 7.70 (s, 1H), 7.12 (dd, 1H,  $J = 8.4$ , 2.1 Hz), 7.01 (d, 1H,  $J = 2.1$  Hz), 5.82 (m, 1H), 4.75 (d, 1H,  $J = 13.4$  Hz), 4.13 (d, 1H,  $J = 13.4$  Hz), 3.57 (d, 1H,  $J = 14.2$  Hz), 3.18 (d, 1H,  $J = 14.2$  Hz), 3.12 (td, 1H,  $J = 13.3$ , 2.4 Hz), 2.73 (dddd, 1H,  $J = 11.9$ , 11.9, 3.8, 3.8 Hz), 2.65 (ddd, 1H,  $J = 13.3$ , 13.3, 2.4 Hz), 2.40 (s, 6H), 2.18–2.32 (m, 4H), 1.60–1.98 (m, 9H). Mass spectrum (ESI,  $m/z$ ): calcd for  $\text{C}_{26}\text{H}_{32}\text{N}_6\text{O}_2$ , 461.3 (M + H); found, 461.2.

**5-Cyano-1H-imidazole-2-carboxylic Acid {2-Cyclohex-1-enyl-4-[1-(R)-(+)-(2,3-dihydroxy-propionyl)-piperidin-4-yl]-phenyl}-amide (25).** a. **5-Cyano-1H-imidazole-2-carboxylic Acid {2-Cyclohex-1-enyl-4-[1-(R)-(+)-(2,2-dimethyl-1,3-dioxolane-4-carbonyl)-piperidin-4-yl]-phenyl}-amide (24).** To a solution of methyl (R)-(+)-2,2-dimethyl-1,3-dioxolane-4-carboxylate (0.16 mL, 1.0 mmol) in  $\text{MeOH}$  (2 mL), 2 N KOH (0.50 mL, 1.0 mmol) was added. The resulting solution was stirred at room temperature for 20 min and concentrated in vacuo. The residue obtained was suspended in ether (10 mL) and sonicated for 5 min. The ether was then removed, and the resulting residue was placed under high vacuum for 4 h to obtain (R)-(+)-2,2-dimethyl-1,3-dioxolane-4-carboxylic acid potassium salt (173 mg, 94%), which was directly used in the next step without purification.

To a solution of 4-cyano-1H-imidazole-2-carboxylic acid (2-cyclohex-1-enyl-4-piperidin-4-yl-phenyl)-amide trifluoroacetic acid salt **8** (40 mg, 0.082 mmol) in  $\text{CH}_2\text{Cl}_2$  (1.5 mL) was added a mixture of (R)-(+)-2,2-dimethyl-1,3-dioxolane-4-carboxylic acid potassium salt

(as prepared above, 18 mg, 0.090 mmol), EDCI (19 mg, 0.090 mmol), HOBt (13 mg, 0.090 mmol), and DIEA (42  $\mu\text{L}$ , 0.24 mmol). The resulting mixture was stirred at room temperature for 6 h. Water (10 mL) was added, and the organic layer was separated, dried ( $\text{Na}_2\text{SO}_4$ ), and concentrated. The residue obtained was chromatographed on silica (2%  $\text{MeOH}/\text{CH}_2\text{Cl}_2$ ) to obtain the title compound (47 mg, 97%).  $^1\text{H}$  NMR ( $\text{CDCl}_3$ , 400 MHz):  $\delta$  9.57 (d, 1H,  $J = 7.9$  Hz), 8.31 (dd, 1H,  $J = 8.4$ , 6.0 Hz), 7.76 (s, 1H), 7.18 (dd, 1H,  $J = 8.6$ , 1.9 Hz), 7.05 (s, 1H), 5.84–5.88 (m, 1H), 4.76–4.82 (m, 2H), 4.45 (dt, 1H,  $J = 8.4$ , 5.7 Hz), 4.30 (d, 1H,  $J = 13.3$  Hz), 4.06–4.21 (m, 2H), 3.08–3.29 (m, 1H), 2.67–2.85 (m, 2H), 2.31 (br s, 2H), 2.25 (br s, 2H), 1.90–2.02 (m, 2H), 1.73–1.90 (m, 6H), 1.43 (d, 6H,  $J = 4.4$  Hz). Mass spectrum (ESI,  $m/z$ ): calcd for  $\text{C}_{28}\text{H}_{33}\text{N}_5\text{O}_4$ , 504.2 (M + H); found, 503.9.

b. **5-Cyano-1H-imidazole-2-carboxylic Acid {2-Cyclohex-1-enyl-4-[1-(R)-(+)-(2,3-dihydroxy-propionyl)-piperidin-4-yl]-phenyl}-amide (25).** To a solution of 5-cyano-1H-imidazole-2-carboxylic acid {2-cyclohex-1-enyl-4-[1-(R)-(+)-(2,2-dimethyl-1,3-dioxolane-4-carbonyl)-piperidin-4-yl]-phenyl}-amide **24** (as prepared in the previous step, 45 mg, 0.090 mmol) in  $\text{MeOH}$  (1 mL) was added aqueous 2 N HCl (2 mL). The resulting mixture was stirred at room temperature for 12 h. Solvents were removed in vacuo, and the resulting residue was placed under vacuum for 4 h. Ether (10 mL) was added, and the mixture was sonicated for 5 min. The ether was removed in vacuo, and the residue was placed under vacuum for 12 h to obtain the title compound (21.3 mg, 52%).  $^1\text{H}$  NMR ( $\text{DMSO}$ , 400 MHz):  $\delta$  14.1 (br s, 1H), 9.85 (s, 1H), 8.32 (s, 1H), 7.92 (d, 1H,  $J = 8.4$  Hz), 7.18 (dd, 1H,  $J = 8.4$ , 2.1 Hz), 7.13 (d, 1H,  $J = 2.1$  Hz), 5.72 (br s, 1H), 4.51 (m, 1H), 4.33 (m, 1H), 4.15 (m, 1H), 3.55 (m, 1H), 3.43 (m, 1H), 3.08 (m, 1H), 2.81 (m, 1H), 2.63 (m, 1H), 2.12–2.24 (m, 4H), 1.31–1.38 (m, 10 H). Mass spectrum (ESI,  $m/z$ ): calcd for  $\text{C}_{25}\text{H}_{29}\text{N}_5\text{O}_4$ , 464.2 (M + H); found, 464.1.

**4-Cyano-1H-imidazole-2-carboxylic Acid {2-Cyclohex-1-enyl-4-[1-(2-(2-hydroxy-ethylamino)-acetyl)-piperidin-4-yl]-phenyl}-amide Trifluoroacetic Acid Salt (28).** a. **[2-(4-[4-(4-Cyano-1H-imidazole-2-carbonyl)-amino]-3-cyclohex-1-enyl-phenyl)-piperidin-1-yl]-2-oxo-ethyl-carbamic Acid tert-Butyl Ester (26).** A solution of *N*-Boc-glycine (286 mg, 1.63 mmol) in  $\text{CH}_2\text{Cl}_2$  (10 mL) was treated with DIEA (854  $\mu\text{L}$ , 4.90 mmol), HOBt (265 mg, 1.96 mmol), and EDCI (376 mg, 1.96 mmol). The mixture was stirred at room temperature for 10 min and added to a suspension of 4-cyano-1H-imidazole-2-carboxylic acid (2-cyclohex-1-enyl-4-piperidin-4-yl-phenyl)-amide trifluoroacetic acid salt **8** (800 mg, 1.63 mmol) in  $\text{CH}_2\text{Cl}_2$  (20 mL). The solution was stirred at room temperature for 17 h. Solvents were evaporated in vacuo. Silica gel chromatography (50%  $\text{EtOAc}$  in hexanes) afforded the title compound (0.41 g, 47%) as a white solid.  $^1\text{H}$  NMR ( $\text{CDCl}_3$ , 400 MHz):  $\delta$  9.53 (s, 1H), 8.26 (d, 1H,  $J = 8.4$  Hz), 7.80–7.78 (m, 1H), 7.71 (s, 1H), 7.45–7.43 (m, 1H), 7.06 (d, 1H,  $J = 8.4$  Hz), 7.00 (s, 1H), 5.83 (br s, 1H), 5.76 (br s, 1H), 4.78–4.68 (m, 1H), 3.96–3.85 (m, 2H), 3.17–3.03 (m, 1H), 2.78–2.63 (m, 2H), 2.29 (br s, 2H), 2.22 (br s, 2H), 1.95–1.87 (m, 2H), 1.86–1.72 (m, 4H), 1.70–1.55 (m, 2H), 1.44 (s, 9H). Mass spectrum (ESI,  $m/z$ ): calcd for  $\text{C}_{29}\text{H}_{36}\text{N}_6\text{O}_4$ , 533.3 (M + H); found, 532.9.

b. **4-Cyano-1H-imidazole-2-carboxylic Acid {2-Cyclohex-1-enyl-4-[1-(2-(2-hydroxy-ethylamino)-acetyl)-piperidin-4-yl]-phenyl}-amide Trifluoroacetic Acid Salt (28).** A solution of [2-(4-[4-(4-cyano-1H-imidazole-2-carbonyl)-amino]-3-cyclohex-1-enyl-phenyl)-piperidin-1-yl]-2-oxo-ethyl-carbamic acid *tert*-butyl ester **26** (as prepared in the previous step, 0.410 g, 0.770 mmol) in  $\text{CH}_2\text{Cl}_2$  (20 mL) was treated with  $\text{EtOH}$  (0.2 mL) and TFA (6 mL). The mixture stirred at room temperature for 45 min, and the solvents were evaporated in vacuo to afford 4-cyano-1H-imidazole-2-carboxylic acid {4-[1-(2-amino-acetyl)-piperidin-4-yl]-2-cyclohex-1-enyl-phenyl}-amide trifluoroacetic acid salt **27**, which was used directly in the next step. Mass spectrum (ESI,  $m/z$ ): calcd for  $\text{C}_{24}\text{H}_{28}\text{N}_6\text{O}_2$ , 433.2 (M + H); found, 433.2.

A suspension of 4-cyano-1H-imidazole-2-carboxylic acid {4-[1-(2-amino-acetyl)-piperidin-4-yl]-2-cyclohex-1-enyl-phenyl}-amide trifluoroacetic acid salt **27** (0.420 g, 0.769 mmol) in  $\text{CH}_2\text{Cl}_2$  (20 mL) was treated with  $\text{Na}(\text{OAc})_3\text{BH}$  (0.326 g, 1.54 mmol) and solid glyoxal (44.6 mg, 0.769 mmol). The mixture was stirred at room temperature



for 1 h, and the solvent was evaporated in vacuo. The residue was taken up in MeOH, the solids were filtered off, and the filtrate was concentrated in vacuo. Reverse phase HPLC (C-18 column) (20–60% acetonitrile in water with 0.1% TFA over 30 min) afforded the title compound (83 mg, 19% over two steps) as a white solid.  $^1\text{H}$  NMR ( $\text{CD}_3\text{OD}$ , 400 MHz):  $\delta$  8.06–8.16 (m, 1H), 7.99–8.05 (m, 1H), 7.18 (m, 1H), 7.07 (m, 1H), 5.81 (m, 1H), 4.64 (m, 1H), 3.74–4.24 (m, 4H), 3.18–3.29 (m, 2H), 2.77–2.93 (m, 2H), 2.27 (m, 4H), 1.52–2.00 (m, 10H). Mass spectrum (ESI,  $m/z$ ): calcd for  $\text{C}_{26}\text{H}_{32}\text{N}_6\text{O}_3$ , 477.2 (M + H); found, 477.2.

**4-Cyano-1H-imidazole-2-carboxylic Acid (2-Cyclohex-1-enyl-4-[1-[2-(2-hydroxy-ethyl)-methyl-amino-acetyl]-piperidin-4-yl]-phenyl)-amide Trifluoroacetic Acid Salt (29).** A solution of 4-cyano-1H-imidazole-2-carboxylic acid (2-cyclohex-1-enyl-4-[1-[2-(2-hydroxy-ethylamino)-acetyl]-piperidin-4-yl]-phenyl)-amide trifluoroacetic acid salt **28** (50 mg, 0.085 mmol) in MeOH (3 mL) was treated with  $\text{Na}(\text{OAc})_3\text{BH}$  (40 mg, 0.19 mmol) and 37% aqueous formaldehyde (8.2  $\mu\text{L}$ , 0.10 mmol). The mixture was stirred at room temperature for 5.5 h, and the solvents were removed in vacuo. Reverse phase HPLC (C-18 column) (10–50% acetonitrile in water with 0.1% TFA over 30 min) afforded the title compound (19.5 mg, 47%) as a white solid.  $^1\text{H}$  NMR ( $\text{CD}_3\text{OD}$ , 400 MHz):  $\delta$  8.12 (d, 1H,  $J$  = 8.4 Hz), 8.02 (s, 1H), 7.19 (dd, 1H,  $J$  = 8.4, 2.0 Hz), 7.09 (d, 1H,  $J$  = 2.0 Hz), 5.84–5.79 (m, 1H), 4.72–4.64 (m, 1H), 4.39–4.23 (m, 2H), 3.84–3.79 (m, 1H), 3.31–3.21 (m, 1H), 3.03–2.94 (m, 6H), 2.92–2.80 (m, 2H), 2.32–2.24 (m, 4H), 2.00–1.90 (m, 2H), 1.90–1.76 (m, 5H), 1.78–1.59 (m, 2H). Mass spectrum (ESI,  $m/z$ ): calcd for  $\text{C}_{27}\text{H}_{34}\text{N}_6\text{O}_3$ , 491.3 (M + H); found, 491.2.

**4-Cyano-1H-imidazole-2-carboxylic Acid [2-Cyclohex-1-enyl-4-[1-(2-methanesulfonyl-acetyl)-piperidin-4-yl]-phenyl]-amide (30).** Methanesulfonyl-acetic acid (14 mg, 0.10 mmol), EDCI (30 mg, 0.15 mmol), HOBt (14 mg, 0.10 mmol), DIEA (36  $\mu\text{L}$ , 0.20 mmol), and 0.5 mL of  $\text{CH}_2\text{Cl}_2$  were stirred at 25  $^\circ\text{C}$ . After 10 min, a solution containing 4-cyano-1H-imidazole-2-carboxylic acid (2-cyclohex-1-enyl-4-piperidin-4-yl-phenyl)-amide TFA salt **8** (40 mg, 0.082 mmol) and  $\text{Et}_3\text{N}$  (14  $\mu\text{L}$ , 0.10 mmol) in 0.5 mL of  $\text{CH}_2\text{Cl}_2$  was added, and the reaction was allowed to proceed for 10 h at 25  $^\circ\text{C}$ . The reaction mixture was loaded on a 5 g SPE cartridge (silica) and eluted with 10%  $\text{EtOH}/\text{EtOAc}$  to give 10 mg (25%) of the title compound as a white solid.  $^1\text{H}$  NMR ( $\text{CDCl}_3$ , 400 MHz):  $\delta$  11.60 (br s, 1H), 9.52 (s, 1H), 8.30 (dd, 1H,  $J$  = 8.4, 1.6 Hz), 7.74 (d, 1H,  $J$  = 2.0 Hz), 7.15 (dd, 1H,  $J$  = 8.6, 1.9 Hz), 7.03 (d, 1H,  $J$  = 2.0 Hz), 5.86 (m, 1H), 4.84 (m, 1H), 4.18 (s, 2H), 4.12 (m, 1H), 3.32 (m, 1H), 3.20 (s, 3H), 2.82 (m, 2H), 2.30 (m, 4H), 1.98 (m, 2H), 1.84 (m, 5H), 1.72 (m, 1H). Mass spectrum (ESI,  $m/z$ ): calcd for  $\text{C}_{25}\text{H}_{29}\text{N}_5\text{O}_4\text{S}$ , 496.2 (M + H); found, 496.2.

**4-Cyano-1H-imidazole-2-carboxylic Acid [2-Cyclohex-1-enyl-4-[1-(1-oxy-pyridine-3-carbonyl)-piperidin-4-yl]-phenyl]-amide (31).** The title compound was prepared in 32% yield from 4-cyano-1H-imidazole-2-carboxylic acid (2-cyclohex-1-enyl-4-piperidin-4-yl-phenyl)-amide trifluoroacetic acid salt **8** and nicotinic acid-N oxide according to the procedure for the preparation of **35**.  $^1\text{H}$  NMR ( $\text{CDCl}_3$ , 400 MHz):  $\delta$  13.95 (br. s., 1H), 9.44 (s, 1H), 8.52 (s, 1H), 8.32 (d,  $J$  = 6.1 Hz, 1H), 8.07 (d,  $J$  = 8.1 Hz, 1H), 7.74 (s, 1H), 7.51–7.56 (m, 1H), 7.41–7.50 (m, 1H), 6.95 (s, 1H), 6.86–6.93 (m, 1H), 5.79 (br. s., 1H), 4.80 (br. s., 1H), 3.88 (d,  $J$  = 12.6 Hz, 1H), 3.17 (br. s., 1H), 2.86 (br. s., 1H), 2.66 (t,  $J$  = 11.6 Hz, 1H), 2.12–2.33 (m, 4H), 2.00 (br. s., 1H), 1.47–1.88 (m, 7H). Mass spectrum (ESI,  $m/z$ ): calcd for  $\text{C}_{28}\text{H}_{28}\text{N}_6\text{O}_3$ , 497.2 (M + H); found, 497.2.

**4-Cyano-1H-imidazole-2-carboxylic Acid [2-Cyclohex-1-enyl-4-[1-(1-oxy-pyridine-4-carbonyl)-piperidin-4-yl]-phenyl]-amide (32).** The title compound was prepared in 42% yield from 4-cyano-1H-imidazole-2-carboxylic acid (2-cyclohex-1-enyl-4-piperidin-4-yl-phenyl)-amide trifluoroacetic acid salt **8** and 1-oxy-isonicotinic acid in 42% yield according to the procedure for the preparation of **35**.  $^1\text{H}$  NMR ( $\text{CDCl}_3$ ):  $\delta$  13.64 (br s, 1H), 11.17 (br s, 1H), 9.50 (s, 1H), 8.53 (d, 2H,  $J$  = 7.0 Hz), 8.30 (d, 1H,  $J$  = 8.6 Hz), 7.73 (s, 1H), 7.46 (d, 2H,  $J$  = 7.0 Hz), 7.28 (m, 1H), 7.09–7.18 (m, 1H), 7.03 (d, 1H,  $J$  = 1.9 Hz), 5.80–5.88 (m, 1H), 3.62–3.76 (m, 2H), 3.11 (qd, 2H,  $J$  = 7.3, 4.9 Hz), 2.81 (t, 1H,  $J$  = 12.8 Hz), 2.29 (br s, 2H), 2.23 (br s, 2H),

1.75–1.89 (m, 6H). Mass spectrum (ESI,  $m/z$ ): calcd for  $\text{C}_{28}\text{H}_{28}\text{N}_6\text{O}_3$ , 497.2 (M + H); found, 497.2.

**4-Cyano-1H-imidazole-2-carboxylic Acid [2-Cyclohex-1-enyl-4-[1-(2-1H-imidazol-4-yl-acetyl)-piperidin-4-yl]-phenyl]-amide Trifluoroacetic Acid Salt (33).** The title compound was prepared from 4-cyano-1H-imidazole-2-carboxylic acid (2-cyclohex-1-enyl-4-piperidin-4-yl-phenyl)-amide TFA salt **8** in 60% yield according to the procedure for the preparation of **35** using (1H-imidazol-4-yl)-acetic acid.  $^1\text{H}$  NMR ( $\text{CD}_3\text{OD}$ , 400 MHz):  $\delta$  8.88 (s, 1H), 8.12 (d, 1H,  $J$  = 1.6 Hz), 8.02 (s, 1H), 7.44 (s, 1H), 7.20 (dd, 1H,  $J$  = 8.4, 2.1 Hz), 7.10 (d, 1H,  $J$  = 2.1 Hz), 5.82 (m, 1H), 4.70 (m, 1H), 4.18 (m, 1H), 4.06 (m, 2H), 3.36 (m, 1H), 2.84 (m, 2H), 2.30 (m, 4H), 2.00–1.70 (m, 7H), 1.64 (m, 1H). Mass spectrum (ESI,  $m/z$ ): calcd for  $\text{C}_{27}\text{H}_{29}\text{N}_7\text{O}_2$ , 484.2 (M + H); found, 484.2.

**4-Cyano-1H-imidazole-2-carboxylic Acid [2-Cyclohex-1-enyl-4-[1-[2-(1-methyl-1H-imidazol-4-yl)-acetyl]-piperidin-4-yl]-phenyl]-amide Trifluoroacetic Acid Salt (34).** The title compound was prepared from 4-cyano-1H-imidazole-2-carboxylic acid (2-cyclohex-1-enyl-4-piperidin-4-yl-phenyl)-amide TFA salt **8** in 66% yield according to the procedure for the preparation of **35** using (1-methyl-1H-imidazol-4-yl)-acetic acid.  $^1\text{H}$  NMR ( $\text{CD}_3\text{OD}$ , 400 MHz):  $\delta$  8.82 (s, 1H), 8.10 (d, 1H,  $J$  = 8.4 Hz), 8.00 (s, 1H), 7.42 (s, 1H), 7.16 (dd, 1H,  $J$  = 8.6, 2.1 Hz), 7.06 (d, 1H,  $J$  = 2.1 Hz), 5.80 (m, 1H), 4.66 (m, 1H), 4.12 (m, 1H), 4.04 (m, 2H), 3.92 (s, 3H), 3.28 (m, 1H), 2.82 (m, 2H), 2.26 (m, 4H), 2.00–1.70 (m, 7H), 1.64 (m, 1H). Mass spectrum (ESI,  $m/z$ ): calcd for  $\text{C}_{28}\text{H}_{31}\text{N}_7\text{O}_2$ , 498.2 (M + H); found, 498.2.

**4-Cyano-1H-imidazole-2-carboxylic Acid [2-Cyclohex-1-enyl-4-[1-(2-pyridin-2-yl-acetyl)-piperidin-4-yl]-phenyl]-amide Trifluoroacetic Acid Salt (35).** 4-Cyano-1H-imidazole-2-carboxylic acid (2-cyclohex-1-enyl-4-piperidin-4-yl-phenyl)-amide TFA salt **8** (25.0 mg, 0.0511 mmol), pyridin-2-yl-acetic acid hydrochloride (9.75 mg, 0.0562 mmol), EDCI (11.7 mg, 0.0613 mmol), HOBt (8.28 mg, 0.0613 mmol), DIEA (26.7  $\mu\text{L}$ , 0.153 mmol), and 0.2 mL of DMF were stirred at 25  $^\circ\text{C}$  for 10 h. The reaction was diluted with 2 mL of  $\text{H}_2\text{O}$ , and the residue was purified by RP-HPLC ( $\text{C}_{18}$ ), eluting with 30–50%  $\text{CH}_3\text{CN}$  in 0.1% TFA/ $\text{H}_2\text{O}$  over 9 min to give 22 mg (70%) of the title compound as a white solid.  $^1\text{H}$  NMR ( $\text{CD}_3\text{OD}$ , 400 MHz):  $\delta$  8.82 (d, 1H,  $J$  = 5.6 Hz), 8.52 (td, 1H,  $J$  = 7.8, 1.7 Hz), 8.14 (d, 1H,  $J$  = 8.4 Hz), 8.04 (s, 1H), 7.96 (m, 2H), 7.20 (dd, 1H,  $J$  = 8.4, 2.1 Hz), 7.10 (d, 1H,  $J$  = 2.1), 5.82 (m, 1H), 4.68 (m, 1H), 4.32 (m, 2H), 4.18 (m, 1H), 3.40 (m, 1H), 2.88 (m, 2H), 2.30 (m, 4H), 2.06–1.60 (m, 8H). Mass spectrum (ESI,  $m/z$ ): calcd for  $\text{C}_{29}\text{H}_{30}\text{N}_6\text{O}_2$ , 495.2 (M + H); found, 495.2.

**4-Cyano-1H-imidazole-2-carboxylic Acid [2-Cyclohex-1-enyl-4-[1-(2-pyridin-3-yl-acetyl)-piperidin-4-yl]-phenyl]-amide Trifluoroacetic Acid Salt (36).** The title compound was prepared from 4-cyano-1H-imidazole-2-carboxylic acid (2-cyclohex-1-enyl-4-piperidin-4-yl-phenyl)-amide TFA salt **8** in 68% yield according to the procedure for the preparation of **35** using pyridin-3-yl-acetic acid.  $^1\text{H}$  NMR ( $\text{CD}_3\text{OD}$ , 400 MHz):  $\delta$  8.80 (s, 1H), 8.77 (d, 1H,  $J$  = 5.7 Hz), 8.54 (d, 1H,  $J$  = 8.0 Hz), 8.10 (d, 1H,  $J$  = 8.4 Hz), 8.06 (dd, 1H,  $J$  = 7.8, 6.1 Hz), 7.98 (s, 1H), 7.18 (dd, 1H,  $J$  = 8.4, 2.0 Hz), 7.08 (d, 1H,  $J$  = 2.0 Hz), 5.78 (m, 1H), 4.68 (m, 1H), 4.20 (m, 1H), 4.18 (s, 2H), 3.36 (m, 1H), 2.84 (m, 2H), 2.28 (m, 4H), 2.06–1.70 (m, 7H), 1.62 (m, 1H). Mass spectrum (ESI,  $m/z$ ): calcd for  $\text{C}_{29}\text{H}_{30}\text{N}_6\text{O}_2$ , 495.2 (M + H); found, 495.2.

**4-Cyano-1H-imidazole-2-carboxylic Acid [2-Cyclohex-1-enyl-4-[1-(2-pyridin-4-yl-acetyl)-piperidin-4-yl]-phenyl]-amide Trifluoroacetic Acid Salt (37).** The title compound was prepared from 4-cyano-1H-imidazole-2-carboxylic acid (2-cyclohex-1-enyl-4-piperidin-4-yl-phenyl)-amide TFA salt **8** in 58% yield according to the procedure for the preparation of **35** using pyridin-4-yl-acetic acid.  $^1\text{H}$  NMR ( $\text{CD}_3\text{OD}$ , 400 MHz):  $\delta$  8.78 (d, 2H,  $J$  = 5.1 Hz), 8.12 (d, 1H,  $J$  = 8.4 Hz), 8.03 (s, 1H), 7.99 (d, 2H,  $J$  = 6.1 Hz), 7.18 (dd, 1H,  $J$  = 8.4, 1.9 Hz), 7.08 (d, 1H,  $J$  = 1.9 Hz), 5.80 (m, 1H), 4.66 (m, 1H), 4.22 (s, 2H), 4.18 (m, 1H), 3.34 (m, 1H), 2.84 (m, 2H), 2.24 (m, 4H), 2.00–1.70 (m, 7H), 1.64 (m, 1H). Mass spectrum (ESI,  $m/z$ ): calcd for  $\text{C}_{29}\text{H}_{30}\text{N}_6\text{O}_2$ , 495.2 (M + H); found, 495.2.

**4-Cyano-1H-imidazole-2-carboxylic Acid [2-Cyclohex-1-enyl-4-[1-(3-morpholin-4-yl-propionyl)-piperidin-4-yl]-phenyl]-amide (38).** 3-Morpholin-4-yl-propionic acid potassium salt

(93.8 mg, 0.475 mmol, prepared from 3-morpholin-4-yl-propionic acid ethyl ester and 6 N KOH as described in the preparation of **39**), 4-cyano-1H-imidazole-2-carboxylic acid (2-cyclohex-1-enyl-4-piperidin-4-yl-phenyl)-amide trifluoroacetic acid salt **8** (179 mg, 0.366 mmol), EDCI (83.7 mg, 0.439 mmol), and HOBT (69.2 mg, 0.512 mmol) were taken up in DMF (4 mL). To the stirred slurry was added DIEA (157  $\mu$ L, 0.901 mmol), and the reaction was allowed to stir overnight. The reaction was diluted with H<sub>2</sub>O (10 mL) and extracted with EtOAc (2  $\times$  25 mL). The combined organic extracts were dried (Na<sub>2</sub>SO<sub>4</sub>) and concentrated in vacuo, and the crude product was purified by silica gel preparative TLC (6% of 7 M NH<sub>3</sub> in MeOH/CH<sub>2</sub>Cl<sub>2</sub>) to afford 10.4 mg (6%) of the title compound as a white solid. <sup>1</sup>H NMR (CDCl<sub>3</sub>, 400 MHz):  $\delta$  9.51 (s, 1H), 8.26 (d, 1H, *J* = 8.2 Hz), 7.70 (s, 1H), 7.09–7.13 (m, 1H), 6.99–7.00 (m, 1H), 6.81–6.82 (m, 1H), 5.81–5.82 (m, 1H), 4.76–4.81 (m, 2H), 3.97–4.02 (m, 2H), 3.72 (br s, 4H), 3.10–3.17 (m, 2H), 2.74–2.76 (m, 4H), 2.58–2.63 (m, 3H), 2.52 (br s, 4H), 2.22–2.31 (m, 3H), 1.49–1.93 (m, 5H). Mass spectrum (ESI, *m/z*): calcd for C<sub>29</sub>H<sub>36</sub>N<sub>6</sub>O<sub>3</sub>, 517.3 (*M* + *H*); found, 517.3.

**4-Cyano-1H-imidazole-2-carboxylic Acid {2-Cyclohex-1-enyl-4-[1-(2-morpholin-4-yl-acetyl)-piperidin-4-yl]-phenyl}-amide (39).** To a solution of morpholin-4-yl-acetic acid ethyl ester (117 mg, 0.675 mmol) in ethanol (4 mL) was added 6 N KOH (110  $\mu$ L, 0.660 mmol) via syringe, and stirring was continued for 3 h. Concentration in vacuo afforded 122 mg (100%) of morpholin-4-yl-acetic acid potassium salt. To a mixture of morpholin-4-yl-acetic acid potassium salt (29.2 mg, 0.160 mmol), 4-cyano-1H-imidazole-2-carboxylic acid **8** (2-cyclohex-1-enyl-4-piperidin-4-yl-phenyl)-amide trifluoroacetic acid salt (65.1 mg, 0.133 mmol), and bromotri-(pyrrolidino)phosphonium hexafluorophosphate (PyBroP) (93.0 mg, 0.199 mmol) in CH<sub>2</sub>Cl<sub>2</sub> (4 mL) was added DIEA (51.0  $\mu$ L, 0.293 mmol), and the reaction was allowed to stir overnight. The reaction was diluted with CH<sub>2</sub>Cl<sub>2</sub> (50 mL), washed with H<sub>2</sub>O (2  $\times$  25 mL), dried (Na<sub>2</sub>SO<sub>4</sub>), and concentrated in vacuo. Purification of the crude product by silica gel preparative TLC (6% of 7 M NH<sub>3</sub> in MeOH/CH<sub>2</sub>Cl<sub>2</sub>) afforded 8.1 mg (12%) of the title compound as a white solid. <sup>1</sup>H NMR (CDCl<sub>3</sub>, 400 MHz):  $\delta$  9.48 (s, 1H), 8.27 (d, 1H, *J* = 8.1 Hz), 7.73 (s, 1H), 7.12 (dd, 1H, *J* = 0.6, 8.0 Hz), 7.00 (s, 1H), 5.82 (s, 1H), 4.73–4.77 (m, 1H), 4.16–4.22 (m, 1H), 3.72 (br s, 4H), 3.35–3.40 (m, 1H), 3.09–3.23 (m, 6H), 2.53–2.78 (m, 5H), 2.20–2.29 (m, 4H), 1.68–2.04 (dt, 5H). Mass spectrum (ESI, *m/z*): calcd for C<sub>28</sub>H<sub>34</sub>N<sub>6</sub>O<sub>3</sub>, 503.3 (*M* + *H*); found, 503.1.

**4-Cyano-1H-imidazole-2-carboxylic Acid {4-[1-(3-Amino-3-methyl-butyl)-piperidin-4-yl]-2-cyclohex-1-enyl-phenyl}-amide Trifluoroacetic Acid Salt (41).** *a.* [3-(4-{4-[(4-Cyano-1H-imidazole-2-carbonyl)-amino]-3-cyclohex-1-enyl-phenyl]-piperidin-1-yl]-1,1-dimethyl-3-oxo-propyl]-carbamic Acid *tert*-Butyl Ester (**40**). To a mixture of 4-cyano-1H-imidazole-2-carboxylic acid (2-cyclohex-1-enyl-4-piperidin-4-yl-phenyl)-amide trifluoroacetic acid salt **8** (40.0 mg, 0.0818 mmol), 3-*tert*-butoxycarbonylamino-3-methyl-butyl acid (21.4 mg, 0.0981 mmol), and PyBroP (55.0 mg, 0.0981 mmol) in 1,2-dichloroethane (2 mL) was added DIEA (42.7  $\mu$ L, 0.245 mmol), and the resulting mixture was stirred at room temperature for 24 h under Ar. The mixture was diluted with EtOAc (30 mL), washed with H<sub>2</sub>O (2  $\times$  10 mL) and brine (10 mL), dried over Na<sub>2</sub>SO<sub>4</sub>, and then concentrated in vacuo. The residue was purified by flash chromatography (silica gel, 10–40% EtOAc/hexane) to give 33.0 mg (70%) of the title compound as a colorless oil. <sup>1</sup>H NMR (CDCl<sub>3</sub>, 400 MHz):  $\delta$  12.93 (br s, 1H), 9.55 (s, 1H), 8.28 (d, 1H, *J* = 8.4 Hz), 7.74 (d, 1H, *J* = 2.5 Hz), 7.15 (dd, 1H, *J* = 8.5, 2.1 Hz), 7.02 (d, 1H, *J* = 2.1 Hz), 5.84 (d, 1H, *J* = 3.5, 2.0 Hz), 5.60 (br s, 1H), 4.85 (d, 1H, *J* = 13.5 Hz), 4.17 (d, 1H, *J* = 13.9 Hz), 3.16 (t, 1H, *J* = 12.1 Hz), 2.56–2.84 (m, 4H), 2.29 (d, 2H, *J* = 3.4 Hz), 2.23 (br s, 2H), 1.67–1.94 (m, 8H), 1.45 (d, 6H, *J* = 1.7 Hz), 1.41 (s, 9H). Mass spectrum (ESI, *m/z*): calcd for C<sub>32</sub>H<sub>42</sub>N<sub>6</sub>O<sub>4</sub>, 575.3 (*M* + *H*); found, 574.8.

*b.* 4-Cyano-1H-imidazole-2-carboxylic Acid {4-[1-(3-Amino-3-methyl-butyl)-piperidin-4-yl]-2-cyclohex-1-enyl-phenyl}-amide Trifluoroacetic Acid Salt (**41**). To a solution of [3-(4-{4-[(4-cyano-1H-imidazole-2-carbonyl)-amino]-3-cyclohex-1-enyl-phenyl]-piperidin-1-yl]-1,1-dimethyl-3-oxo-propyl]-carbamic Acid *tert*-butyl ester (33.0 mg, 0.0574 mmol) (as prepared in the previous step) in 3 mL

of CH<sub>2</sub>Cl<sub>2</sub> and 0.10 mL of EtOH at 0 °C was added 1.0 mL of TFA, and the mixture was warmed to room temperature and stirred for 3 h. The reaction was diluted with 3 mL of *n*-PrOH and then concentrated in vacuo. The residue was purified by flash chromatography (silica gel, 3–8% MeOH/CH<sub>2</sub>Cl<sub>2</sub>) to give 33.5 mg (99%) of the title compound as a white solid. <sup>1</sup>H NMR (CDCl<sub>3</sub>, 400 MHz):  $\delta$  13.3 (s, 1H), 9.52 (s, 1H), 8.57 (br s, 2H), 8.26 (d, 1H, *J* = 8.6 Hz), 7.69 (s, 1H), 7.02 (dd, 1H, *J* = 8.6, 1.7 Hz), 6.98 (d, 1H, *J* = 1.7 Hz), 5.78 (m, 1H), 4.67 (br d, 1H, *J* = 13.4 Hz), 3.88 (br d, 1H, *J* = 13.4 Hz), 3.10 (m, 1H), 2.55–2.85 (m, 4H), 2.23 (m, 4H), 1.72–2.01 (m, 8H), 1.50 (s, 6H). Mass spectrum (ESI, *m/z*): calcd for C<sub>27</sub>H<sub>34</sub>N<sub>6</sub>O<sub>2</sub>, 475.3 (*M* + *H*); found, 475.1.

**5-Cyano-1H-imidazole-2-carboxylic Acid {4-[1-(2-Amino-2-methyl-propionyl)-piperidin-4-yl]-2-cyclohex-1-enyl-phenyl}-amide Trifluoroacetic Acid Salt (43).** *a.* {2-[4-(4-{4-Cyano-1-(2-trimethylsilylanyl-ethoxymethyl)-1H-imidazole-2-carbonyl]-amino}-3-cyclohex-1-enyl-phenyl)-piperidin-1-yl]-1,1-dimethyl-2-oxo-ethyl]-carbamic Acid *tert*-Butyl Ester (**42**). To a solution of 4-{4-[(4-cyano-1-(2-trimethylsilylanyl-ethoxymethyl)-1H-imidazole-2-carbonyl]-amino}-3-cyclohex-1-enyl-phenyl)-piperidine-1-carboxylic acid *tert*-butyl ester **7** (231 mg, 0.380 mmol) in 2.5 mL of CH<sub>2</sub>Cl<sub>2</sub> and 0.4 mL of EtOH was added 700  $\mu$ L of TFA, and the solution stirred for 3 h at 25 °C. The reaction was diluted with 4 mL of EtOH and then concentrated to give ca. a 2:1 mixture of 5-cyano-1-(2-trimethylsilylanyl-ethoxymethyl)-1H-imidazole-2-carboxylic acid (2-cyclohex-1-enyl-4-piperidin-4-yl-phenyl)-amide trifluoroacetic acid salt **19** and starting material by <sup>1</sup>H NMR and LC/MS, which was used in the following step without further purification. The mixture in 3 mL of CH<sub>2</sub>Cl<sub>2</sub> was added to a solution of 2-*tert*-butoxycarbonylamino-2-methyl-propionic acid (53.0 mg, 0.261 mmol), DIEA (122  $\mu$ L, 0.700 mmol), and PyBroP (144 mg, 0.309 mmol) in 3 mL of CH<sub>2</sub>Cl<sub>2</sub>, and the reaction was stirred at 25 °C overnight. The reaction was diluted with EtOAc (25 mL) and washed with saturated aqueous NaHCO<sub>3</sub> (1  $\times$  25 mL) and brine (25 mL), and the organic layer was dried over Na<sub>2</sub>SO<sub>4</sub> and then concentrated. Purification of the residue by preparative TLC (50% EtOAc–hexanes) afforded 40.0 mg (15%) of the title compound as a white solid. <sup>1</sup>H NMR (CDCl<sub>3</sub>, 400 MHz):  $\delta$  9.67 (s, 1H), 8.24 (d, 1H, *J* = 8.4 Hz), 7.78 (s, 1H), 7.68–7.76 (m, 1H), 7.48–7.59 (m, 1H), 7.10 (dd, 1H, *J* = 8.5, 1.9 Hz), 7.00 (d, 1H, *J* = 2.1 Hz), 5.96 (s, 2H), 5.78–5.85 (m, 1H), 4.24–4.38 (m, 1H), 3.62–3.76 (m, 3H), 2.66–2.77 (m, 1H), 2.28 (br s, 2H), 2.22 (br s, 2H), 1.42–1.57 (s, 18H), 0.94–1.01 (m, 2H), 0.81–0.92 (m, 6H), 0.01 (s, 9H). Mass Spectrum (ESI, *m/z*): calcd for C<sub>37</sub>H<sub>54</sub>N<sub>6</sub>O<sub>5</sub>Si, 691.3 (*M* + *H*); found, 691.1.

*b.* 5-Cyano-1H-imidazole-2-carboxylic Acid {4-[1-(2-Amino-2-methyl-propionyl)-piperidin-4-yl]-2-cyclohex-1-enyl-phenyl}-amide Trifluoroacetic Acid Salt (**43**). To a solution of {2-[4-(4-{4-cyano-1-(2-trimethylsilylanyl-ethoxymethyl)-1H-imidazole-2-carbonyl]-amino}-3-cyclohex-1-enyl-phenyl)-piperidin-1-yl]-1,1-dimethyl-2-oxo-ethyl]-carbamic acid *tert*-butyl ester **42** (40.0 mg, 0.0579 mmol, as prepared in the previous step) in 2 mL of CH<sub>2</sub>Cl<sub>2</sub> and 20  $\mu$ L of EtOH was added 1.5 mL of TFA. The solution was stirred for 3 h at 25 °C, diluted with 2 mL of EtOH, and concentrated in vacuo. Trituration of the residue with ether afforded 8.4 mg (29%) of the title compound as a white solid. <sup>1</sup>H NMR (CD<sub>3</sub>OD, 400 MHz):  $\delta$  8.10 (d, 1H, *J* = 8.4 Hz), 8.00 (s, 1H), 7.16 (d, 1H, *J* = 8.4 Hz), 7.07 (s, 1H), 5.79 (s, 1H), 4.55–4.48 (m, 1H), 3.30 (s, 6H), 2.89–2.87 (m, 2H), 2.40–2.25 (m, 4H), 1.96–1.93 (m, 2H), 1.86–1.83 (m, 6H), 1.64–1.61 (m, 2H). Mass spectrum (ESI, *m/z*): calcd for C<sub>26</sub>H<sub>32</sub>N<sub>6</sub>O<sub>2</sub>, 461.3 (*M* + *H*); found, 461.3.

**4-{4-[(4-Cyano-1H-imidazole-2-carbonyl)-amino]-3-cyclohex-1-enyl-phenyl}-piperidine-1-carboxylic Acid (2-Hydroxy-ethyl)-amide (44).** *a.* 4-{4-[(4-Cyano-1-(2-trimethylsilylanyl-ethoxymethyl)-1H-imidazole-2-carbonyl)-amino]-3-cyclohex-1-enyl-phenyl}-piperidine-1-carboxylic Acid (2-Hydroxy-ethyl)-amide. A solution of 4-cyano-1-(2-trimethylsilylanyl-ethoxymethyl)-1H-imidazole-2-carboxylic acid (2-cyclohex-1-enyl-4-piperidin-4-yl-phenyl)-amide trifluoroacetic acid salt **19** (116 mg, 0.192 mmol) and DIEA (134  $\mu$ L, 0.770 mmol) in 4 mL of CH<sub>2</sub>Cl<sub>2</sub> was added slowly to solution of triphosgene (22.8 mg, 0.0770 mmol) in 4 mL of CH<sub>2</sub>Cl<sub>2</sub> at –78 °C under Ar. The mixture was stirred at –78 °C for 15 min, warmed to



room temperature, stirred for 15 min, and cooled to  $-78^{\circ}\text{C}$  again. A suspension of 2-amino-ethanol (350  $\mu\text{L}$ , 5.77 mmol) in 4 mL of THF was added, and the resulting mixture was warmed to room temperature and stirred for 20 h under Ar. Treated with 100 mL of EtOAc, the mixture was washed with  $\text{H}_2\text{O}$  ( $3 \times 20\text{ mL}$ ) and brine (20 mL) and was dried ( $\text{Na}_2\text{SO}_4$ ). Removal of the solvent in vacuo followed by flash chromatography of the residue on silica gel (10% EtOAc/ $\text{CH}_2\text{Cl}_2$  then 5% MeOH/ $\text{CH}_2\text{Cl}_2$ ) gave 95 mg (83%) of the title compound as a colorless oil.  $^1\text{H}$  NMR ( $\text{CDCl}_3$ , 400 MHz):  $\delta$  9.68 (s, 1H), 8.25 (d, 1H,  $J = 8.4\text{ Hz}$ ), 7.77 (s, 1H), 7.12 (dd, 1H,  $J = 8.4$ , 2.2 Hz), 7.01 (d, 1H,  $J = 2.2\text{ Hz}$ ), 5.94 (s, 2H), 5.83 (m, 1H), 4.96 (t, 1H,  $J = 5.6\text{ Hz}$ ), 4.11 (d, 2H,  $J = 13.3\text{ Hz}$ ), 3.75 (ddd, 2H,  $J = 4.4\text{ Hz}$ ), 3.66 (t, 2H,  $J = 8.3\text{ Hz}$ ), 3.44 (ddd, 2H,  $J = 5.0\text{ Hz}$ ), 3.36 (t, 1H,  $J = 4.6\text{ Hz}$ ), 2.91 (ddd, 2H,  $J = 13.0$ , 2.2 Hz), 2.66 (dddd, 1H,  $J = 12.2$ , 12.2, 3.3, 3.3 Hz), 2.18–2.33 (m, 4H), 1.75–1.91 (m, 6H), 1.67 (dddd, 2H,  $J = 12.9$ , 12.9, 12.9, 4.0 Hz), 0.97 (t, 2H,  $J = 8.3\text{ Hz}$ ), 0.00 (s, 9H). Mass spectrum (ESI,  $m/z$ ): calcd for  $\text{C}_{31}\text{H}_{44}\text{N}_6\text{O}_4\text{Si}$ , 593.3 ( $M + \text{H}$ ); found, 593.1.

**b.** 4-[4-[(4-Cyano-1H-imidazole-2-carbonyl)-amino]-3-cyclohex-1-enyl-phenyl]-piperidine-1-carboxylic Acid (2-Hydroxy-ethyl)-amide (44). To a solution of 4-[4-[(4-cyano-1-(2-trimethylsilyl-ethoxy-methyl)-1H-imidazole-2-carbonyl]-amino]-3-cyclohex-1-enyl-phenyl]-piperidine-1-carboxylic acid (2-hydroxy-ethyl)-amide (as prepared in the previous step, 95 mg, 0.16 mmol) in 3 mL of  $\text{CH}_2\text{Cl}_2$  was added 0.10 mL of EtOH followed by 1.0 mL of TFA. The resulting solution was stirred at room temperature for 6 h. Removal of the solvent under reduced pressure followed by flash chromatography of the residue on silica gel (2–8% MeOH/ $\text{CH}_2\text{Cl}_2$ ) gave 68 mg (92%) of the title compound as a white solid.  $^1\text{H}$  NMR ( $\text{CD}_3\text{OD}$ , 400 MHz):  $\delta$  8.09 (d, 1H,  $J = 8.4\text{ Hz}$ ), 8.00 (s, 1H), 7.15 (dd, 1H,  $J = 8.4$ , 2.2 Hz), 7.06 (d, 1H,  $J = 2.2\text{ Hz}$ ), 5.79 (m, 1H), 4.15 (dd, 2H,  $J = 13.3$ , 1.1 Hz), 3.61 (t, 2H,  $J = 5.9\text{ Hz}$ ), 3.27–3.32 (m, 2H), 2.90 (ddd, 2H,  $J = 13.0$ , 13.0, 2.5 Hz), 2.73 (dddd, 1H,  $J = 12.1$ , 12.1, 2.6, 2.6 Hz), 2.26 (m, 4H), 1.73–1.88 (m, 6H), 1.62 (dddd, 2H,  $J = 12.6$ , 12.6, 12.6, 4.0 Hz). Mass spectrum (ESI,  $m/z$ ): calcd for  $\text{C}_{25}\text{H}_{30}\text{N}_6\text{O}_3$ , 463.2 ( $M + \text{H}$ ); found, 463.2.

**4-[4-[(4-Cyano-1H-imidazole-2-carbonyl)-amino]-3-cyclohex-1-enyl-phenyl]-piperidine-1-carboxylic Acid Amide (45).** 4-Cyano-1H-imidazole-2-carboxylic acid (2-cyclohex-1-enyl-4-piperidin-4-yl-phenyl)-amide TFA salt (51.0 mg, 0.104 mmol) 8,  $\text{Et}_3\text{N}$  (21.7  $\mu\text{L}$ , 0.156 mmol), trimethylsilyl isocyanate (15.5  $\mu\text{L}$ , 0.114 mmol), and 1.0 mL of  $\text{CH}_2\text{Cl}_2$  were stirred for 10 h at  $25^{\circ}\text{C}$ . The solvent was evaporated, and the residue was purified by RP-HPLC ( $\text{C}_{18}$ ), eluting with 35–60%  $\text{CH}_3\text{CN}$  in 0.1% TFA/ $\text{H}_2\text{O}$  over 11 min to give 30 mg (70%) of the title compound as a white solid.  $^1\text{H}$  NMR ( $\text{DMSO}-d_6$ , 400 MHz):  $\delta$  14.28 (br s, 1H), 9.76 (s, 1H), 8.34 (d, 1H,  $J = 2.56\text{ Hz}$ ), 7.84 (d, 1H,  $J = 8.1\text{ Hz}$ ), 7.18 (dd, 1H,  $J = 8.5$ , 2.2 Hz), 7.08 (d, 1H,  $J = 1.9\text{ Hz}$ ), 6.00 (br s, 2H), 5.72 (m, 1H), 4.18 (m, 2H), 2.80–2.60 (m, 3H), 2.24–2.10 (m, 4H), 1.80–1.60 (m, 6H), 1.50 (m, 2H). Mass spectrum (ESI,  $m/z$ ): calcd for  $\text{C}_{23}\text{H}_{26}\text{N}_6\text{O}$ , 419.2 ( $M + \text{H}$ ); found, 419.0.

**Biology. Kinase Assays.** Assays for FMS and the other kinases listed in Table 5 were carried out using a fluorescence polarization competition immunoassay format and have been described elsewhere in detail.<sup>24</sup> The full cytoplasmic regions of FMS (538–972) encompassing the tyrosine kinase domain were expressed and purified from a baculovirus system.<sup>30</sup> The FMS kinase assay measured FMS-mediated phosphorylation of tyrosine residues present on a synthetic FMS<sub>555–568</sub> peptide (SYEGNSYTFIDPTQ). To each well of a black 96-well microplate (catalog no. 42-000-0117, Molecular Devices, Sunnyvale, CA), 5  $\mu\text{L}$  of compound solution (in 4% DMSO in assay buffer) was mixed with 2  $\mu\text{L}$  of 3.5 nM FMS, 25 mM  $\text{MgCl}_2$  in assay buffer (100 mM HEPES, pH 7.5, 1 mM DTT, and 0.01% Tween-20), and 2  $\mu\text{L}$  of 1540  $\mu\text{M}$  peptide in assay buffer. The kinase reaction was initiated by adding 1  $\mu\text{L}$  of 10 mM ATP in assay buffer. The final concentrations in the 10  $\mu\text{L}$  reaction mixture were 100 mM HEPES, pH 7.5, 1 mM DTT, 0.01% Tween-20, 2% DMSO, 308  $\mu\text{M}$  SYEGNSYTFIDPTQ, 1 mM ATP, 5 mM  $\text{MgCl}_2$ , and 0.7 nM FMS. The plates were incubated at room temperature for 80 min. Reactions were stopped by the addition of 1.2  $\mu\text{L}$  of 50 mM EDTA. Each well

then received 10  $\mu\text{L}$  of a 1:1:3 mixture of 10 $\times$  antiphosphotyrosine antibody, 10 $\times$  PTK green tracer, and fluorescence polarization dilution buffer (catalog no. P2837, Invitrogen, Carlsbad, CA). The plates were incubated for 30 min at room temperature, and the fluorescence polarization was read (485 nm excitation, 530 nm emission) on an Analyst plate reader (Molecular Devices). Fluorescence polarization values for positive (EDTA) and negative (DMSO) controls were used to define 100 and 0% inhibition of the FMS reaction.

**Cellular Assays.** Functional inhibition of CSF-1R was assessed using murine bone marrow-derived macrophages as previously described.<sup>24</sup> Macrophages were plated in 96-well culture plates at a density of 5000 cells/well in 100  $\mu\text{L}$  of  $\alpha$ -MEM containing 10% FCS. After overnight culture, wells were supplemented with the addition of 50  $\mu\text{L}$  of media containing 15 ng/mL CSF-1, 3  $\mu\text{M}$  indomethacin, and a dilution series of test compound. The cells were cultured for 30 h at  $37^{\circ}\text{C}$  and 5%  $\text{CO}_2$ . During the final 6 h, cultures were supplemented with an additional 30  $\mu\text{L}$  of media containing a 1:500 dilution of bromodeoxyuridine (BrdU) reagent, and incorporation of BrdU into cellular DNA was quantified using a specific ELISA (catalog no. X1327K) from Exalpha Corporation (Watertown, MA). Inhibition of cellular LCK was determined as described.<sup>65</sup> Jurkat cells ( $10^5$ /well) (ATCC) with graded concentrations of 23 were plated into wells precoated with CD3 $\epsilon$  antibody (R&D Systems). PMA was added to a final concentration of 10 ng/mL, and IL-2 secreted into 24 h culture supernatants was measured by ELISA (R&D Systems). As described previously in detail, inhibition of cellular AXL was based on measurement of GAS6-induced AXL phosphorylation in HEK cells transfected to express AXL, and cellular ITD-FLT3, KIT, and TRKA inhibition were based assays of ITD-FLT3, KIT, and TRKA-dependent cell proliferation.<sup>24</sup>

**MV-4-11 and M-07e Leukemia Cell Line Proliferation Assays.** The functional impact on cellular FLT3 activity was determined by measuring compound inhibition of MV-4-11 (ATCC no. CRL-9591) cell proliferation, and M-07e (DSMZ no. ACC 104) cells were used to assess compound effects on cellular KIT activity. MV-4-11 cells grew independent of growth factor due to expression of a constitutive active FLT3 mutation, and M-07e cells were driven to proliferate in a KIT-dependent fashion by 25 ng/mL stem cell factor. Following a culture period of 72 h, relative cell numbers were determined using CellTiterGlo reagent (Promega).

**Biochemical PD Mouse Model.** Groups of six B6C3F1 mice (Taconic Farms) were given oral doses of vehicle [aqueous 20% hydroxypropyl- $\beta$ -cyclodextrin (HP $\beta$ CD)] or test article in vehicle. Eight hours later, mice were administered saline alone or saline containing 1  $\mu\text{g}$  of recombinant mouse CSF-1 (Cell Biosciences Inc., Norwood, MA) via the tail vein. Fifteen minutes after CSF-1 injection, mice were sacrificed, and spleens were isolated and snap-frozen on dry ice. The frozen tissue was homogenized in 1 mL of Trizol (Invitrogen) per 50 mg of tissue, RNA was purified, and RT-PCR was performed to assess c-fos mRNA expression as described previously.<sup>24</sup>

**CIA-Induced Arthritis Model.** The CIA model was performed by Bolder BioPath, Inc. (Boulder, CO). Male B10RIII (Jackson Laboratories) were immunized with type II collagen (Elastin Products), in Freund's complete adjuvant (with supplemental *M. tuberculosis* 4 mg/mL, Difco) on days 0 and 15. On day 12, animals were randomized by body weight into groups ( $n = 15$ ), and dosing was initiated and continued every day (BID, 12 h intervals) for a total of 14 days. On day 26, mice were euthanized, paws were fixed in buffered formalin, and toluidine blue stained sections were prepared for histopathology. Inflammation, cartilage damage, pannus invasion, and bone erosion were each scored using five-point scales corresponding to minimal, mild, moderate, marked, and severe changes. Inflammation was scored as the presence of inflammatory cells and edema. Pannus was scored as tissue invasion of cartilage and subchondral bone and destruction of joint architecture. Cartilage damage was scored as the loss of toluidine blue staining, chondrocyte loss, and collagen disruption. Bone resorption was scored for areas of resorption of medullary trabecular and cortical bone and for the abundance of osteoclasts.

**Adjuvant-Induced Arthritis Model.** The adjuvant-induced arthritis study was performed by Bolder BioPath, Inc. Male Lewis rats (Harlan

catalog no. 1439444), 165–185 g, were anesthetized with isoflurane and injected with 100  $\mu$ L of Freund's complete adjuvant (FCA, Sigma)/lipoidal amine (LA, Sigma) at the base of the tail on day 0. Twice daily oral dosing was initiated on day 8 (the first day of clinical disease) with 23 or vehicle (0.5% hydroxypropylmethylcellulose/0.5% Tween-80). Rats were sacrificed on day 14, and spleens and hind paws were weighed. Both hind paws were then fixed in formalin, decalcified in 5% formic acid, and processed for H&E microscopy. H&E sections of paws were scored for bone resorption using a five-point scale as described in detail previously.<sup>20</sup> Sections were scored additionally for inflammation using a five-point scale for minimal, mild, moderate, marked, and severe leukocytic infiltration and edema. Osteoclast counts ( $n = 5$ , 400 $\times$  fields) were performed on ankles in the areas of greatest bone resorption. Histological sections prepared for ED1 immunohistochemistry were treated for 3 min with proteinase K to expose masked epitopes, and the endogenous peroxidase activity was deactivated with 3% hydrogen peroxidase. Sections were blocked for 1 h with 5% horse serum and for 30 min with Avidin–Biotin solution (SP-2001, Vector Corporation, Burlingame, CA) prior to a 1 h of incubation with ED1 primary antibody (mouse antirat CD68, MCA341R, Serotec, Oxford, United Kingdom). Bound antibody was detected using the ABC-AP Rat kit (PK-6102, Vector) and a DAB Substrate kit (SK-4100, Vector). The sections were lightly counterstained, and the each section was visually scanned under 40 $\times$  magnification. Hot spots were defined as areas with markedly increased ED1 positive cell density containing >30 ED1 positive cells. Only hot spots in the soft tissue were counted to avoid inclusion of ED1 positive osteoclasts.

**SCW-Induced Arthritis Model.** Female Lewis rats (80–100 g each) were purchased from Charles River. SCW peptidoglycan-polysaccharide polymers (PG-PS 10S) were purchased from Becton Dickinson (catalog no. 210866). On day 0, rats were anesthetized using isoflurane and injected ip with PG-PS 10S equivalent to 15  $\mu$ g of rhamnose/gram (body weight) in the lower left quadrant of the abdomen. Control rats were treated in a similar manner with sterile saline. On day 5, rats injected with PG-PS 10S that showed a robust acute phase arthritic response based on joint swelling were randomized into the treatment groups. In an initial study, animals were dosed orally BID beginning on day 8 until sacrifice on day 19. In a second study, animals were dosed orally BID beginning on day 18 until sacrifice on day 39. Compound 23 was formulated in 20% HP $\beta$ CD, and the dose volume was 6 mL/kg. Calipers were used to measure the width (anterior to posterior surface) of the left and right hind ankles of each rat. Each ankle was measured three times and averaged. Hind paw inflammation clinical scores were assigned based on swelling and erythema as follows: 1 = ankle involvement only; 2 = involvement of ankle and proximal 1/2 of tarsal joint; 3 = involvement of the ankle and entire tarsal joint down to the metatarsal joints; and 4 = involvement of the entire paw including the digits. Scores of both hind paws were summed for a maximal score of 8. Digital radiographs of the left paws were prepared using a VetTek Universal AP500 (Del Medical Imaging Corporation, Franklin Park, IL). Hind paws were assessed for ED1 positive cells using immunohistochemistry as described above for the adjuvant arthritis model.

**Statistical Analysis.** Ankle thickness, bone erosion scores, osteoclast counts, and c-fos expression values (means  $\pm$  SEs) were analyzed for group differences using the Student's *t* test. Significance was set at  $p \leq 0.05$  unless indicated otherwise.

## ■ ASSOCIATED CONTENT

### ● Supporting Information

Supplementary data collection, refinement statistics, and crystallization/soaking conditions for cocrystal structures of FMS with compounds 8 and 49. This material is available free of charge via the Internet at <http://pubs.acs.org>.

### Accession Codes

PDB IDs are as follows: 3KRL and 3KRJ.

## ■ AUTHOR INFORMATION

### Corresponding Author

\*E-mail: [cillig@its.jnj.com](mailto:cillig@its.jnj.com).

## ■ ACKNOWLEDGMENTS

We thank Alison Bendele and Mike Bendele at Bolder BioPath Inc. for performing the mouse CIA and the rat adjuvant-induced arthritis studies.

## ■ ABBREVIATIONS

BMDM, bone marrow-derived macrophage (cellular assay); CIA, collagen-induced arthritis; CSF-1, colony-stimulating factor-1; CSF-1R, colony-stimulating factor-1 receptor; CV, cardiovascular; CYP, cytochrome P450 enzyme; EDCI, *N*-(3-dimethylaminopropyl)-*N'*-ethylcarbodiimide hydrochloride; FMS, the product of the cellular proto-oncogene homologue of the feline McDonough sarcoma virus oncogene; H&E stain, hematoxylin and eosin stain; hERG, human ether-a-go-go-related gene potassium channel; HOBt, 1-hydroxybenzotriazole; HP $\beta$ CD, 2-hydroxypropyl- $\beta$ -cyclodextrin; IDR, idiosyncratic drug reaction; M-CSF, macrophage colony-stimulating factor; M-CSFR, macrophage colony-stimulating factor receptor; MTX, methotrexate; PD, pharmacodynamic; PK, pharmacokinetics; QT, the interval in a heartbeat measured from the beginning of the QRS complex to the end of the T wave; SCW, streptococcal cell wall; RA, rheumatoid arthritis; SAR, structure–activity relationship; SEM, trimethylsilylethoxymethyl; TNF, tumor necrosis factor

## ■ REFERENCES

- (1) Lundkvist, J.; Kastang, F.; Kobelt, G. The burden of rheumatoid arthritis and access to treatment: Health burden and costs. *Eur. J. Health Econ.* **2008**, *8* (Suppl. 2), S49–S60.
- (2) Maggon, K. Global arthritis market review 2008 (World top ten RA drugs); <http://knol.google.com/k/global-arthritis-market-review-2008-world-top-ten-ra-drugs#> (accessed January 3, 2011).
- (3) Lipsky, P. E.; van der Heijde, D. M. F. M.; Clair, E. W. St.; Furst, D. E.; Breedveld, F. C.; Kalden, J. R.; Smolen, J. S.; Weisman, M.; Emery, P.; Feldmann, M.; Harriman, G. R.; Maini, R. N. Infliximab and methotrexate in the treatment of rheumatoid arthritis. *N. Engl. J. Med.* **2000**, *343*, 1594–1602.
- (4) (a) Esposito, E.; Cuzzocrea, S. TNF-alpha as a therapeutic target in inflammatory diseases, ischemia-reperfusion injury and trauma. *Curr. Med. Chem.* **2009**, *16*, 3152–3167. (b) Ranganathan, P. An update on pharmacogenomics in rheumatoid arthritis with a focus on TNF-blocking agents. *Curr. Opin. Mol. Ther.* **2008**, *10*, 562–567.
- (5) Fujiwara, N.; Kobayashi, K. Macrophages in inflammation. *Curr. Drug Target Inflamm. Allergy* **2005**, *4*, 281–286.
- (6) Tak, P. P.; Smeets, T. J.; Daha, M. R.; Kluin, P. M.; Meijers, K. A.; Brand, R.; Meinders, A. E.; Breedveld, F. C. Analysis of the synovial cell infiltrate in early rheumatoid synovial tissue in relation to disease activity. *Arthritis Rheum.* **1997**, *40*, 217–25.
- (7) Haringman, J. J.; Gerlag, D. M.; Zwiderman, A. H.; Smeets, T. J. M.; Kraan, M. C.; Baeten, D.; McInnes, I. B.; Bresnahan, B.; Tak, P. P. Synovial tissue macrophages: A sensitive biomarker for response to treatment in patients with rheumatoid arthritis. *Ann. Rheum. Dis.* **2005**, *64*, 834–838.
- (8) Pixley, F. J.; Stanley, E. R. CSF-1 regulation of the wandering macrophage: complexity in action. *Trends Cell Biol.* **2004**, *14*, 628–638.
- (9) Hamilton, J. A. Colony-stimulating factors in inflammation and autoimmunity. *Nature Rev. Immunol.* **2008**, *8*, 533–544.
- (10) Hamilton, J. A.; Filonzi, E. L.; Ianches, G. Regulation of macrophage colony-stimulating factor (CSF-1) production in cultured human synovial fibroblasts. *Growth Factors* **1993**, *9*, 157–65.

- (11) Campbell, I. K.; Ianches, G.; Hamilton, J. A. Production of macrophage colony-stimulating factor (CSF-1) by human articular cartilage and chondrocytes. Modulation by interleukin-1 and tumor necrosis factor alpha. *Biochim. Biophys. Acta* **1993**, *1182*, 57–63.
- (12) Nakano, K.; Okada, Y.; Saito, K.; Tanikawa, R.; Sawamukai, N.; Sasaguri, Y.; Kohro, T.; Wada, Y.; Kodama, T.; Tanaka, Y. Rheumatoid synovial endothelial cells produce macrophage colony-stimulating factor leading to osteoclastogenesis in rheumatoid arthritis. *Rheumatology* **2007**, *46*, 597–603.
- (13) Kawaji, H.; Yokomuro, K.; Kikuchi, K.; Somoto, Y.; Shirai, Y. Macrophage colony-stimulating factor in patients with rheumatoid arthritis. *Nippon Ika Daigaku Zasshi* **1995**, *62*, 260–270.
- (14) Ritchlin, C.; Dwyer, E.; Bucala, R.; Winchester, R. Sustained and distinctive patterns of gene activation in synovial fibroblasts and whole synovial tissue obtained from inflammatory synovitis. *Scand. J. Immunol.* **1994**, *40*, 292–298.
- (15) Takei, I.; Takagi, M.; Ida, H.; Ogino, T.; Santavirta, S.; Konttinen, Y. T. High macrophage-colony stimulating factor levels in synovial fluid of loose artificial hip joints. *J. Rheumatol.* **2000**, *27*, 894–899.
- (16) Bischof, R. J.; Zafropoulis, D.; Hamilton, J. A.; Campbell, I. K. Exacerbation of acute inflammatory arthritis by the colony-stimulating factors CSF-1 and granulocyte macrophage (GM-CSF): Evidence of macrophage infiltration and local proliferation. *Clin. Exp. Immunol.* **2000**, *119*, 361–367.
- (17) Abd, A. H.; Savage, N. W.; Halliday, W. J.; Hume, D. A. The role of macrophages in experimental arthritis induced by *Streptococcus agalactiae* sonicate: actions of macrophage colony-stimulating factor (CSF-1) and other macrophage-modulating agents. *Lymphokine Cytokine Res.* **1991**, *10*, 43–50.
- (18) Campbell, I. K.; Rich, M. J.; Bischof, R. J.; Hamilton, J. A. The colony-stimulating factors and collagen-induced arthritis: Exacerbation of disease by M-CSF and G-CSF and requirement for endogenous M-CSF. *J. Leukocyte Biol.* **2000**, *68*, 144–150.
- (19) Ohno, H.; Uemura, Y.; Murooka, H.; Takanashi, H.; Tokieda, T.; Ohseki, Y.; Kubo, K.; Serizawa, I. The orally-active and selective c-Fms tyrosine kinase inhibitor Ki20227 inhibits disease progression in a collagen-induced arthritis mouse model. *Eur. J. Immunol.* **2008**, *38*, 283–298.
- (20) Huang, H.; Hutta, D. A.; Rinker, J. M.; Hu, H.; Parsons, W. H.; Schubert, C.; Desjarlais, R. L.; Crysler, C. S.; Chaikin, M. A.; Donatelli, R. R.; Chen, Y.; Cheng, D.; Zhou, Z.; Yurkow, E.; Manthey, C. L.; Player, M. R. Pyrido[2,3-*d*]pyrimidin-5-ones: A novel class of antiinflammatory macrophage colony-stimulating factor-1 receptor inhibitors. *J. Med. Chem.* **2009**, *52*, 1081–1091.
- (21) Meyers, M. J.; Pelc, M.; Kamtekar, S.; Day, J.; Poda, G. I.; Hall, M. K.; Michener, M. L.; Reitz, B. A.; Mathis, K. J.; Pierce, B. S.; Parikh, M. D.; Mischke, D. A.; Long, S. A.; Parlow, J. J.; Anderson, D. A.; Thorarensen, A. Structure-based drug design enables conversion of a DFG-in binding CSF-1R kinase inhibitor to a DFG-out binding mode. *Bioorg. Med. Chem. Lett.* **2010**, *20*, 1543–1547.
- (22) Paniagua, R. T.; Chang, A.; Mariano, M. M.; Stein, E. A.; Wang, Q.; Lindstrom, T. M.; Sharpe, O.; Roscow, C.; Ho, P. P.; Lee, D. M.; Robinson, W. H. c-Fms-mediated differentiation and priming of monocyte lineage cells plays a central role in autoimmune arthritis. *Arthritis Res. Ther.* **2010**, *12*, R32.
- (23) Ando, W.; Hashimoto, J.; Nampai, A.; Tsuboi, H.; Tateishi, K.; Ono, T.; Nakamura, N.; Ochi, T.; Yoshikawa, H. Imatinib mesylate inhibits osteoclastogenesis and joint destruction in rats with collagen-induced arthritis (CIA). *J. Bone Miner. Metab.* **2006**, *24*, 274–282.
- (24) Manthey, C. L.; Johnson, D. L.; Illig, C. R.; Tuman, R. W.; Zhou, Z.; Baker, J. F.; Chaikin, M. A.; Donatelli, R. R.; Franks, C. F.; Zeng, L.; Crysler, C.; Chen, Y.; Yurkow, E. J.; Boczon, L.; Meegalla, S. K.; Wilson, K. J.; Wall, M. J.; Chen, J.; Ballentine, S. K.; Ott, H.; Baumann, C.; Lawrence, D.; Tomczuk, B. E.; Molloy, C. J. JNJ-28312141, a novel orally active colony-stimulating factor-1 receptor/FMS-related receptor tyrosine kinase-3 receptor tyrosine kinase inhibitor with potential utility in solid tumors, bone metastases, and acute myeloid leukemia. *Mol. Cancer Ther.* **2009**, *8*, 3151–3161.
- (25) Miyaura, N.; Suzuki, A. Palladium-catalyzed cross-coupling reactions of organoboron compounds. *Chem. Rev.* **1995**, *95*, 2457–2483.
- (26) Wustrow, D. J.; Wise, L. D. Coupling of arylboronic acid with a partially reduced pyridine derivative. *Synthesis* **1991**, 993–995.
- (27) Wall, M. J.; Schubert, C.; Illig, C. R. Cyano-substituted 2-carboxyimidazoles: Synthesis of 4-cyano-1-[[2-(trimethylsilyl)-ethoxy]methyl]-1H-imidazole-2-carboxylate potassium salt. *Synthesis* **2008**, 3377–3379.
- (28) Wall, M. J.; Chen, J.; Meegalla, S.; Ballentine, S. K.; Wilson, K. J.; Desjarlais, R. L.; Schubert, C.; Chaikin, M. A.; Crysler, C. S.; Petrounia, I.; Donatelli, R. R.; Yurkow, E. J.; Boczon, L.; Mazzula, M.; Player, M. R.; Patch, R. J.; Manthey, C. L.; Molloy, C. J.; Tomczuk, B. E.; Illig, C. R. Synthesis and evaluation of novel 3,4,6-substituted 2-quinolones as FMS kinase inhibitors. *Bioorg. Med. Chem. Lett.* **2008**, *18*, 2097.
- (29) Patch, R. J.; Brandt, B. M.; Asgari, D.; Baidur, N.; Chadra, N. K.; Georgiadas, T.; Cheung, W. S.; Petrounia, I.; Donatelli, R. R.; Chaikin, M. A.; Player, M. R. Potent 2-aminoanilide inhibitors of cFMS as potential anti-inflammatory agents. *Bioorg. Med. Chem. Lett.* **2007**, *17*, 6070.
- (30) Schubert, C.; Schalk-Hihi, C.; Struble, G. T.; Ma, H. C.; Petrounia, I. P.; Brandt, B.; Deckman, I. C.; Patch, R. J.; Player, M. R.; Spurlino, J. C.; Springer, B. A. Crystal structure of the tyrosine kinase domain of colony-stimulating factor-1 receptor (cFMS) in complex with two inhibitors. *J. Biol. Chem.* **2007**, *282*, 4094–4101, PDB ID: 2I0Y.
- (31) Illig, C. R.; Chen, J.; Wall, M. J.; Wilson, K. J.; Ballentine, S. K.; Rudolph, M. J.; Desjarlais, R. L.; Chen, Y.; Schubert, C.; Petrounia, I.; Crysler, C. S.; Molloy, C. J.; Chaikin, M. A.; Manthey, C. L.; Player, M. R.; Tomczuk, B. E.; Meegalla, S. K. Discovery of novel FMS kinase inhibitors as anti-inflammatory agents. *Bioorg. Med. Chem. Lett.* **2008**, *18*, 1642–1648.
- (32) (a) Kaplowitz, N. Idiosyncratic drug hepatotoxicity. *Nature Rev. Drug Discovery* **2005**, *4*, 489–499. (b) Ju, C.; Uetrecht, J. P. Mechanism of idiosyncratic drug reactions: Reactive metabolite formation, protein binding and the regulation of the immune system. *Curr. Drug Metab.* **2002**, *3*, 367–377.
- (33) Singh, R.; Silva Elipse, M. V.; Pearson, P. G.; Arison, B. H.; Wong, B. K.; White, R.; Yu, X.; Burgey, C. S.; Lin, J. H.; Baillie, T. A. Metabolic activation of a pyrazinone-containing thrombin inhibitor. Evidence for novel biotransformation involving pyrazinone ring oxidation, rearrangement, and covalent binding to proteins. *Chem. Res. Toxicol.* **2003**, *16*, 198–207.
- (34) Meegalla, S. K.; Wall, M. J.; Chen, J.; Wilson, K. J.; Ballentine, S. K.; Desjarlais, R. L.; Schubert, C.; Crysler, C. S.; Chen, Y.; Molloy, C. J.; Chaikin, M. A.; Manthey, C. L.; Player, M. R.; Tomczuk, B. E.; Illig, C. R. Structure-based optimization of a potent class of arylamide FMS inhibitors. *Bioorg. Med. Chem. Lett.* **2008**, *18*, 3632–3637.
- (35) Illig, C. R.; Ballentine, S. K.; Chen, J.; Meegalla, S.; Rudolph, J.; Wall, M. J.; Wilson, K. J.; Desjarlais, R.; Manthey, C. L.; Flores, C. M.; Molloy, C. J. Preparation of aromatic amides as inhibitors of c-fms kinase. PCT Int. Pat. Appl. WO 2006047504 A1, 2006.
- (36) RCSB Protein Data Bank. An Information Portal to Biological Macromolecular Structures. <http://www.rcsb.org/pdb/explore/explore.do?structureId=3KRL> (accessed December 30, 2010).
- (37) RCSB Protein Data Bank. An Information Portal to Biological Macromolecular Structures. <http://www.rcsb.org/pdb/explore/explore.do?structureId=3KRJ> (accessed December 30, 2010).
- (38) DeLano, W. L. *The PyMOL Molecular Graphics System*; DeLano Scientific: Palo Alto, CA, 2002; <http://www.pymol.org> (accessed November 17, 2010).
- (39) Orloffsky, A.; Stanley, E. R. CSF-1-induced gene expression in macrophages; dissociation from the mitogenic response. *EMBO J.* **1987**, *6*, 2947–2952.
- (40) The Cerep high-throughput profile consists of a broad collection of 50 transmembrane and soluble receptors, ion channels, and monoamine transporters designed to provide information not only on potential limitations or liabilities of drug candidates but also for



off-target activity identification. For the test compounds, the results are expressed as a percent inhibition of control-specific binding (mean values,  $n = 2$ ); <http://www.cerep.fr/Cerep/Users/index.asp> (accessed December 30, 2010).

(41) The  $pK_a$  of the conjugate acid of the piperidine was calculated using Advanced Chemistry Development (ACD/Labs) Software v12.0; <http://www.acdlabs.com> (accessed September 10, 2010).

(42) (a) Peters, J.-U.; Schnider, P.; Mattei, P.; Kansy, M. Pharmacological promiscuity: Dependence on compound properties and target specificity in a set of recent Roche compounds. *ChemMedChem* **2009**, *4*, 680–686. (b) Azzaoui, K.; Hamon, J.; Faller, B.; Whitebread, S.; Jacoby, E.; Bender, A.; Jenkins, J. J.; Urban, L. Modeling promiscuity based on in vitro safety pharmacology profiling data. *ChemMedChem* **2007**, *2*, 874–880. (c) Leeson, P. D.; Springthorpe, B. The influence of drug-like concepts on decision-making in medicinal chemistry. *Nature Rev. Drug Discovery* **2007**, *6*, 881–890. (d) Macchiarulo, A.; Nuti, R.; Eren, G.; Pellicciari, R. Charting the chemical space of target sites: Insights into the binding modes of amine and amidine groups. *J. Chem. Inf. Model.* **2009**, *49*, 900–912.

(43) (a) Starmer, C. F.; Lancaster, A. R.; Lastra, A. A.; Grant, A. O. Cardiac instability amplified by use-dependent sodium channel blockade. *Am. J. Physiol.* **1992**, *262*, H1305–H1310. (b) Hiroaka, M. In *Electrical Diseases of the Heart: Genetics, Mechanisms, Treatment, Prevention*; Gussak, I., Antzelevitch, C., Wilde, A. A. M., Friedman, P. A., Ackerman, M. J., Shen, W.-K., Eds.; Springer: London, 2008; pp 691–704.

(44) (a) Clusin, W. T. Calcium and cardiac arrhythmias: DADs, EADs, and alternans. *Crit. Rev. Clin. Lab. Sci.* **2003**, *40*, 337–375. (b) Salhanick, S. D.; Shannon, M. W. Management of calcium channel antagonist overdose. *Drug Saf.* **2003**, *26*, 65–79. (c) Packer, M. Pathophysiological mechanisms underlying the adverse effects of calcium channel-blocking drugs in patients with chronic heart failure. *Circulation* **1989**, *80*, IV59–IV67.

(45) Wilson, K. J.; Illig, C. R.; Chen, J.; Wall, M. J.; Ballentine, S. K.; Desjarlais, R. L.; Chen, Y.; Schubert, C.; Donatelli, R.; Petrounia, I.; Crysler, C. S.; Molloy, C. J.; Chaikin, M. A.; Manthey, C. L.; Player, M. R.; Tomczuk, B. E.; Meegalla, S. K. Reducing ion channel activity in a series of 4-heterocyclic arylamide FMS inhibitors. *Bioorg. Med. Chem. Lett.* **2010**, *20*, 3925–3929.

(46) Collins, I.; Rowley, M.; Davey, W. B.; Emms, F.; Marwood, R.; Patel, S.; Patel, S.; Fletcher, A.; Ragan, I. C.; Leeson, P. D.; Scott, A. L.; Broten, T. 3-(1-Piperazinyl)-4,5-dihydro-1H-benzo[g]indazoles: High affinity ligands for the human dopamine  $D_4$  receptor with improved selectivity over ion channels. *Bioorg. Med. Chem.* **1998**, *6*, 743–753.

(47) (a) Ladduwahetty, T.; Boase, A. L.; Mitchinson, A.; Quin, C.; Patel, S.; Chapman, K.; MacLeod, A. M. A new class of selective, non-basic 5-HT $_2A$  receptor antagonists. *Bioorg. Med. Chem. Lett.* **2006**, *16*, 3201–3204. (b) Jamieson, C.; Moir, E. M.; Rancovic, Z.; Wishart, G. Medicinal chemistry of hERG optimizations: Highlights and hang-ups. *J. Med. Chem.* **2006**, *49*, 5029–5046.

(48) Bertz, R. J.; Granneman, G. R. Use of in vitro and in vivo data to estimate the likelihood of metabolic pharmacokinetic interactions. *Clin. Pharmacokinet.* **1997**, *32*, 210–258.

(49) Masimirembwa, C. M.; Thompson, R.; Andersson, T. B. In vitro high throughput screening of compounds for favorable metabolic properties in drug discovery. *Comb. Chem. High Throughput Screening* **2001**, *4*, 245–263.

(50) Morgenthaler, M.; Schwiezer, E.; Hoffmann-Roder, A.; Benini, F.; Martin, R. E.; Jaeschke, G.; Wagner, B.; Fischer, H.; Bendels, S.; Zimmerli, D.; Schneider, J.; Diederich, F.; Kansy, M.; Muller, K. Predicting and tuning physicochemical properties in lead optimization: amine basicities. *ChemMedChem* **2007**, *2*, 1100–1115.

(51) (a) Sanguinetti, M. C.; Tristani-Firouzi, M. hERG potassium channels and cardiac arrhythmia. *Nature* **2006**, *440*, 463–469. (b) Sanguinetti, M. C.; Mitcheson, J. S. Predicting drug-hERG channel interactions that cause acquired long QT syndrome. *Trends Pharmacol. Sci.* **2005**, *26*, 119–124.

(52) (a) Geissler, E. N.; Ryan, M. A.; Housman, D. E. The dominant-white spotting (W) locus of the mouse encodes the c-kit proto-oncogene. *Cell* **1988**, *55*, 185–192. (b) Bijangi-Vishehsaraei, K.; Saadatzaheh, M. R.; Werne, A.; Wilson McKenzie, K. A.; Kapur, R.; Ichijo, H.; Haneline, L. S. Enhanced TNF- $\alpha$ -induced apoptosis in Fanconi anemia type C-deficient cells is dependent on apoptosis signal-regulating kinase 1. *Blood* **2005**, *106*, 4124–4130.

(53) Trentham, D. E.; Townes, A. S.; Kang, A. H. Autoimmunity to type II collagen: an experimental model of arthritis. *J. Exp. Med.* **1977**, *146*, 857–868.

(54) Bendele, A. M. Animal models of rheumatoid arthritis. *J. Musculoskeletal Interact.* **2001**, *1*, 377–385.

(55) Joosten, L. A. B.; Helsen, M. M. A.; Van de Loo, F. A. J.; Van den Berg, W. B. Anticytokine treatment of established type II collagen-induced arthritis in DBA/1 mice: A comparative study using anti-TNF $\alpha$ , anti-IL-1 $\alpha/\beta$ , and IL-1Ra. *Arthritis Rheum.* **1996**, *39*, 797–809.

(56) De Clerck, F.; Van de Water, A.; D'Aubouli, J.; Lu, H. R.; van Rossem, K.; Hermans, A.; Van Ammel, K. In vivo measurement of QT prolongation, dispersion and arrhythmogenesis: Application to the preclinical cardiovascular safety pharmacology of a new chemical entity. *Fundam. Clin. Pharmacol.* **2002**, *16*, 125–140.

(57) Ueno, Y.; Okazaki, S.; Isogaya, M.; Nishio, S.; Tanaka, H.; Kato, Y.; Shigenobu, K. Positive inotropic and chronotropic effects of beraprost sodium, a stable analog of prostacyclin, in isolated guinea pig myocardium. *Gen. Pharmacol.* **1996**, *27*, 101–103.

(58) Pearson, C. M. Development of arthritis, periarthritis and periostitis in rats given adjuvants. *Proc. Soc. Exp. Biol. Med.* **1956**, *91*, 95–100.

(59) Carlson, R. P.; Datko, L. J.; O'Neil-Davis, L.; Blazek, E. M.; Delustro, F.; Beideman, R.; Lewis, A. J. Comparison of inflammatory changes in established type II collagen and adjuvant induced arthritis using outbred Wistar rats. *Int. J. Immunopharmacol.* **1985**, *7*, 811–826.

(60) Benslay, D. N.; Bendele, A. M. Development of a rapid screen for detecting and differentiating immunomodulatory vs. anti-inflammatory compounds in rats. *Agents Actions* **1991**, *34*, 254–256.

(61) Chang, Y. Adjuvant polyarthritis. *Arthritis Rheum.* **1980**, *23*, 62–71.

(62) Cromartie, W. J.; Craddock, J. G.; Schwab, J. H.; Anderlie, S. K.; Yang, C. Arthritis in rats after systemic injection of streptococcal cells or cell walls. *J. Exp. Med.* **1977**, *146*, 1585–1602.

(63) Richards, P. J.; Williams, B. D.; Williams, A. S. Suppression of chronic streptococcal cell wall-induced arthritis in lewis rats by liposomal clodronate. *Rheumatology* **2001**, *40*, 978–987.

(64) Wustrow, D. J.; Wise, L. D. Coupling of arylboronic acids with a partially reduced pyridine derivative. *Synthesis* **1991**, 993–995.

(65) Maier, J. A.; Brugel, T. A.; Sabat, M.; Golebiowski, A.; Laufersweiler, M. J.; VanRens, J. C.; Hopkins, C. R.; De, B.; Hsieh, L. C.; Brown, K. K.; Easwaran, V.; Janusz, M. J. Development of N-4,6-pyrimidine-N-alkyl-N'-phenyl ureas as orally active inhibitors of lymphocyte specific tyrosine kinase. *Bioorg. Med. Chem. Lett.* **2006**, *16*, 3646–3650.